UNIVERSITÉ DU QUÉBEC

MÉMOIRE
PRÉSENTÉ À
L'UNIVERSITÉ DU QUÉBEC À CHICOUTIMI
COMME EXIGENCE PARTIELLE
DE LA MAÎTRISE EN SCIENCES DE LA TERRE

PAR

ALICE SHIRLEY PELOQUIN

THE PETROGRAPHIC AND GEOCHEMICAL VARIATIONS IN ARCHEAN META-BASALTIC PILLOWS FROM THE KINOJEVIS GROUP OF THE ABITIBI GREENSTONE BELT, ROUYN-NORANDA, QUEBEC

(LES VARIATIONS PÉTROGRAPHIQUES ET GÉOCHIMIQUES DES COUSSINS BASALTIQUES ARCHÉENS DU GROUPE DE KINOJEVIS, SOUS-PROVINCE DE L'ABITIBI, ROUYN-NORANDA, QUÉBEC)

MARS 1990

Bibliothèque
Paul-Émile-Boulet

UQAC
Université du Québec
à Chicoutimi

Mise en garde/Advice

Afin de rendre accessible au plus grand nombre le résultat des travaux de recherche menés par ses étudiants gradués et dans l'esprit des règles qui régissent le dépôt et la diffusion des mémoires et thèses produits dans cette Institution, **l'Université du Québec à Chicoutimi (UQAC)** est fière de rendre accessible une version complète et gratuite de cette œuvre.

Motivated by a desire to make the results of its graduate students' research accessible to all, and in accordance with the rules governing the acceptation and diffusion of dissertations and theses in this Institution, the **Université du Québec à Chicoutimi (UQAC)** is proud to make a complete version of this work available at no cost to the reader.

L'auteur conserve néanmoins la propriété du droit d'auteur qui protège ce mémoire ou cette thèse. Ni le mémoire ou la thèse ni des extraits substantiels de ceux-ci ne peuvent être imprimés ou autrement reproduits sans son autorisation.

The author retains ownership of the copyright of this dissertation or thesis. Neither the dissertation or thesis, nor substantial extracts from it, may be printed or otherwise reproduced without the author's permission.

ABSTRACT

Cross-sections of four pillows from a prehnite-pumpellyite facies meta-basalt flow were compared, in this study, to the massive facies of the same flow. The tholeiitic flow belongs to the Kinojevis Group of the Abitibi Sub-province of the Archean Superior Province.

The pillow centres exhibit a greater geochemical variation than the massive facies; the average of the pillow centre analyses, however, approaches that of the average massive basalt. The variations observed may be explained by either a primary variation in the lava between the two facies, or by deuteric alteration of the pillow centres due to introduction of sea water through fractures.

The textural zones observed in the pillows are: 1) the hyaloclastite (epidotized, chloritized and sericitized glass fragments); 2) the spherulitic rim (albitized plagioclase and interstitial chlorite); 3) the vesicular zone (albitized plagioclase, interstitial chlorite, and quartz - chlorite filled vesicule trains); and 4) the interior zones including the pillow centre (relic clinopyroxene, epidotized and albitized microlitic plagioclase, and interstitial chlorite and epidote).

In general, all four pillows exhibit similar variations in major, trace and REE elements. The variations observed in the major elements from one pillow zone to another directly reflect the mineralogical variations in the zones. Trace elements are generally enriched in the hyaloclastite. The enrichment begins in the spherulitic rim for Sc, Rb, Zr and Zn, and in the vesicular zone for B and Ba. Sr, Y and Cu exhibit negative anomalies in the vesicular zone. B and Sc decrease in abundance from the pillow centre toward the vesicular zone, whereas the other trace elements are virtually constant. Pb, Co, Nb and Hf have erratic trends. The REE's are also enriched in the hyaloclastite. The spherulitic rim exhibits negative anomalies for La and Sm; anomalies begin in the vesicular zone for Ce and Nd.

The alteration stages envisioned for these pillows are:
1) Deuteric alteration, which slightly modified the original chemistry of the pillow centre.
2) Submarine alteration or interaction with sea water, which palagonitized the hyaloclastite and smectitized the intersitial glass of the spherulitic rim and vesicular zone. The REE's are mobilized during this alteration and migrate to the external zones of the pillow.
4) Submarine metamorphism, or diagenesis after burial, resulted in the albitization of plagioclase. The spherulitic rim and vesicular zone are the most affected due to their greater porosity and high plagioclase content. The mobility of the trace elements and REE's is unknown for this stage.
5) Regional prehnite-pumpellyite facies metamorphism, which only affects the element distribution through the distribution of the metamorphic minerals.

RÉSUMÉ

L'objectif de cette étude était de définir les changements géochimiques correspondant aux variations texturales observées dans les bordures de coussins archéens, et de les comparer à celles des coussins récents.

La région de l'étude est située dans la Sous-Province de l'Abitibi, environ 40 km au nord de Rouyn-Noranda, dans le Canton d'Aiguebelle du nord-ouest du Québec (figure 1). Elle fait partie de la Formation de Deguisier du Groupe de Kinojévis.

La région fut étudiée en détail par Yves Sanschagrin et Maxime Leduc sous la direction d'Erich Dimroth dans le cadre d'un contrat du M.E.R.Q. et d'études de maîtrise (Sanschagrin et Leduc 1979, Sanschagrin 1981, Leduc 1981). La coulée étudiée se trouve sur le terrain de Sanschagrin (1981) qui a défini 18 coulées de basaltes tholéiitiques métamorphisés au faciès préhnite-pumpellyite (figure 3). Ces coulées comprennent des faciès massifs, coussinés et bréchiques.

Deux affleurements de la coulée 9, qui montre les faciès massifs et coussinés, furent échantillonnés en détail (figures 3 et 4). Dix-neuf échantillons de la partie massive furent collectés, et des neuf coussins échantillonnés (figure 6), quatre furent retenus pour cette étude.

Les variations texturales mentionnées ci-haut apparaissent à la figure 6 (modifiée d'après Dimroth et Lichtblau 1979) et se définissent comme suit:

I. La zone hyaloclastique qui consiste en verre fragmenté.

II. La zone de croûte hyaline. Cette zone comprend du verre avec des microphénocrystaux de plagioclase ou d'olivine comme phases principales.

III. La zone des sphérolites isolés. Dans cette zone, les sphérolites sont composés de microlites, souvent squelettiques, de plagioclase sur lesquels des fibres de plagioclase et de clinopyroxène se sont developpées pour donner des formes sphériques et fibro-radiées.

IV. La zone des sphérolites agglomérés. Les sphérolites de la zone III deviennent graduellement plus nombreux et le verre moins abondant vers le centre du coussin. Les sphérolites individuels passent graduellement à des sphérolites agglomérés aux bordures nettes, puis à des sphérolites agglomérés aux bordures floues.

V. Le centre du coussin. Le centre du coussin a une texture microlitique avec des microlites de plagioclase dans une matrice de clinopyroxène squelettique.

Les textures décrites sont les produits de surfusion (Kirkpatrick 1978, Natland 1978 et 1980). La surfusion (- T) est définie comme un différentiel négatif de température, entre la température d'équilibre du liquidus et la température réelle à laquelle la cristallisation se produit. Donc, la surfusion est plus élevée à l'interface eau - lave (près de la croûte), où elle limite la cristallisation. La surfusion diminue vers le centre du coussin où, conséquemment, le taux de cristallisation augmente.

Les textures de surfusion restent préservées dans les coussins archéens; même sur l'affeurement on note une variation de couleur qui indique un changement textural (planche 1). En plaque coupée, ces variations texturales sont encore plus évidentes (planche 4), et certaines nuances peuvent être définies. Par exemple, la zone de sphérolites agglomérés montrent toujours la présence de trainées de vacuoles perpendiculaires à la bordure du coussin, et un coussin (S4-P3) montre un rubanement dans la zone microlitique (planche 5), tandis que dans d'autres coussins les mêmes zones sont homogènes.

L'échelle réduite des zones texturales a rendu l'échantillonage difficile; conséquemment, certains regroupements ont dû être faits:

I. La zone hyaloclastique (Celle-ci inclut la croûte de verre non-sphérolitique.).

II. La bordure de verre à sphérolites isolés. Des échantillons de 0,5 cm furent prélevés dans cette zone.

III. La zone de trainées de vacuoles dans les sphérolites agglomérés. (1,0 cm)

IV. Zone microlitique. Trois à quatre échantillons consécutifs de la zone microlitique ont été prélevés de la bordure vers le centre du coussin. Dans tous les coussins, sauf celui avec le rubanement, les deux premiers échantillons font 2,0 cm chacun, et le troisième, 5,0 cm. Dans un seul cas, un quatrième échantillon a été pris. Le coussin avec le rubanement a été échantillonné de la bordure vers le centre aux intervalles suivants: 1,0 cm, 1,0 cm, 2,0 cm, 2,0 cm et 5,0 cm.

V. Centre du coussin. Un échantillon a été pris au centre de tous les coussins.

Des échantillons de basaltes massifs ont été prélevés pour comparer leur géochimie à celle des coussins. En lames minces, le basalte est microporphyrique à plagioclase; il contient du clinopyroxène relique, et sa texture est essentiellement sub-ophitique (planche 2). Le basalte massif, d'affinité tholéiitique, est métamorphisé au faciès préhnite-pumpellyite (Sanschagrin 1981, Sanschagrin et Leduc 1979, Dimroth et al. 1983). En utilisant le logiciel SOMA (Appleyard and de Beer 1982), qui calcule les pertes et ajouts des éléments dans une roche altérée comparée à sa roche parente, des differences majeures entre la moyenne des éléments majeurs des analyses de cette étude et des tholéiites récentes (Cox et al. 1980, Nockolds et al. 1979) apparaissent (figure 10). Toutefois, la conservation des textures primaires et du clinopyroxène primaire dans les échantillons de basalte archéen, rend l'explication des variations chimiques par l'altération peu plausible. Donc, il est probable que les différences soient primaires, c'est-à-dire que les laves archéennes étaient fondamentalement distinctes des laves récentes.

Malgré ces différences, la lave massive est sub-alcaline (figure 7) et tholéiitique (figure 8). Sur les diagrammes pétrochimiques utilisés couramment pour déterminer les environments tectoniques des laves, cette coulée couvre divers champs: basaltes des fonds océaniques (figure 11b et c), basaltes d'arcs insulaires et calco-alcalins (figure 11c) et basaltes calco-alcalins (figure 11a). Ceci démontre l'utilité restreinte de ces diagrammes pour définir les environnements tectoniques archéens.

Six centres de coussins ont été étudiés pour fin de comparaison avec la lave massive. Bien que la minéralogie ressemble à celle de la lave massive, la texture est surtout microlitique et pilotaxitique avec du clinopyroxène squelettique entre les microlites de plagioclase. Leur géochimie montre des tendances sub-alcaline (figure 7) et tholéiitique (figure 8) similaires à la lave massive. Sur les diagrammes des éléments (oxydes, éléments traces et éléments de terres rares) en fonction de SiO_2 (figures 12, 14 et 15), les centres de coussins montrent une plus grande dispersion que les échantillons de lave massive pour les oxydes et les éléments traces à l'exception du Ce. Par contre, la moyenne des échantillons des centres de coussins se rapproche de la moyenne des laves massives pour tous les éléments. Les diagrammes "Spider" des éléments de terres rares montrent des patrons sensiblement plats pour les centres de coussins et pour la lave massive (figure 9).

Le programme SOMA a été encore utilisé pour comparer les centres de coussins à la moyenne du faciès massif (figure 13). La perte en Al_2O_3 avec l'augmentation en CaO et Na_2O est attribuée à l'albitisation des plagioclases. L'augmentation en Fe_2O_3 et FeO et la perte en MgO est due à l'épidotisation de la matrice hyaline.

Les teneurs en éléments traces sont plutôt constantes, à l'exception des éléments métalliques Cr, Ni, Cu et Zn qui montrent plus de variations. Le Sr montre un gain alors que le Ba indique une grande perte.

Les terres rares sont essentiellement immobiles, à l'exception du Cerium, qui croît de façon notable.

Des trois façons de traiter les données des sections de coussins avec le programme Soma (figures 16 et 17), le mode sans changement en volume a été retenu pour comparer la composition des coussins à celle de la moyenne de la lave massive. Les figures produites avec le centre du coussin comme roche mère ressemblent à celles de la lave massive comme parente (figures 16c et 17c). Le mode avec changement de volume n'a pas été retenu; les courbes obtenues, à l'exception de la hyaloclastite, montrent des patrons identiques à ceux avec mode à volume constant. Pour la hyaloclastite, les variation proviennent surtout du fait que nous avons assumé sa densité identique à celle de la lave massive.

Les diagrammes de SiO_2, Na_2O, CaO et Al_2O_3 (figure 18a-c et e) montrent les effets de l'albitisation des plagioclases vers la bordure des coussins, suivie par l'épidotisation et la chloritisation de la hyaloclastite. L'augmentation en K_2O (figure 18d) est due à la présence des petites quantités de séricite dans la hyaloclastite.

Le FeO et le Fe_2O_3 (figure 18f-g) sont plutôt complémentaires à l'intérieur des coussins. L'augmentation en FeO et FE_2O_3 dans l'hyaloclastite est causée par la chloritisation et l'épidotisation.

L'abondance en MgO (figure 18h) reflète problablement le rapport épidote/chlorite interstitielle. Dans le coussin rubané (S4-P3), le MgO augmente dans la partie rubanée.

Le MnO (figure 18i) ne montre aucun patron majeur.

Le TiO_2 et le P_2O_5 (figure 18j et 18k) montrent une dichotomie; le coussin S4-P5 montre un contenu en TiO_2 plus bas que les autres coussins et un taux de P_2O_5 plus haut.

Au niveau des éléments traces (figure 19), la hyaloclastite est très enrichie. Le Bore (figure 19a) montre une diminution du centre vers la bordure du coussin, suivie par une forte augmentation dans la hyaloclastite. Le Ba (figure 19b) est sensiblement stable jusqu'à la bordure, sauf dans le cas du coussin S4-P3 où il y a une anomalie positive à l'extérieur du rubanement. Le Cr et le Sc (figure 19c-d) sont un peu plus erratiques à l'intérieur mais augmentent quand même dans l'hyaloclastite. Rb, Sr, Y et Zr (figure 19i-l) montrent tous un enrichissement dans la hyaloclastite. Le Rb montre la même dichotomie que le Titane. Le Sr montre un diminution vers la bordure analogue à celle observée pour

le Calcium. Le Y est essentiellement stable à l'intérieur des coussins avec une anomalie négative dans la zone sphérolitique. Le Zr est un peu plus erratique, mais la courbe est surtout plate. Il y a une petite anomalie positive à l'intérieur du rubanement en S4-P3.

Le Cu, le Zn, le Pb et le Ni (figure 19e-h) sont enrichis dans la hyaloclastite. Souvent, une petite anomalie négative précède l'augmentation. A l'intérieur, les courbes sont souvent erratiques sauf pour le Cu (figure 19e) qui a une courbe plate.

Les lignes évolutives du Li, du Co, du Nb et du Hf (figure 19m-l) ne sont pas très claires, à l'exception d'une forte anomalie en Co à l'intérieur du rubanement de l'échantillon S4-P2.

Les Terres Rares (figure 20) sont aussi enrichies dans la hyaloclastite. Les courbes du La, du Ce, du Nd et du Sm (figure 20a-d) sont en générales plates avec une petite anomalie positive à l'intérieur des coussins, suivie d'anomalies négatives dans les zones de sphérolites isolés à agglomérés. L'échantillon S4-P3 est parmi ceux qui montrent des anomalies positives.

Les éléments Eu et Ho (figure 20e-f) montrent des courbes presque parfaitement plates sauf dans la hyaloclastite où il y a enrichissement.

Dans les coussins S4-P5 et S4-P3, l'Yb (figure 20g) montre des anomalies positives dans la zone interne, redevient ensuite plat, et augmente à nouveau dans la hyaloclastite.

Les diagrammes "Spider" des terres rares montrent que les courbes des zones centrales et interne de coussins sont similaires aux courbes du faciès massif de la coulée (figure 9). La zone vacuolaire montre plus de variation (lessivage en terres rares légères). La zone des sphérolites est en moyenne un peu lessivée en terres rares, et certains coussins montrent aussi une lixiviation en terres rares légères. La hyaloclastite, qui est en général enrichie en terres rares, montre des patrons erratiques (figure 9). Des anomalies positives marquées en La, Sm, Eu et Ho sont observées.

Les étapes d'altération subies par ces coussins sont:

1- L'altération deutérique qui a modifié légèrement la géochimie originale. (Tableaux 3 et 4)

2- L'altération sous-marine (interaction eau de mer-coussin) qui a produit la palagonitisation des hyaloclastites et la smectitisation du verre interstitiel (surtout dans la bordure sphérolitique et la zone vacuolaire). Les terres rares sont mobilisées dans cette phase, et se trouvent à l'extérieur des coussins. (Tableau 5)

3- La troisième phase est une albitisation qui se produit probablement lors de l'enfouissement de la coulée. La bordure sphérolitique et la zone vacuolaire sont les plus effectées, leur porosité et leur contenu en plagioclase étant plus élevé que ceux des zones internes et de la hyaloclastite. La mobilité des éléments traces et des terres rares est connue à ce point. (Tableau 7)

4- La dernière étape est le métamorphisme régional au faciès préhnite - pumpellyite qui produit la minéralogie observée mais n'affecte pas la chimie des roches de façon sensible.

TABLE OF CONTENTS

LIST OF FIGURES

LIST OF TABLES

LIST OF PLATES

LIST OF ANNEXES

INTRODUCTION

This thesis was undertaken with the goal of studying the textural zonation in Archean meta-basaltic[1] pillows, and defining the associated alteration pattern. The massive and pillowed facies of a single flow were sampled; the massive facies being considered the "parent" composition of the pillows, and thus, being used as a basis for comparison of the chemical variations within individual pillows.

The area studied is in the Aiguebelle Provincial Park in Aiguebelle Township, Quebec, approximately 40km north of Rouyn-Noranda (figure 1). The flow studied is from the Kinojevis Group of the Western Abitibi Greenstone Belt (figure 2) and has been previously documented in detail by Sanschagrin (1981) under the direction of the late Erich Dimroth.

The chemical differences observed between the massive basalt and the microlitic pillow centre, and within the individual pillows from centre to rim can be explained by a number of successive, overlapping phenomena: 1) different crystallization histories between facies and within pillows; 2) deuteric alteration of the pillow centre; 3) sea water-basalt interaction on the seafloor (seafloor weathering); 4) sea water - basalt interaction sub-surface (seafloor metamorphism); and 5) regional prehnite - pumpellyite facies metamorphism.

---

[1] The term "meta-basalt" has been simplified to "basalt" in the remainder of the text.

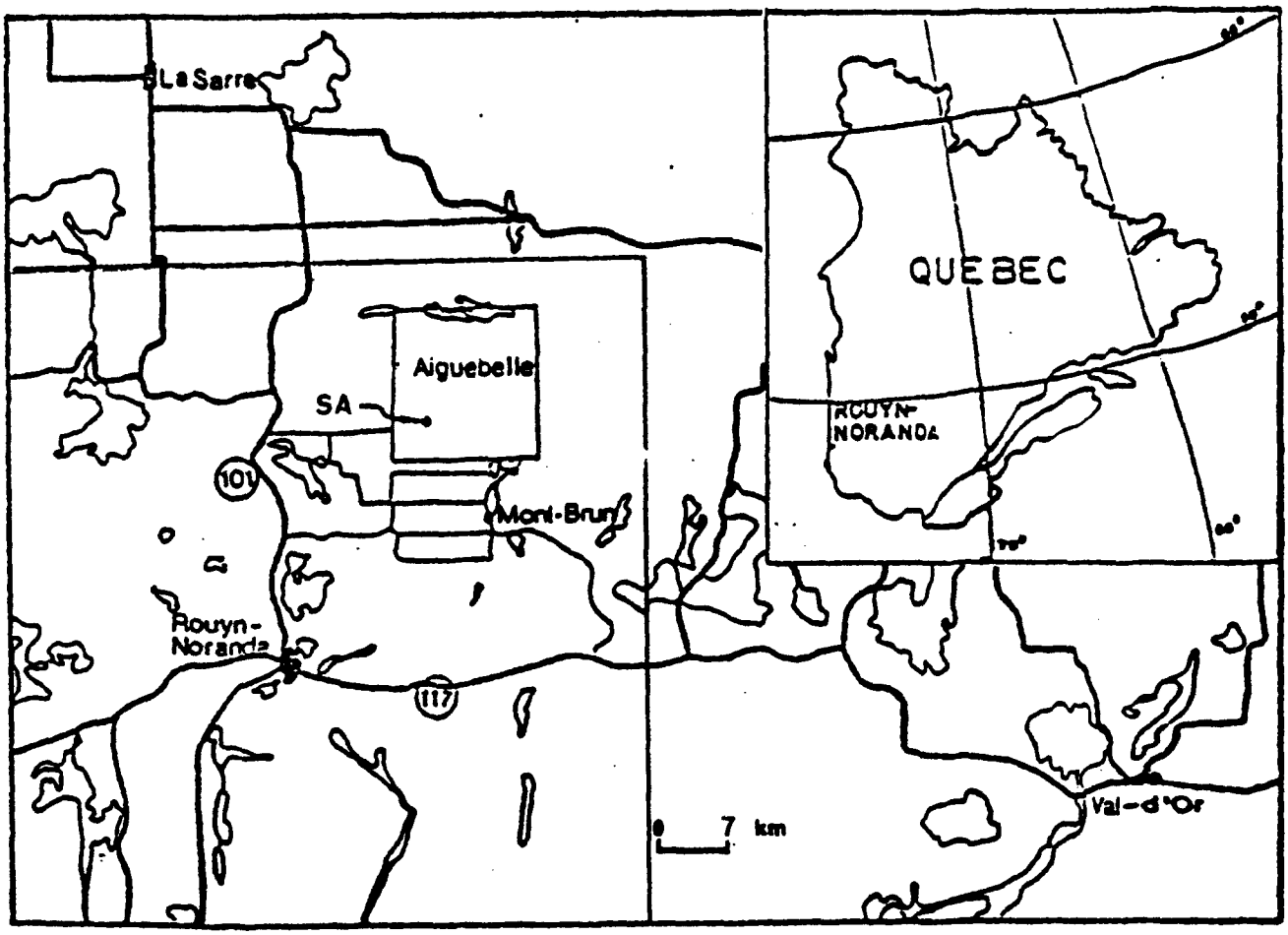

Figure 1: Localisation of study area (SA). (reproduced from Sanschagrin, 1981)

Localisation de la région d'étude. (tiré de Sanschagrin, 1981)

GENERAL GEOLOGY

The study area is in the Ruisseau Deguisier Formation of the Kinojevis Group of the Abitibi Greenstone Belt of the Superior Province of the Canadian Pre-Cambrian Shield (Dimroth et al. 1973, Sanschagrin 1981). The Kinojevis Group north of Rouyn-Noranda is part of the Tholeiitic Division of the Cycle III volcanism defined in the Lithostratigraphic map of the Abitibi Subprovince (M.E.R.Q. and O.G.S 1983). It is underlain by the Cycle III Ultramafic Division (Stoughton-Roquemaure and Malartic Groups), and overlain by the Cycle III Upper Varied Division (Blake River Group) (figure 2).

The Malartic Group is divided into the La Motte-Vassan, Dubuisson and Caste Formations. The Roquemaure-Stoughton Group is the stratigraphic equivalent of the La Motte-Vassan Formation, both being ultramafic sequences. The Dubuisson Formation is composed of alternating ultramafic (komatiitic) and mafic (tholeiitic) flows. The Caste Formation is an argillite and graywacke unit occurring entirely within the Dubuisson Formation (M.E.R.Q. and O.G.S. 1983). The Blake River Group is comprised of tholeiitic andesites, and less commonly basalts, alternating with calc-alcaline andesites and rhyolites in a bimodal series (Gélinas et al. 1984).

The Kinojevis Group sandwiched between the Stoughton-Roquemaure-Malartic and Blake River Groups is divided into the Paré and Deguisier Formations (Dimroth et al. 1973, Sanschagrin 1981). The older of the formations, the Paré, is comprised of komatiite and basalt flows, and rhyolite domes.

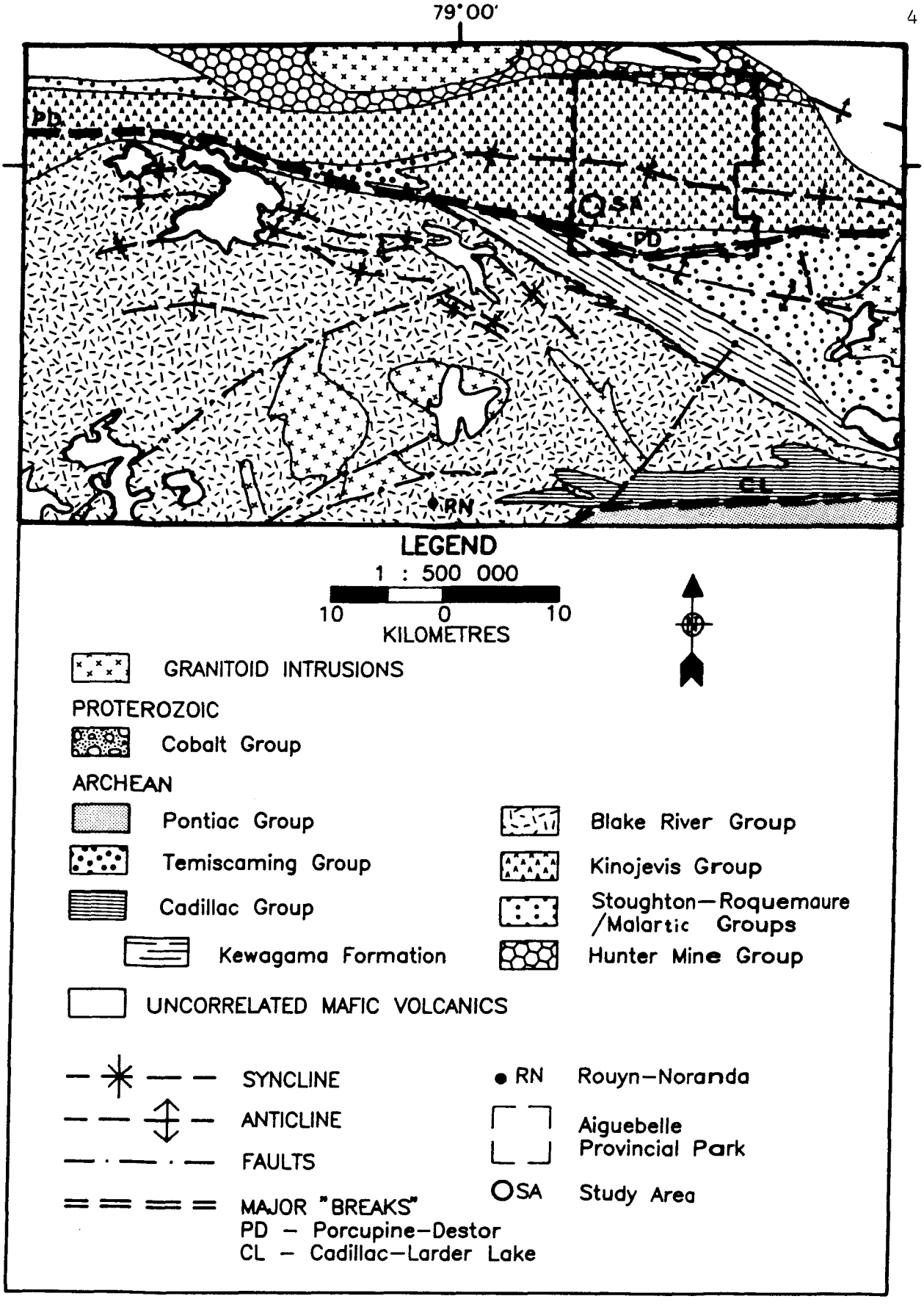

Figure 2: Regional geology of the area. (after M.E.R.Q. and O.G.S. 1983)

Géologie régionale du secteur. (d'après M.E.R.Q. et O.G.S. 1983)

The Deguisier Formation is, on the other hand, a tholeiitic basalt pile, the majority of which is aphyric, with rare glomeroporphyritic lavas. These latter have been used as marker horizons to define the stratigraphy and structure in the Kinojevis Group (Sanschagrin 1981). The basalts of the Deguisier Formation have been metamorphosed to prehnite-pumpellyite facies and are virtually unfoliated.

LOCAL GEOLOGY:

Sanschagrin (1981) defined a tholeiitic basalt pile consisting of nineteen individual flows exhibiting massive, pillowed and brecciated facies in the area south of lac Vose (figure 3). The pile strikes at approximately 267° and dips 60° to the north.

While the majority of the basalts were found to be aphyric, two plagioclase glomeroporphyritic basalts (flows 18 and 19) cap the sequence and are used as marker units. The area is considered to be a part of the Destor Volcanic Complex; the source of the flows, thus being located approximately 10 km west of the study area, in Destor Township. This idea is supported by the findings of Sanschagrin and Leduc (1979), Sanschagrin (1981) and Leduc (1981) that the massive to pillowed basalt ratio decreased to the East; that rhyolites, associated with the basalts to the east, are absent in the Aiguebelle Area, and that the grain sizes in pyroclastic rocks decrease to the West.

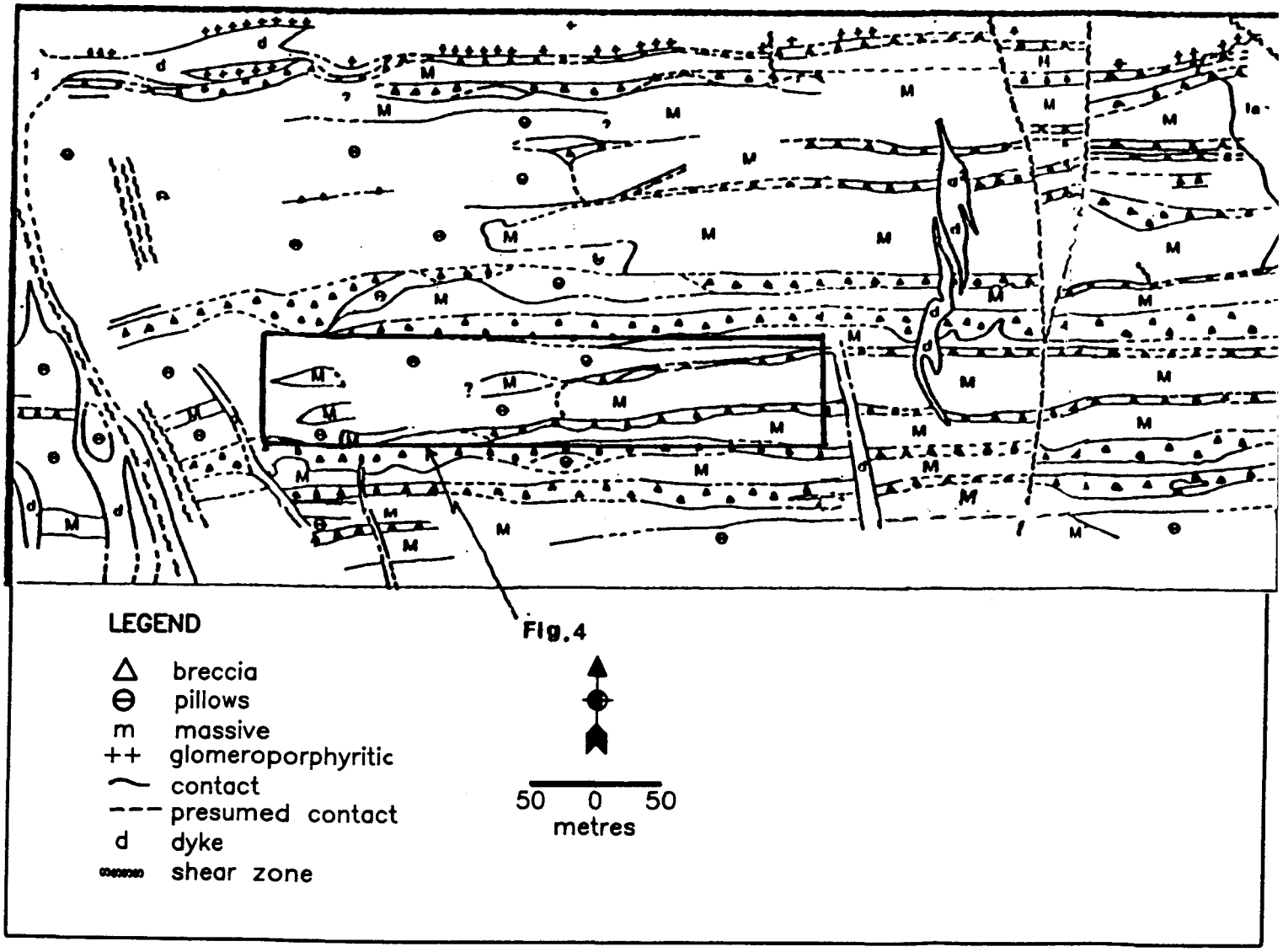

Figure 3: Local geology of the area, showing the position of the flow studied. (reproduced from Sanschagrin 1981).

Géologie locale du secteur montrant la position de la coulée étudiée. (tirée de Sanschagrin 1981).

SAMPLE LOCATION AND METHODOLOGY

Of the nineteen individual flows delineated by Sanschagrin (figure 3), flow 9, consisting of a massive and pillowed facies (figure 4), was studied. Flow 9 is aphyric or sparsely plagioclase microphyric. The pillows of this flow are generally 1m in size and are well-formed, indicating an east-west stratification and a polarity toward the north.

Two outcrops (SP-S3 and SP-S4) were sampled (figure 4). The southern extremity of SP-S3 consists of the pillowed section of flow 8, followed to the north by the massive facies of flow 9 and finally the pillowed section of flow 9 (figure 4). On SP-S4 only the pillowed facies of flow 9 is present. Three pillows from outcrop SP-S4 and one from SP-S3, along with samples of three other pillow centres and nine samples of the massive facies were chosen for geochemical analysis.

In sampling the massive facies, the least altered, most homogenous areas were chosen from throughout the exposed section, and detailed sampling approaching the massive - pillowed facies boundary was undertaken (figure 5a). Unfortunately, these latter samples proved to be too altered for chemical analysis.

Sampling of the pillows was performed to include entire cross-sections from the rim to the pillow centre. On outcrop SP-S4, entire pillows were taken as samples. Attempts to sample specific pillow zones using a GSC "pack drill" met

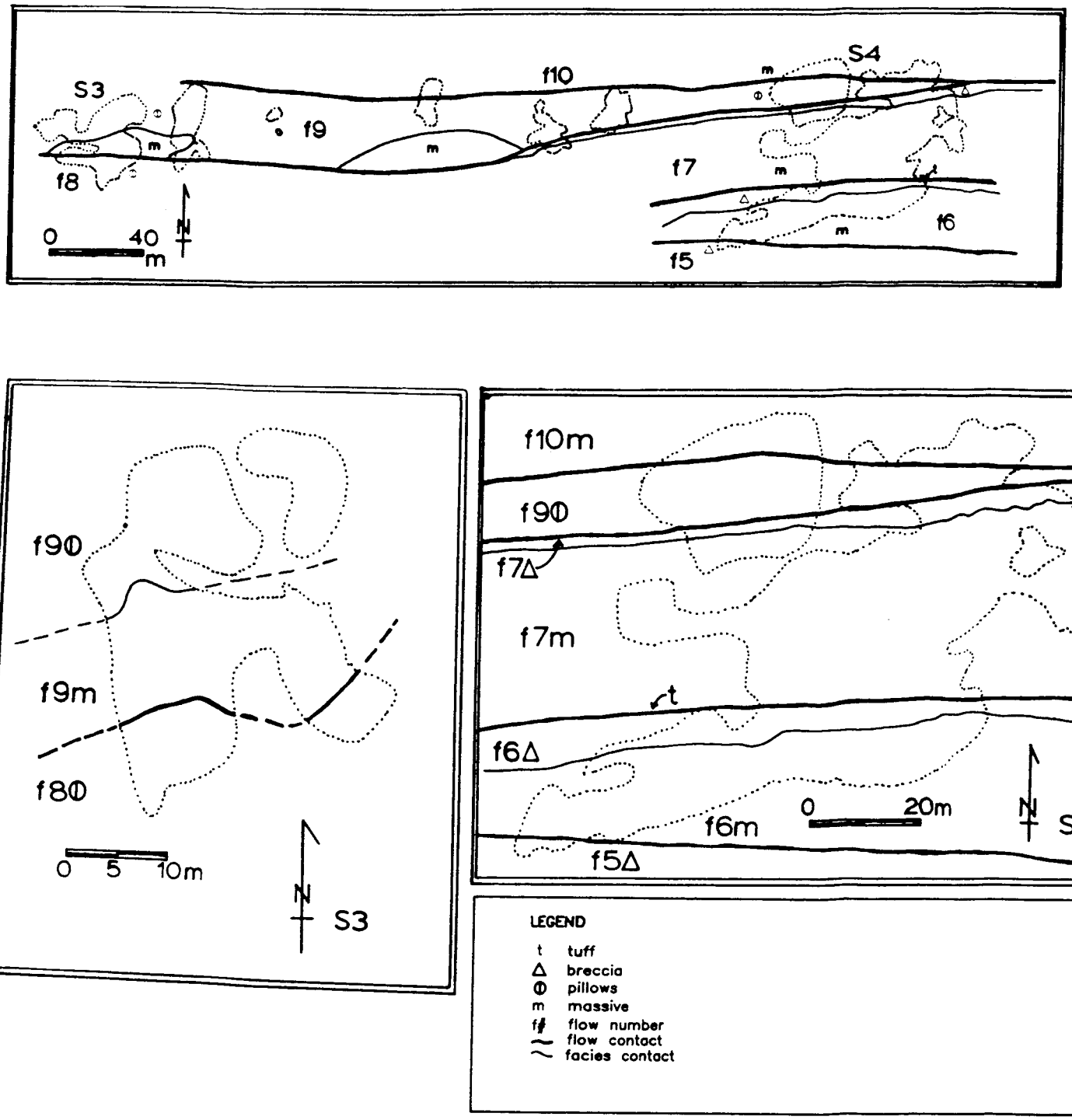

Figure 4: Detailed map of the outcrops studied.
a) Spatial relationship of the outrcrops.
b) Facies present on outcrop S3.
c) Facies present on outcrop S4.

Carte détaillée des affleurements étudiés.
a) Relation spatiale des affleurements.
b) Faciès présents sur l'affleurement S3.
c) Faciès présents sur l'affleurement S4.

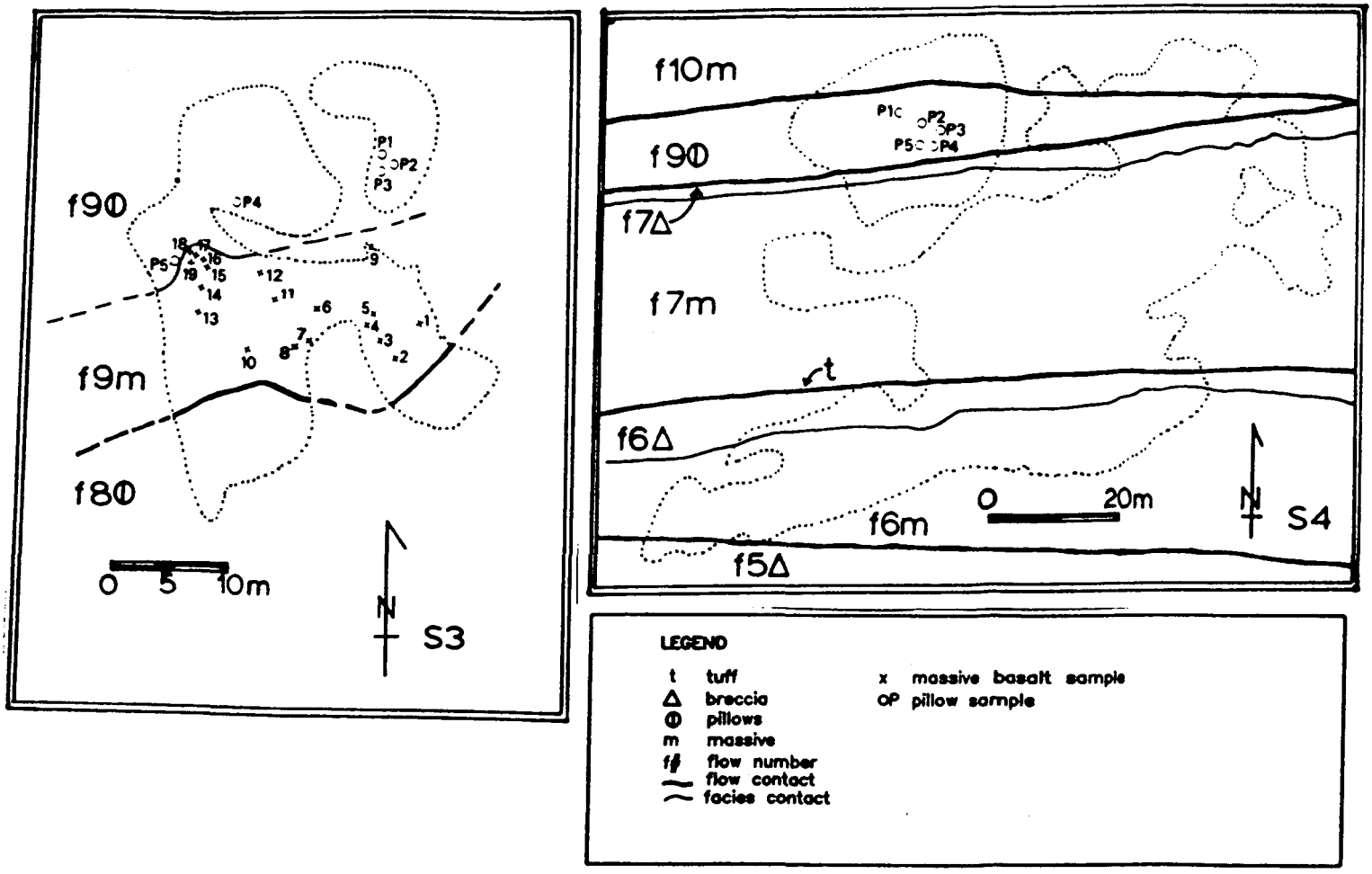

Figure 5: Sample locations
a) Outcrop S3
b) Outcrop S4

Localisation des échantillons
a) Affleurement S3
b) Affleurement S4

with limited success. Thus, samples were taken by hammer and chisel.

Three pillows from outcrop SP-S4 and one from SP-S3, along with three samples from pillow centres, two from SP-S3 and one from SP-S4, and nine samples from the massive facies were chosen for major element analysis (figure 5a and b). Of these, five of the massive samples and all of the entire pillow samples were analysed for trace elements using XRF. Rare Earth Element analyses were performed on the five massive basalt samples and the pillow samples from outcrop SP-S4.

The pillows exhibit the classic crystallization textures of pillow lavas (Kirkpatrick 1978, Natland 1978 and 1980, Dimroth and Lichtblau 1979; figure 6): a hyaloclastite border, a non-spherulitic glass rim, a thin zone of isolated spherulites grading into a zone of coalesced spherulites, which itself grades from spherulites having distinct boundaries to those having indistinct boundaries, and an increasingly massive microlitic central zone. This textural zonation is easily visible in the pillows of flow 9 due to slight, concentric variations in the colour of the weathered surface (plate 1).

An average of six samples per pillow cross-section were analysed; these being, the glass border (hyaloclastite) including the isolated spherulite rim, the zone of gradually coalescing spherulites (0.5 cm), a zone of crystalline vesicular lava grading from the spherulitic zone to the microlitic zone (1.0 cm), two samples in 2 cm increments from

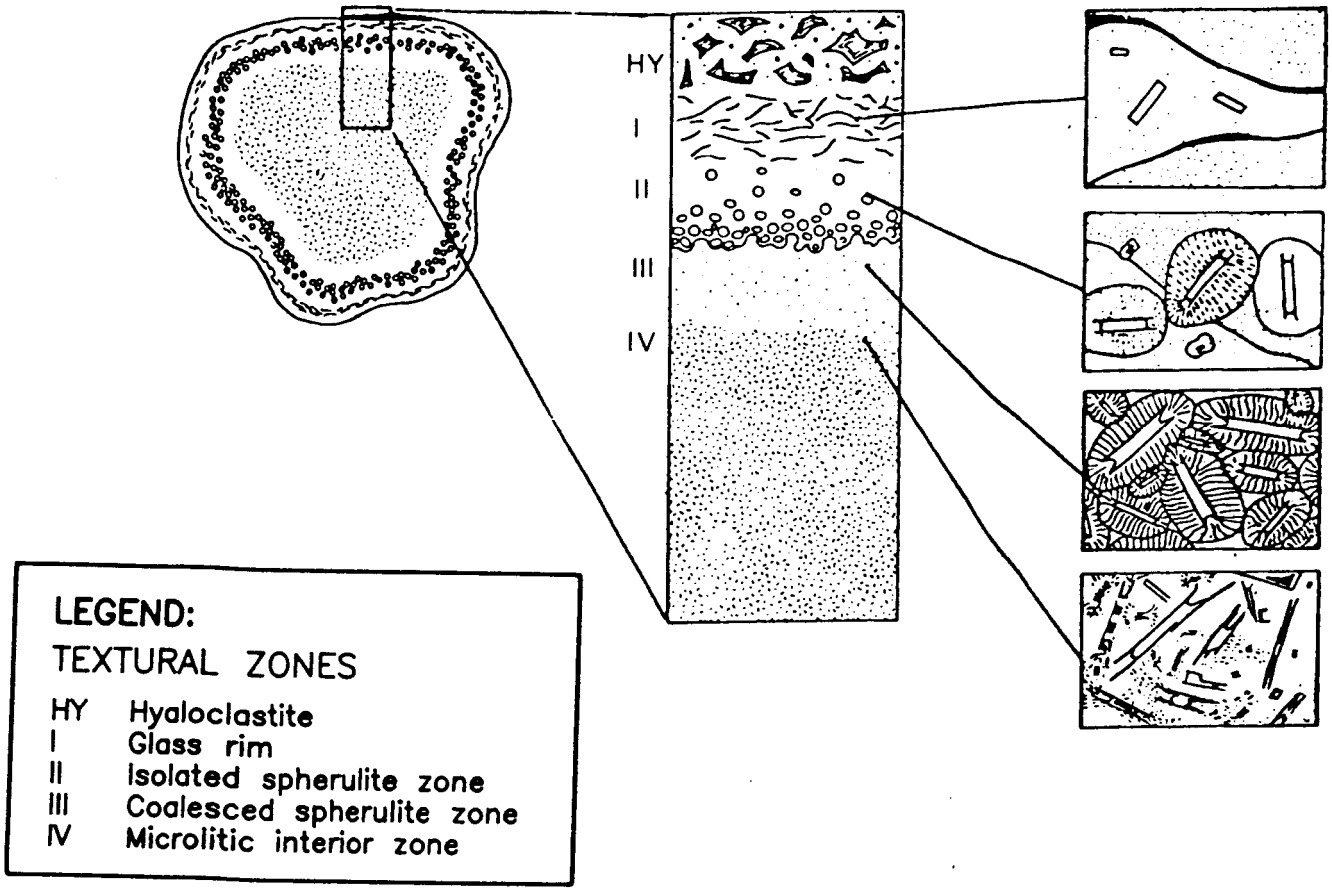

Figure 6: Zonal crystallization textures of pillow lavas. (reproduced from Dimroth and Lichtblau 1979.)

Zones des textures de cristallisation des laves coussinées. (tirée de Dimroth et Lichtblau 1979.)

the beginning of the microlitic zone, one 4 cm sample, and in one case, a sample consisting of the remainder of the internal zone. A final sample representing the centre of the pillow was taken in each case.

The exception to this sampling division is pillow SP-S4-P3. In this case, due to a banded structure occurring 4 cm within the pillow, two 1 cm samples and two 2 cm samples were taken following the vesicular zone; the third of these samples being the banded zone.

The individual textural samples were separated in the whole pillow sample by cutting thin slabs, preferably of 1/2 cm width, polishing the slabs, using tungsten-carbide grinding powder to remove any contamination from the saw, and "clipping" the appropriate sample from the slab using a ceramic-tile clipper. The sample chips were then sandblasted using Ottawa quartz sand, such as is used in sample grinding, to remove any contamination by the tile clippers. After washing and drying in an oven at 95° for 8 hours, the samples were quartered into a fifty gram sample for grinding with a tungsten carbide shatterbox, and a 10 gram sample for grinding with an agate mortar. In one case, SP-S3-P5-2H, the initial sample was not sufficient for the two types of grinding and a second sample was taken for the grinding by agate mortar.

The major element analyses, Loss On Ignition (LOI), and CO2, S and FeO/Fe2O3 determinations were performed at the Université du Québec à Chicoutimi geochemistry laboratory. Fe_2O_3, Na_2O, K_2O, CaO, MgO, MnO and TiO_2 were determined by

Plate 1: Pillow sample exhibiting a concentric variation in colour due to the variation in texture.

Echantillon de coussin montrant une variation concentrique de couleur due au changement de texture.

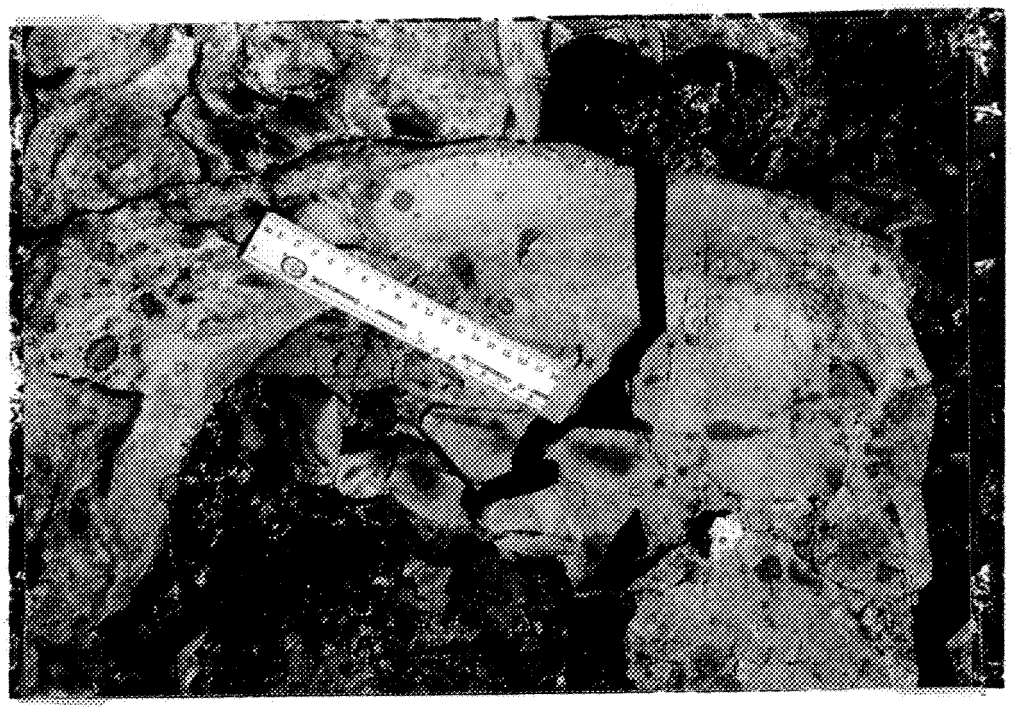

Atomic Absorption; SiO_2, Al_2O_3 and P_2O_5 by XRF using a Philips PW-1420 machine (in the cases were the H2O content of the sample exceeded 3%, the LOI powders were used in the XRF pastilles); CO2 and S were determined using a LECO apparatus; and FeO/Fe_2O_3, by titration. The trace element analyses; Li, B, Cr, Ni, Cu, Zn, Rb, Sr, Y, Zr, Nb, Ba and Pb; were performed by XRF at Neutron Activation Services Limited and X-Ray Assay Laboratories, Hamilton, Ontario. The REE and the trace elements; La, Ce, Nd, Sm, Eu, Tb, Ho, Yb and Lu, and Ba, Rb, Cs, Sc, Hf, Cr, U, Th, Ta, Au, and Zn; were analysed by Neutron Activation at the Université du Québec à Chicoutimi Neutron Activation Laboratory.

PETROGRAPHY

MASSIVE BASALT

The entire thickness of the massive facies of Flow 9 is exposed on outcrop SP-S3 (figure 4), only the immediate contact with Flow 8 being overburden covered. It varies in thickness from 10 m to 15 m, the contact with the pillowed section being very irregular. The flow is dominantly subophitic to ophitic, and slightly (1%) vesicular; approaching the contacts, both inter-flow and inter-facies, the basalt passes from sub-ophitic to intergranular, and skeletal quench clinopyroxenes are observed.

Nineteen samples were collected across this facies (figure 5a). The flow can be characterized as being composed of 30% (0.2-1mm) plagioclase microlites, <1% (2-4mm) sausseritized plagioclase phenocrysts, and 40% (0.2-1mm) xenomorphic to hypidomorphic clinopyroxene in a quartz--clinozoisite--pistacite--FeTi oxide mesostasis (plate 2). The texture is intergranular to sub-ophitic, rarely ophitic. The plagioclase microlites define a pilotaxitic texture. The clinopyroxene exhibits skeletal to anhedral granular crystal habits; in one sample it occurs as acicular crystals. Chlorite (+/- carbonate, clinozoisite, quartz, and rarely pumpellyite) fill vesicles, which make up 1% of the rock. Concentric cooling fractures locally visible on the outcrop and in handsamples are not evident in the thin sections; they

Plate 2: Texture common to the massive section of Flow 9. (SP-S3-10: crossed nickels; bar = 0.5mm).

Texture commune du faciès massif de la coulée 9. (SP-S3-10: lumière polarisée; barre = 0,5mm).

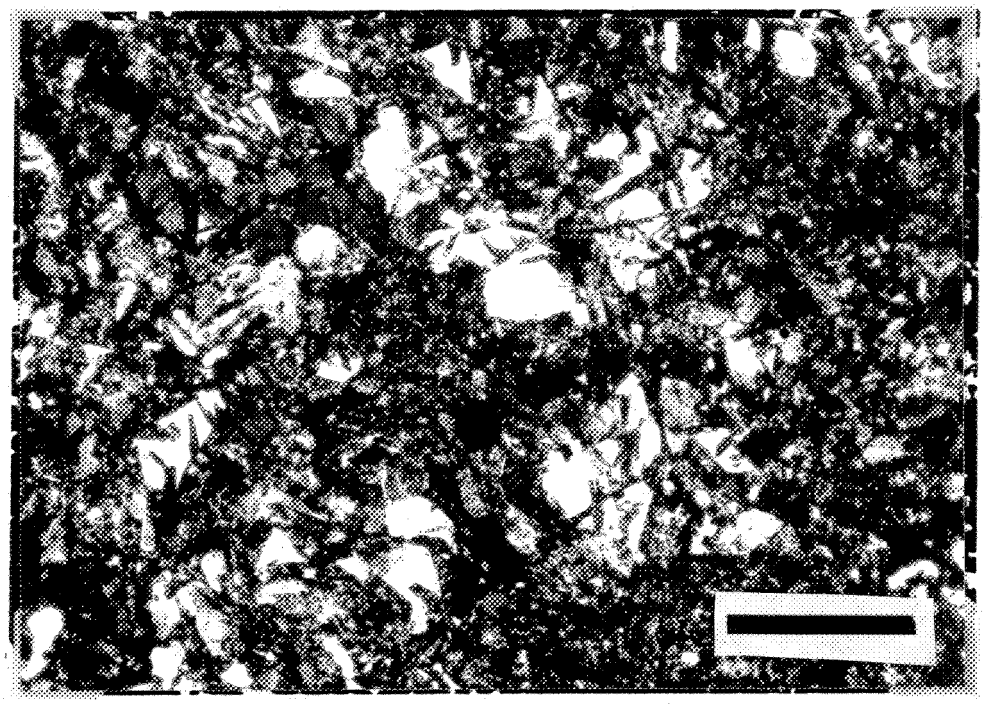

Plate 3: Trachytic texture observed near the massive - pillowed facies contact. (S3-18: plane light; bar = 0.25mm).

Texture trachytique observée près du contact faciès massif - faciès coussiné. (S3-18: lumière naturelle; barre = 0,25mm).

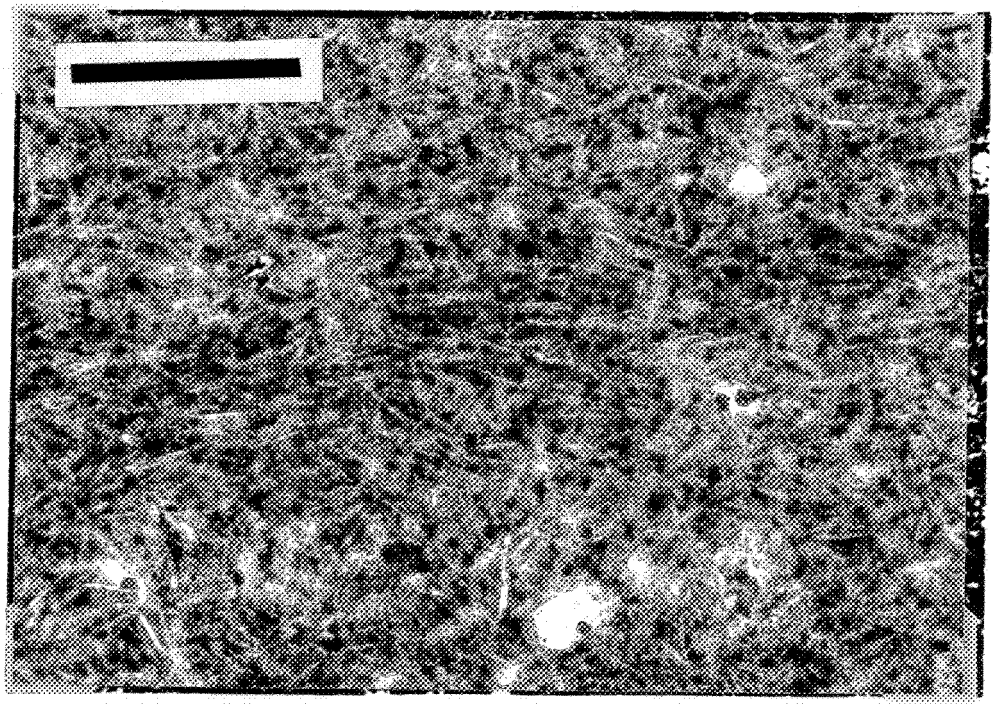

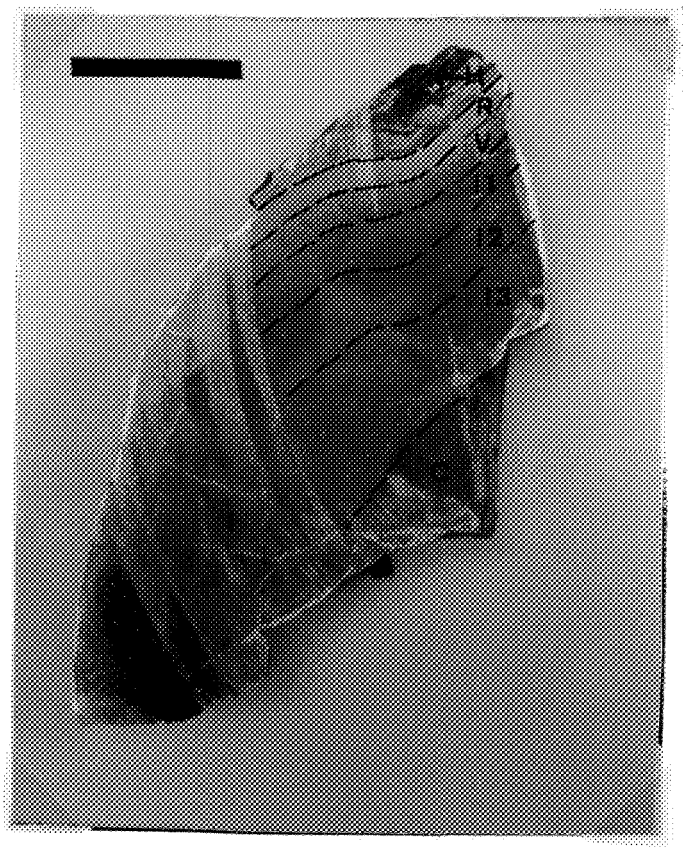

Plate 4: The textural zones sampled seen in handsample: H - hyaloclastite and glass rim; R - isolated to coalesced spherulite rim; V -vesicular zone; I 1-3 - microlitic interior zones; C - pillow centre.

Echantillon montrant les zones texturales échantillonées. H - bordure de hyaloclastite et de verre; R - bordure des sphérolites isolées à agglomérées; V - zone vacuolaire; I 1-3 - zones internes microlitiques; C - centre du coussin.

Plate 5: The banded texture observed in the interior zones of S4-P3.

Texture rubanée observée dans les zones internes de S4-P3.

appear to be simply irregular concentrations of FeTi-oxides in the mesostasis.

Five samples, S3-15 through S3-19, were taken in a 1.5 metre section approaching the exposed massive-pillowed facies contact (figure 5a). S3-15 is at 1.5 metres from the contact, followed by S3-16 at 1.2 metres, S3-17 and S3-19 at 1.0 metres, and S3-18 at the immediate contact. S3-15 resembles the samples from the centre of the flow, except that the texture is dominantly interstitial to isogranular, rather than sub-ophitic. In S3-16, S3-17 and S3-19 herring-bone quench clinopyroxene appear. Small hematite veins cut the three samples; S3-19 being more pervasively hematitized. While S3-18 exhibits the herring bone clinopyroxene, the 1% vesicles and the hematitization observed in the previous samples of this section, it is the only sample studied from the entire massive facies to possess a trachytic rather than pilotaxitic plagioclase microlite texture (plate 3).

PILLOWED BASALT

Five cross-sections were studied from the four pillows sampled. A single section was taken from each of S3-P3, S4-P3 and S4-P4; two cross-sections were studied from S4-P5. Three pillow centres, in addition to those of the four entire pillows studied, were sampled and analysed (S3-P2, S3-P4 and S4-P2).

As previously mentionned, the pillow cross-sections studied have been divided into zones on the basis of textural variation and physical possibility of separating of the zones for the purpose of geochemical analysis (plate 4). That is to say, that some textural zones, in particular the hyaloclastite and isolated spherulite zones, were grouped together for geochemical analysis due to the impossibility of manually separating them. The zones described herein are as follows: The hyaloclastite zone consisting of the glass rim of the pillows, including the zone of isolated crystallization spherulites; The spherulitic or rim zone, extending 0.5 cm below the hyaloclastite zone and consisting of semi-coalesced to coalesced crystallization spherulites. The vesicular zone, extending 1 cm below the spherulite zone, being characterized by vesicle trains and skeletal plagioclase microlites and clinopyroxene. The interior zone has been sub-divided into three to four sections: the first 2 centimetres of the interior zone has been designated I1, is increasingly microlitic toward the centre of the pillow and

is commonly trachytic. I2 consists of the succeeding 2 cm of the pillow interior and is commonly microlitic and pilotaxitic; the clinopyroxene in this zone is increasingly evident and skeletal in nature. I3 extends 4 cm from the base of I2; it too is microlitic and pilotaxitic, differing little texturally from I2 except in the degree of crystallinity, which increases toward the pillow centre. I4 was sampled in only one pillow and consists of the remainder of the sample (5cm) extending from the base of I3. In one case S4-P3, the interior zones were further sub-divided due the presence of an uncommon banded texture in the first 4 cm of the microlitic zone (plate 5). The final zone described and sampled for geochemical analysis is the centre of the pillows, each being a sample taken specifically from that section of the pillow.

THE HYALOCLASTITE

The hyaloclastite zones of the five pillow sections studied (plate 6) are composed predominantly of chloritized and epidotized fragments. Quartz and pumpellyite are also common, although less abundant. Fe-Ti oxides are ubiquitous in minor amounts. Carbonate occurs locally, and sericite is rare.

The fragments occur in-situ or with minor displacement. They are commonly mineralogically zoned, and in one case (S4-P5.2), banded. The zonation is further defined by oxide

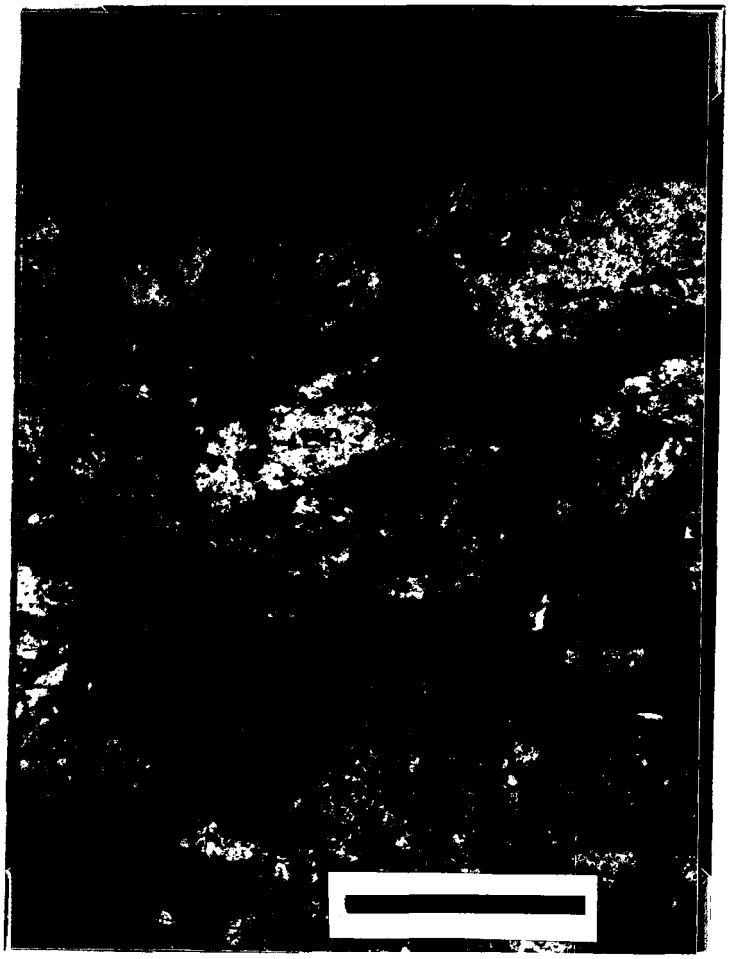

Plate 6: The general texture of the hyaloclastite zone. (example: S4-P3; CHL = chlorite; EP = epidote; plane light; bar = 1mm)

Texture générale de la zone de hyaloclastite. (exemple: S4-P3; CHL = chlorite; EP = épidote; lumière naturelle; barre = 1mm).

Plate 7: The general texture of the spherulitic rim. (example: S4-P3; IS = isolated spherulites; CS = coalesced spherulites; plane light; bar = 1mm).

Texture générale de la bordure sphérolitique. (exemple: S4-P3; IS - sphérolites isolées; CS = sphérolites agglomérées; lumière naturelle; barre = 1mm).

liesengang rings. Nebulous conchoidal fractures and bubble-wall shards were observed in one sample (S4-P5.1).

Chlorite pseudomorphs of 0.1mm olivine crystals and epidote ± carbonate pseudomorphs of 0.25mm plagioclase crystals constitute <1% of the hyaloclastite. Small 0.1mm quartz amygdules are rare. Crystallization and devitrification spherulites occur. The former increase in size and number toward the centres of the individual fragments and toward the pillow border; they are nucleated on small, 0.08 - 0.15mm plagioclase microlites. The devitrification spherulites are nucleated on fragment walls and along fractures within the fragments.

Quartz, chlorite, epidote, carbonate and minor oxides occur interstitial to the fragments. Carbonate, quartz and minor chlorite cement the hyaloclastite. Chlorite, carbonate, epidote, quartz, pumpellyite and locally hematite veins cut the hyaloclastite zones.

THE SPHERULITIC PILLOW RIM

The contacts between the hyaloclastite and the pillow rims of the five pillow sections studied are characterized by the presence of an oxide ± chlorite ± epidote rim. The pillow rims themselves are characterized by the transition from isolated to coalesced spherulites (plate 7). These spherulites, nucleated on plagioclase microlites and less commonly olivine crystals, range from 0.01mm to 0.25mm in

diameter, and from 5-10% of the rock at the hyaloclastite boundary to 60-90% at the Vesicular Zone boundary. The mineralogy of the spherulites could not be determined; two populations were observed: pale brown and dark red-brown. The former dominate near the hyaloclastite boundary; the latter, near the vesicular zone boundary. In one sample (S4-P5.2) the spherulites exhibit local carbonatization.

The plagioclase microlites in the pillow rim vary from 0.1-0.3mm in length, and from 1-2% at the hyaloclastite boundary to 10% at the vesicular zone boundary. They exhibit acicular to skeletal crystal forms, and in one case (S4-P5.1) a trachytic texture. Epidote - sericite - carbonate-quartz - pumpellyite - albite pseudomorphs of 0.4mm plagioclase laths make up ≤1% of the rock, while chlorite-quartz - carbonate - epidote pseudomorphs of 0.15mm olivine crystals constitute 1-2%.

Chlorite is the most common interstitial mineral in the pillow rim, followed by carbonate and epidote. Quartz occurs in minor amounts, as do oxides. In two cases (S4-P4 and SP5.1), epidote - oxide agglomerates up to 0.7mm in size make up ≤1% of the rock. Amygdules are 0.1mm in diameter, quartz - chlorite - carbonate - epidote filled and ≤2% of the rock. Quartz - chlorite - carbonate ± epidote veins cut the pillow rim; hematite and stilpnomelane also occur in veins.

THE VESICULAR ZONE

The vesicular zones of the five pillow sections are characterized by vesicle trains perpendicular to the pillow surface (plate 8). These vesicles are 2-5mm in length, filled with carbonate - chlorite - quartz ± epidote, and constitute 3-7% of this zone. A second population of vesicles, 0.25mm in diameter, are also quartz - carbonate-chlorite ± epidote filled; they make up ≤2% of the zone.

The rock in the vesicular zone is composed of poorly trachytic to trachytic plagioclase microlites in a fibrous clinopyroxene matrix. The microlites exhibit skeletal crystal forms, and are commonly sericitized and epidotized. They increase in abundance from 10% of the rock at the pillow rim boundary to 25-30% at the interior boundary.

Chlorite - quartz - carbonate ± epidote pseudomorphs of 0.15mm olivine crystals make up 1-3% of the vesicular zone; epidote - sericite - quartz - albite - carbonate-pumpellyite - chlorite pseudomorphs of 0.2-0.8mm plagioclase crystals being <1%. Very rare 1.5mm and 4.5mm plagioclase pseudomorphs were also observed (S4-P5.1 and S4-P4, respectively).

Chlorite is the most common mineral interstitial to the clinopyroxene of the matrix, followed by carbonate and epidote; oxides occur in minor amounts. Epidote and oxides also occur together in small 0.1mm agglomerates. These agglomerates commonly make up <1% of the vesicular zone,

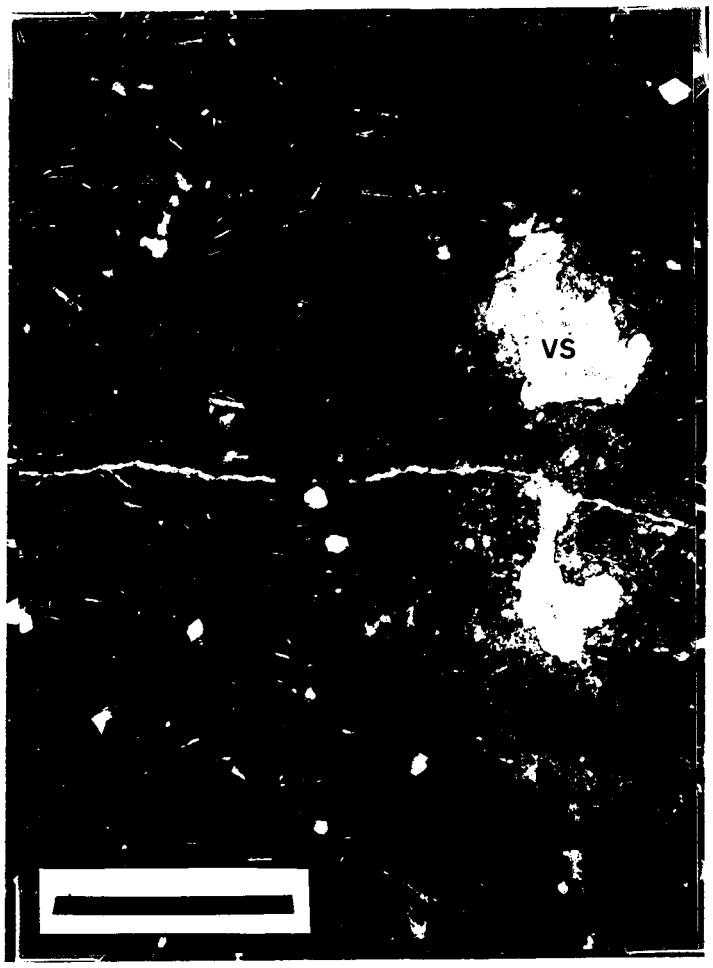

Plate 8: The general texture of the vesicular zone. (example: S4-P3; VS = vesicule train; plane light; bar = 1mm).

Texture générale de la zone vacuolaire. (exemple: S4-P3; VS = trainée de vacuole; lumière naturelle; barre = 1mm).

except in the case of S4-P5.1, where they attain dimensions of 0.3mm and abundances of 3% of the rock.

Quartz - chlorite - carbonate ± epidote and minor Fe-Ti oxide veins cut the vesicular zone.

THE INTERIOR (I1) ZONE
(and I2 of S4-P3)

The interior (I1) of four of the five pillow sections studied is 2cm in width. In the fifth sample (S4-P3), this zone was subdivided in two 1cm zones (I1 and I2) in order to better delineate the banded zone observed.

All the samples are composed of 20-35%, 0.1-0.3mm, epidotized, skeletal plagioclase microlites in a skeletal clinopyroxene matrix. They generally exhibit poorly trachytic to pilotaxitic textures; S4-P5.1 and P5.2 are the exceptions, exhibiting well-developed trachyitic textures (plate 9). Both samples from S4-P3 are pilotaxitic. The I2 zone, approaching the banded texture of the interior I3, is characterized by a slight decrease in abundance of plagioclase microlites (plate 10).

Carbonate - chlorite - epidote - quartz and oxides occur as minor constituents of the matrix. Epidote and oxide occur as up to 0.2-0.5mm agglomerates, and constitute <1% of the rock, except in S4-P5.1 where they attain up to 5%. Quartz-chlorite - carbonate - epidote pseudomorphs of 0.1-0.3mm olivine crystals make up 1-3% of the I1 zone; epidote -

Plate 9: The general texture of the Interior (I1) zone.
a) S3-P3; pilotaxitic texture; plane light; bar = 0.5mm.
b) S4-P5.1; trachytic texture; plane light; bar = 0.5mm.

Texture générale de la zone interne (I1).
a) S3-P3; texture pilotaxitique; lumière naturelle; barre = 0,5mm.
b) S4-P5.1; texture trachytique; lumière naturelle; barre = 0,5mm.

Plate 10: Texture of Interior (I1 and I2) zones of S4-P3.
a) microlitic, pilotaxitic texture of I1 (plane light; bar = 1mm).
b) decrease in plagioclase microlite developement in I2 (banded structure; plane light; bar = 1mm).

Textures des zones internes (I1 and I2) dans S4-P3.
a) texture microlitique, pilotaxitique dans I1 (lumière naturelle; barre = 1mm).
b) diminution du développement des microlites de plagioclase dans la zone I2 (structure rubanée; lumière naturelle; barre = 1mm).

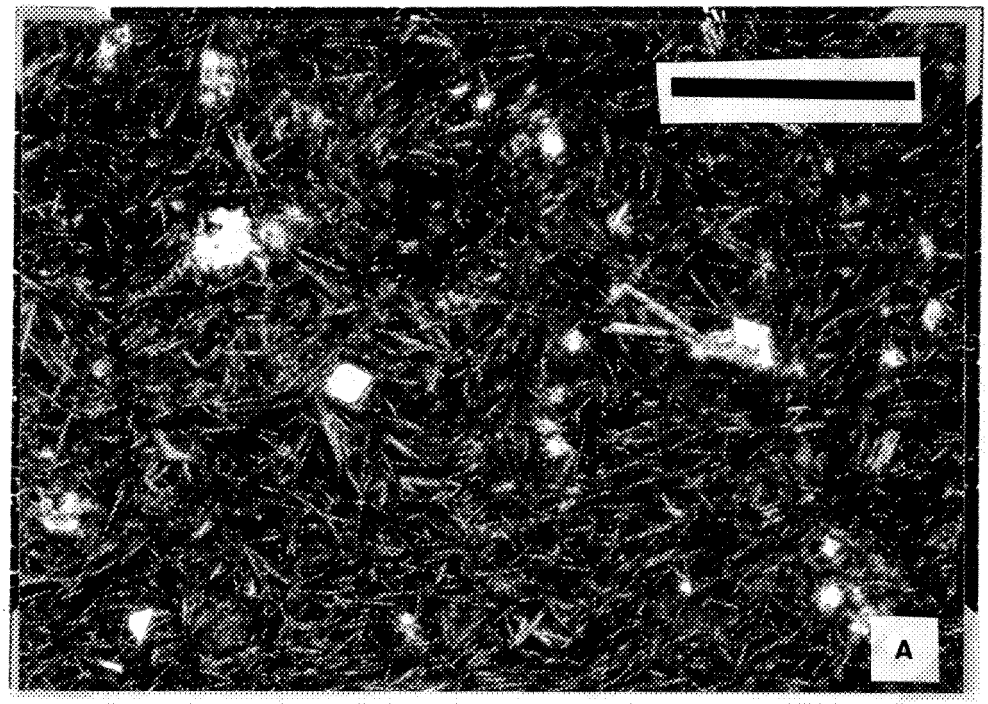

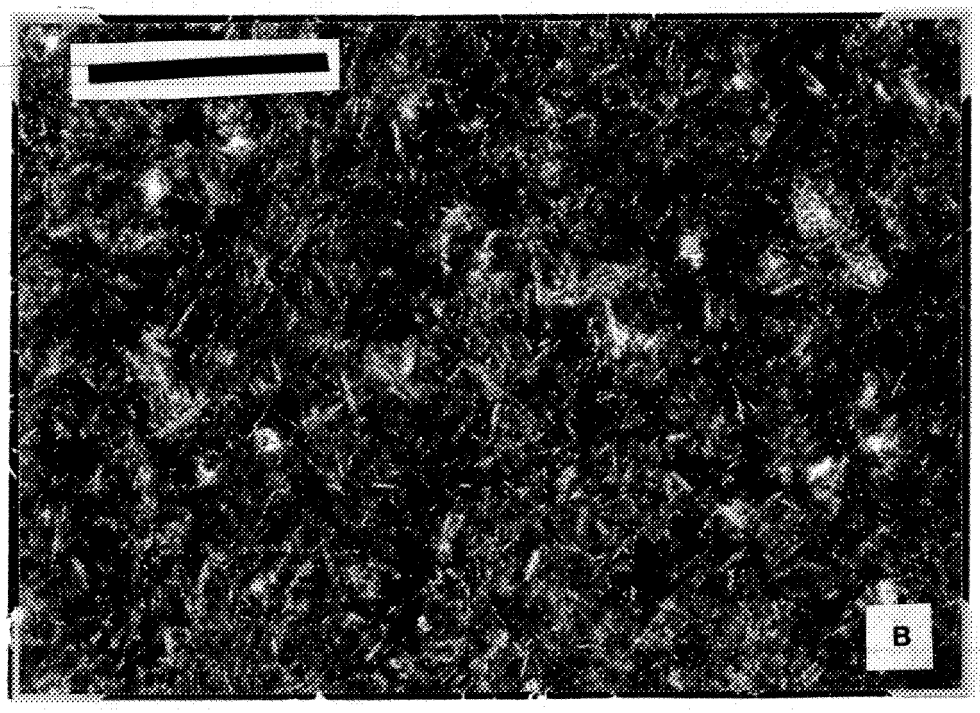

quartz - carbonate - pumpellyite - chlorite - plagioclase pseudomorphs of 0.3-0.5mm plagioclase crystals, 1%. In both the S4-P3 samples, the plagioclase crystals are acicular rather than lath-shaped as in the other samples. A single 2mm plagioclase pseudomorph was observed in S4-P5.1.

Amygdules commonly make up 1% of the interior (I1) zone, are 0.2-0.4mm in diameter and are carbonate - chlorite - epidote - quartz filled. Segregation vesicles (Baragar et al. 1977) occur in all samples, except S4-P3. These 0.3-0.5mm vesicles are composed of skeletal clinopyroxene and exhibit central amygdules (plate 11a).

Quartz - carbonate - epidote - chlorite - pumpellyite veins with minor hematite and stilpnomelane cut the interior (I1) zone.

THE INTERIOR (I2) ZONE
(I3 of S4-P3)

The interior (I2) zone (I3 of S4-P3) is 2cm in width. In S4-P3, this zone (I3) is a single band of the banded structure previously mentionned.

The interior (I2) zone resembles the interior (I1) zone with minor exceptions (plate 12). The plagioclase microlites are slightly more abundant than in I1, up to 40% of the rock; they commonly exhibit a pilotaxitic texture, or in the case of S4-P5.1 and P5.2 an increasingly convoluted trachytic texture. The interstitial clinopyroxene is generally

Plate 11: a) Segregation vesicle exhibiting a central amygdule. (Interior (I1) zone S3-P3; plane light; bar = 0.25mm).
and b) filled segregation vesicles (Interior (I2) zone S3-P3; plane light; bar = 0.25mm).

a) Vacuole de ségrégation avec une amygdale au centre. (zone interne (I1) de S3-P3; lumière naturelle; barre = 0,25mm).
et b) vacuoles de ségrégation. (zone interne (I2) de S3-P3; lumière naturelle; bar = 0.25mm).

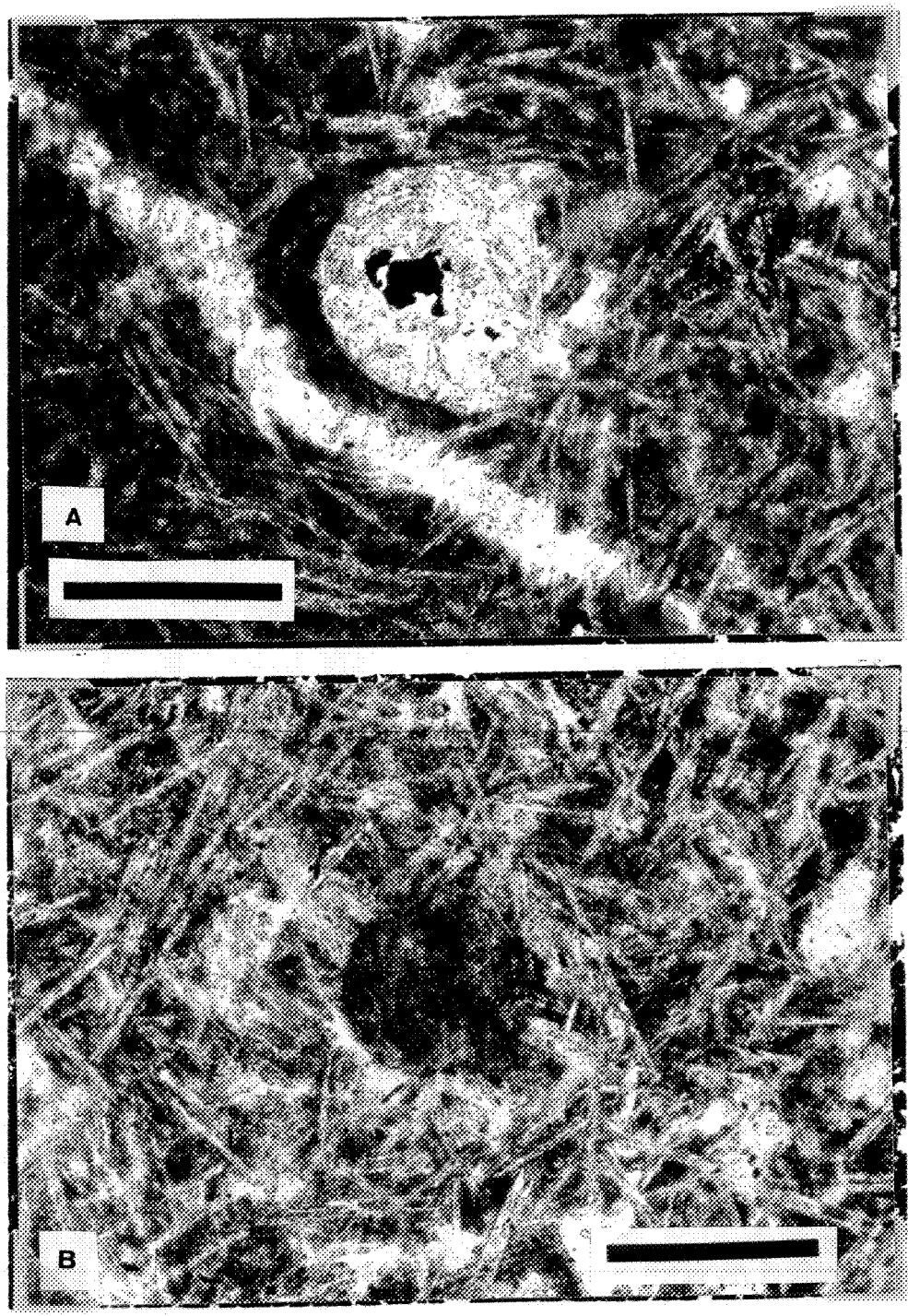

Plate 12: The general texture of the Interior (I2) zone.
a) microlitic, pilotaxitic (S3-P3; plane light; bar = 0.5mm).
b) microlitic, trachytic texture (S4-P5.1; plane light; bar = 1mm).

Texture générale de la zone interne (I2).
a) texture microlitique, pilotaxitique (S3-P3; lumière naturelle; barre = 0,5mm).
b) texture microlitique, trachytique (S4-P5.1; lumière naturelle; barre = 1mm).

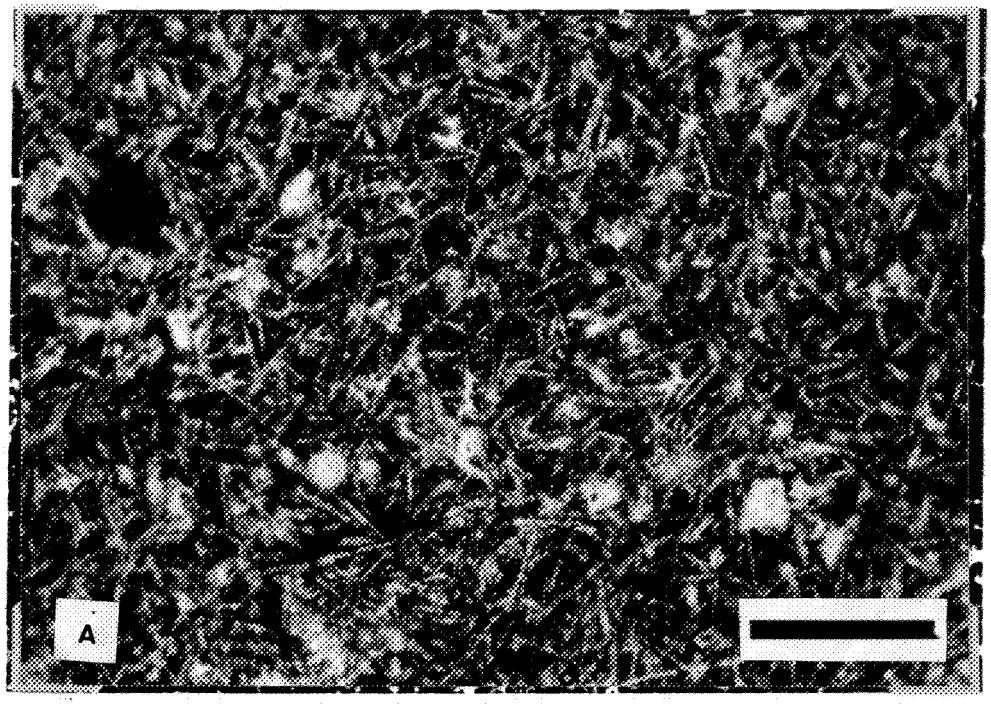

skeletal, except in S3-P3 and S4-P3, where it occurs locally as xenomorphic grains. No differences between the interior zones I1 and I2 were observed in accessory minerals in the matrix, nor in the size and percentages of olivine and plagioclase pseudomorphs. The epidote - oxide agglomerates are larger, 0.5-0.8mm, in S4-P3, where they occur concentrated in thin zones parallel to the pillow border (i.e. parallel to the banding). This being the only variation unique to S4-P3 it is interpreted as being the cause of the banded structure visible in handsample.

While the amygdules do not vary in size and abundance between I1 and I2, the segregation vesicle containing central amygdules become wider, 0.5-0.7mm, and locally filled segregation vesicles up to 0.4mm in diameter occur (plate 11b). Such vesicles are not observed in S4-P3.

Veins cutting the I2 zone are commonly filled with quartz - carbonate - epidote - chlorite, less commonly pumpellyite, and rare sericite and hematite.

THE INTERIOR (I3) ZONE
(I4 and I5 of S4-P3; and I4 of S4-P5.2)

The interior (I3) zones of S3-P3, S4-P4, S4-P5.1 and S4-P5.2 extends 4cm below the I2 zone. In S4-P5.2 a fourth interior zone (I4), extending 5cm below I3, was sampled, and in S4-P3, this zone was subdivided into a 2cm zone (I4) and a succeeding 4cm zone (I5).

Again, this zone differs little from the previous interior zones (plate 13). The plagioclase microlites exhibit a pilotaxitic texture, except in S4-P3 (I4), where they are poorly trachytic, and in S4-P5.1, where the trachytic texture is convoluted. The interstitial clinopyroxene becomes increasingly granular in nature, although skeletal crystals are still most common. In S4-P4 and S4-P3 (I5), the rock is locally sub-ophitic. No variation in minor matrix mineralogy is observed, and the increase in size and abundance of epidote - oxide agglomerates, which characterized the S4-P3 banded structure (I3), is not evident in S4-P3 (I4 and I5).

The size and abundance of olivine and plagioclase crystal pseudomorphs is constant. However, the olivine crystal forms are better preserved; skeletal crystals being recognizable.

Amygdules exhibit no variation from the previous zones; nor do the segregation vesicles described above. Veins in the I3 zone are composed of epidote - carbonate - chlorite-quartz, and locally pumpellyite and hematite.

Plate 13: The general texture of the Interior (I3) zone. (example: S3-P3; plane light; bar = 1mm).

Texture générale de la zone interne (I3). (exemple: S3-P3; lumière naturelle; barre = 1mm).

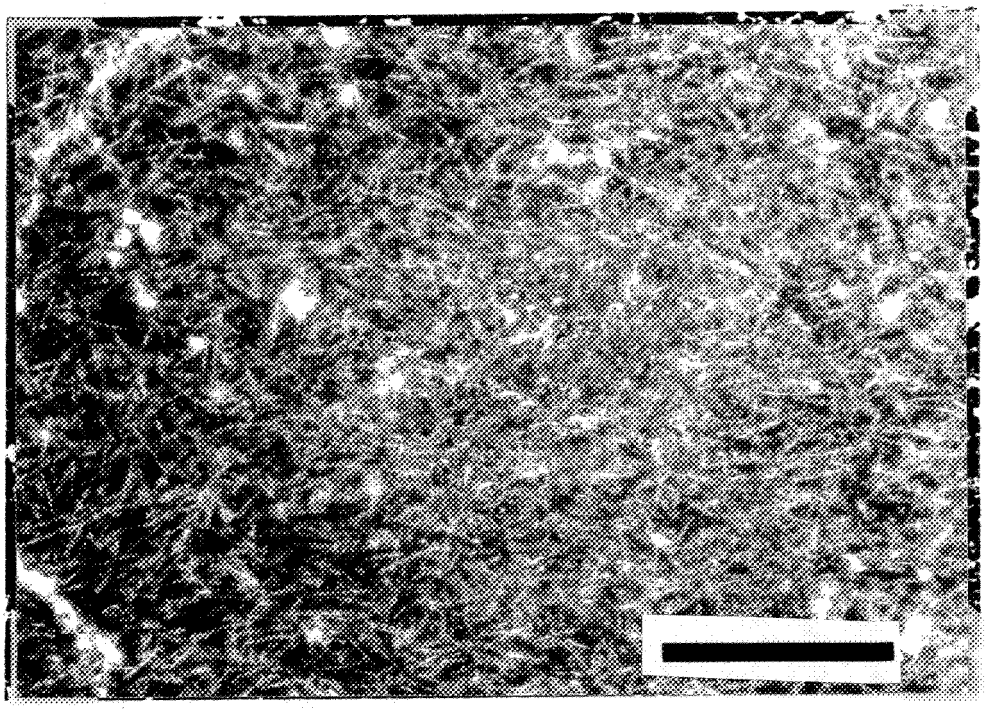

Plate 14: The general texture of the pillow centres. (example: S3-P3; plane light; bar = 0.5mm).

Texture générale des centres de coussins. (exemple: S3-P3; lumière naturelle; barre = 0,5mm).

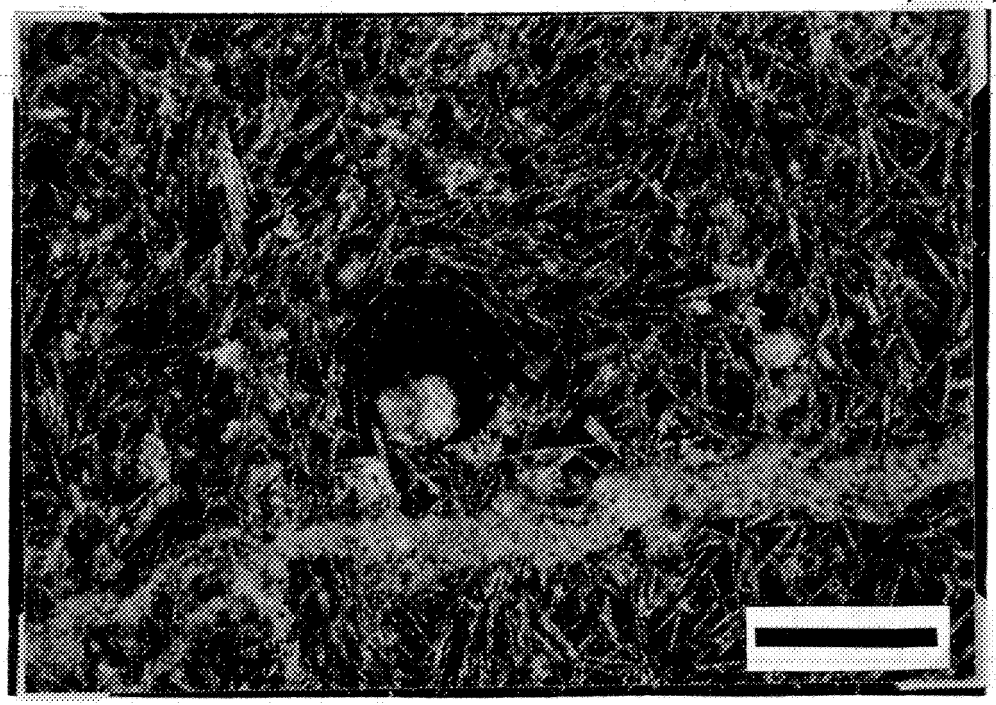

THE PILLOW CENTRE

The seven pillow centres studied are composed of 20-30% plagioclase microlites in a clinopyroxene matrix. The microlites range in length from 0.2-0.5mm and commonly exhibit a pilotaxitic texture, except in the cases of S3-P3 and S4-P3 where the microlites are trachytic and poorly trachytic, respectively. The clinopyroxene is commonly skeletal in nature, although acicular and granular forms do occur (S4-P4 and S3-P4). In these latter cases, the overall texture of the rock is intergranular to subophitic. Chlorite, quartz and clinozoisite are the dominant minerals interstitial to the plagioclase--clinopyroxene; pumpellyite, oxides and carbonate are rare (<1%). Carbonate content, however, varies, being higher in S4-P5 and S4-P2. Epidote-oxide agglomerates are very rare in the pillow centres (<1%).

Chlorite - carbonate - quartz ± epidote ± pumpellyite pseudomorphs of 0.2-0.4mm olivine crystals constitute 1-3% of the pillow centres; epidote - carbonate - quartz-pumpellyite - chlorite pseudomorphs of 0.3-0.5mm plagioclase laths, <1%. Rare 1.5mm epidote - pumpellyite pseudomorphs of plagioclase also occur (S4-P4 and S3-P4).

Amygdules are 0.1-0.3mm in diameter, make up <1% of the pillow centres and are carbonate - quartz ± epidote filled. In two cases (S3-P3 and S4-P5), segregation vesicles with central amygdules, as observed in the interior zones, occur.

Epidote - carbonate - chlorite - quartz and minor hematite veins cut the pillow centres.

GEOCHEMISTRY

The chemical variations observed in basalt pillow cross-sections, both recent (Scott and Hajash 1976, Hart 1970, Cann 1969, Andrews 1977, Ludden and Thompson 1979, Baragar et al. 1977) and ancient (Baragar et al. 1979, Mellinger 1976, Ludden et al. 1982, Bartley, 1986), are well documented, as are the textural variations observed in both ages (Kirkpatrick 1978, Natland 1978 and 1980, Dimroth and Lichlblau 1979). Rarely, however, have attempts been made to associate these two phenomena (Humphris et al. 1978). Here, the chemical variations have been defined for individual textural zones in order to determine the association between the texture and the subsequent alteration.

To define the gains and losses of individual elements within the textural zones of a pillow, the parent composition must first be known. Within an individual pillow, the microlitic centre is assumed to be the least affected by water - rock interaction (halmolysis or hydrothermal), as it is the least accessible. However, some doubt exists as to the "unaltered" nature of pillow centres (Hart 1970 after Paster 1968, Scott and Hajash 1976). Therefore, the pillow centres of this study were compared, individually and as an average, to the massive facies of the flow, which is, in turn, considered to be the least altered facies of an individual flow.

First, however, the average composition of the massive Archean basalt has been compared to average compositions of

recent basalts of the same affinity. The purpose of such a comparison is to determine to what extent comparisons between present-day processes and Archean processes are valid.

MASSIVE BASALT

Ten samples of the nineteen massive basalt samples collected were analysed for major elements (Annexe 1: Table I); five of these were further analysed for trace and rare earth elements (Annexe 1: Table II). The average of the analyses was calculated for use in the comparisons with the pillow analyses (Annexe 1: Tables I and II).

Plotting of the data on Alkali vs. Silica and Nepheline - Olivine - Quartz diagrams (figure 7), shows the flow to indeed be sub-alkaline. AFM, FeO/MgO vs. SiO_2, and Al_2O_3 vs Anorthite diagrams (figure 8) exhibit the tholeiitic affinity of the flow. The massive basalt samples have flat, non-fractionated (Schilling and Winchester 1967), 10x chondrite REE patterns (figure 9).

The average major element analysis of the flow was compared to average tholeiite analyses (Nockolds et al. 1979, Cox et al. 1979). The Fortran program SOMA (Appleyard and de Beer 1982) available on the Université du Québec mainframe CYBER was used to calculate the variations between the Archean and Recent lavas (figure 10). The program SOMA calculates the change in rock composition due to metasomatism using the metasomatic equations of Poldervaart (1953) and Gresens (1967). The program assumes that the variations

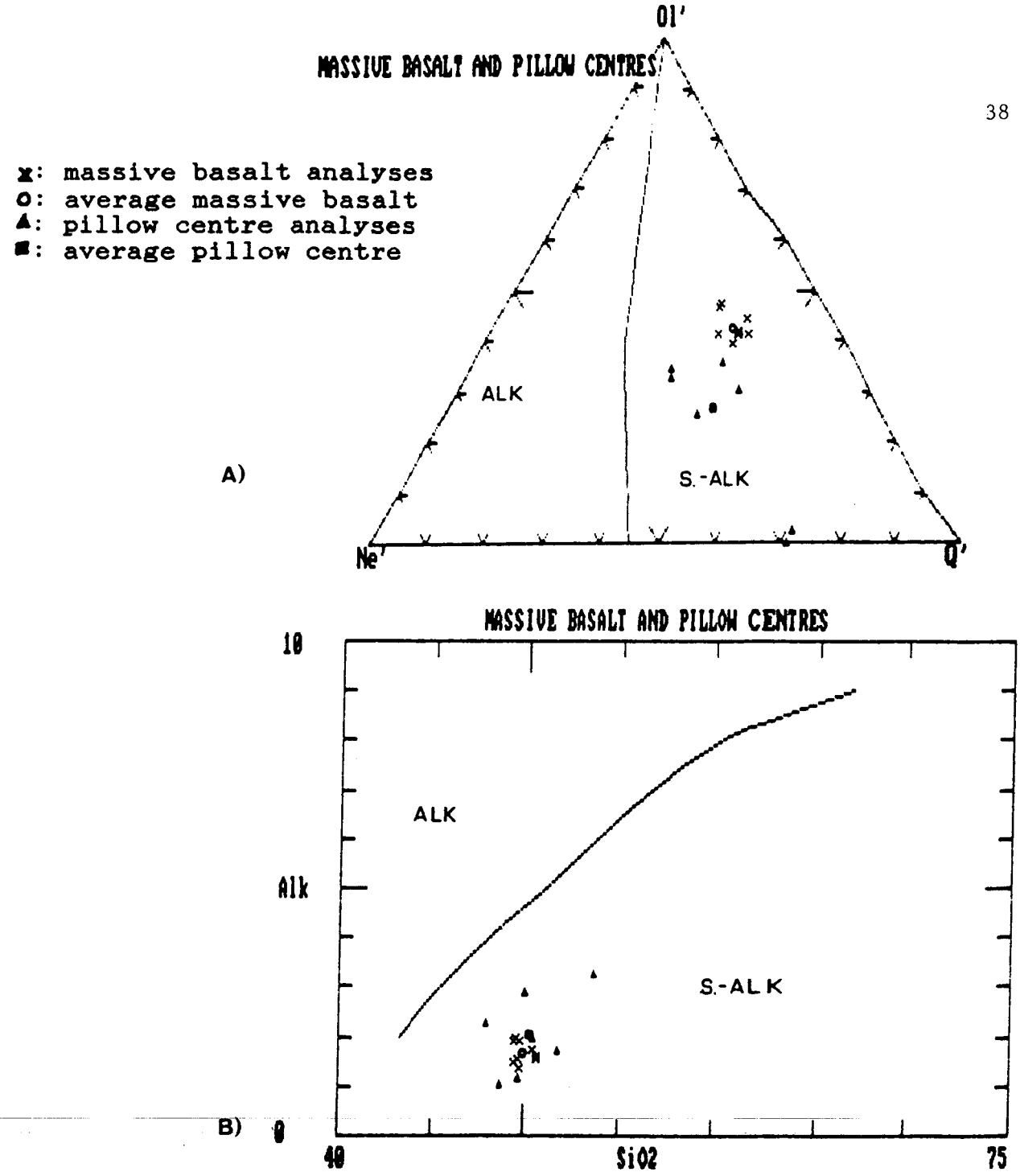

Figure 7: Alkaline versus sub-alkaline differentiation diagrams (Carr 1987 after Irvine and Baragar 1971).
a) normative nepheline - olivine - quartz
b) alkalis versus silica

Diagrammes de différenciation entre les affinités alcalines et sub-alcalines (Carr 1987 d'après Irvine et Baragar 1971).
a) néphéline - olivine - quartz normatifs
b) alcalis versus silice

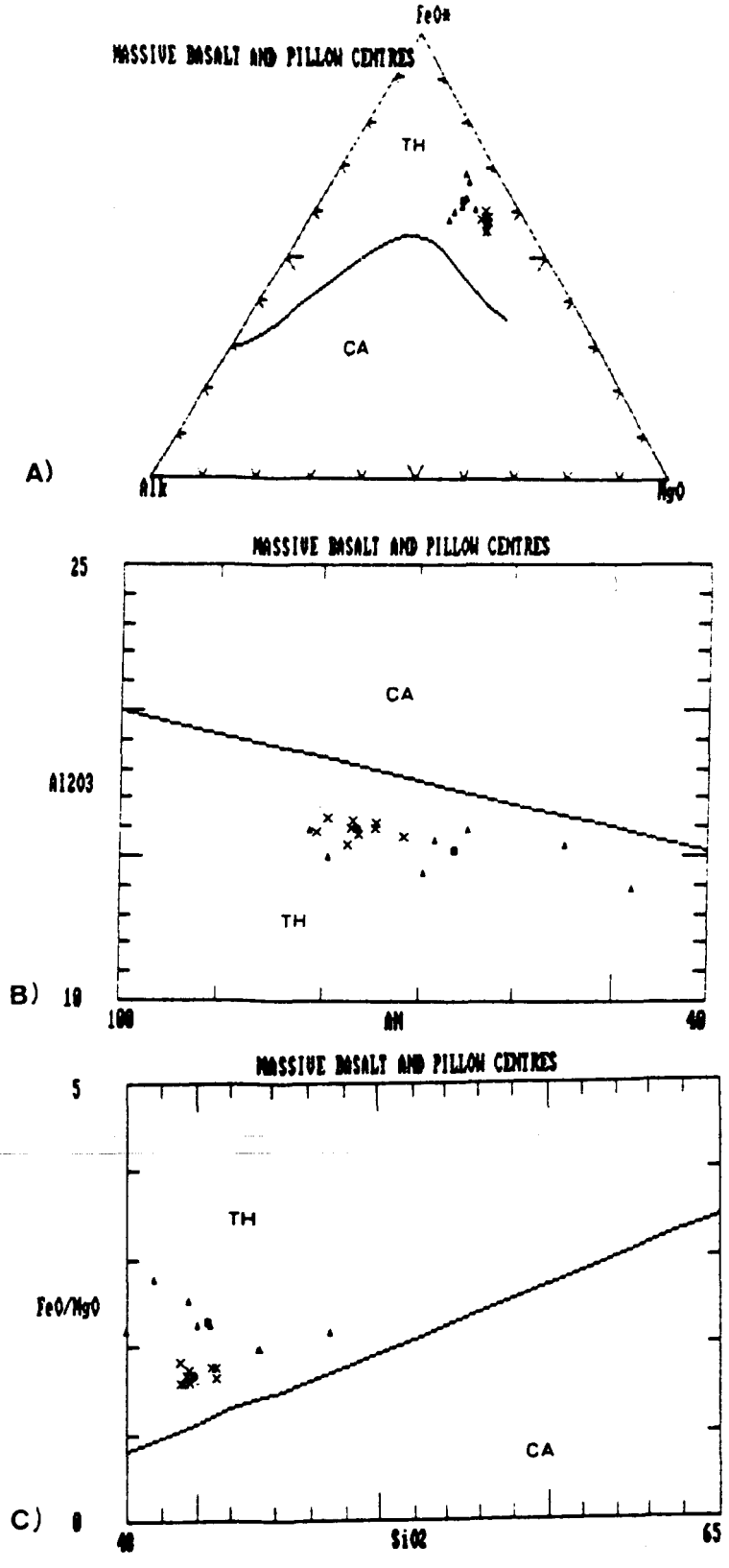

Figure 8: Tholeiitic versus calc-alkaline differentiation diagrams (Carr 1987: a) and b) after Irvine and Baragar (1971), and c) after Miyashiro (1974)).
a) AFM diagram
b) Aluminum versus normative anorthite
c) FeO/MgO versus SiO2

(symbols are the same as figure 7)

Diagrammes de différenciation entre les affinités tholéiitique et calco-alcaline (Carr 1987: a) et b) d'après Irvine et Baragar (1971), et c) d'après Miyashiro (1974)).
a) Diagramme AFM
b) Al_2O_3 versus anorthite normative
c) FeO/MgO versus SiO2

(les symboles sont les même qu'à la figure 7)

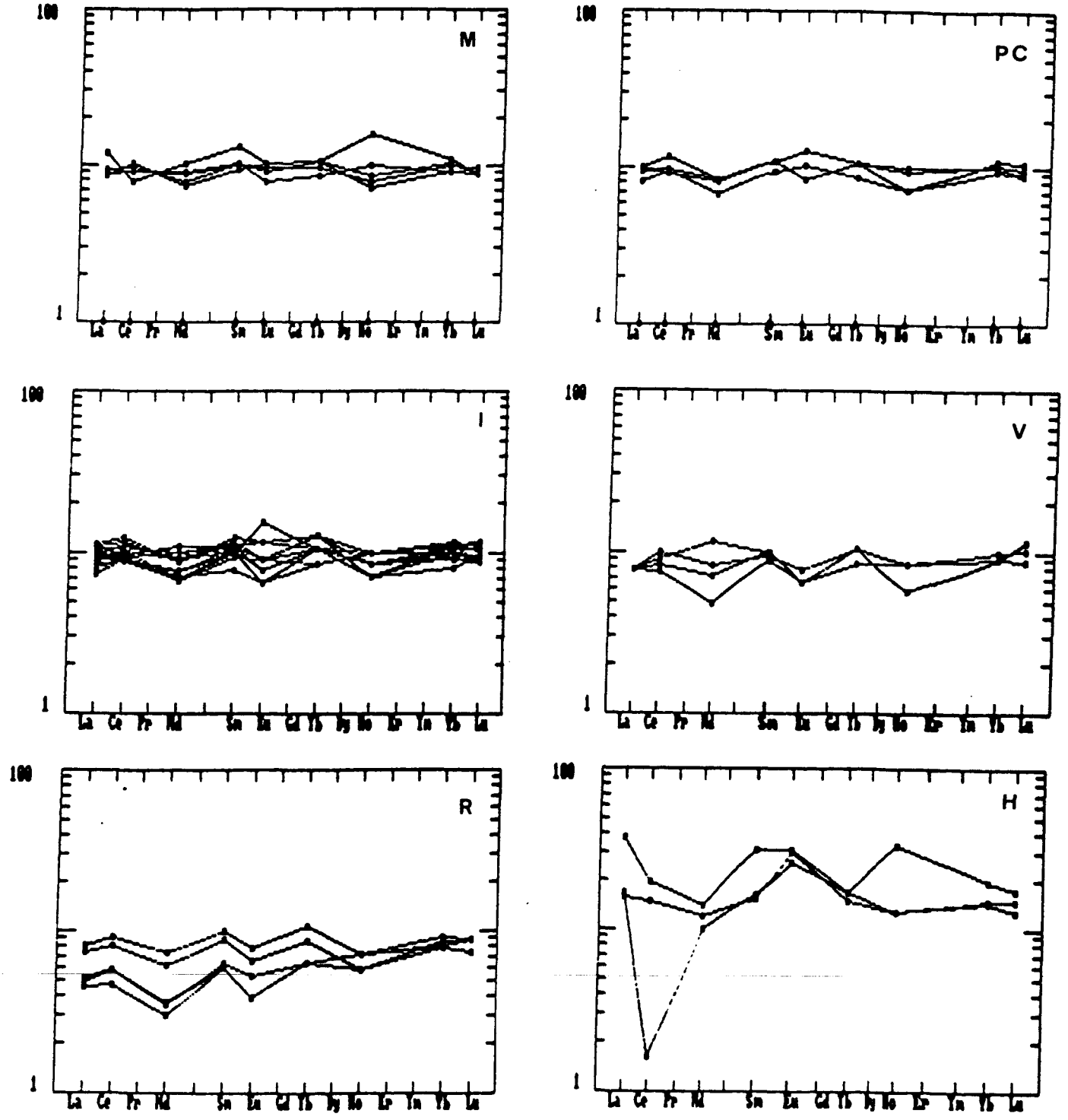

Figure 9: REE patterns for the massive basalts samples and the pillow cross sections.
M - massive basalt; PC - pillow centre; I - interior zones; V - vesicular zone; R - spherulitic rim; and H- hyaloclastite.

Diagrammes des élements des terres rares pour le basalte massif et les sections des coussins.
M - basalte massif; PC - centre des coussins; I - zone interne; V - zone vacuolaire; R - bordure sphérolitique; et H - hyaloclastite.

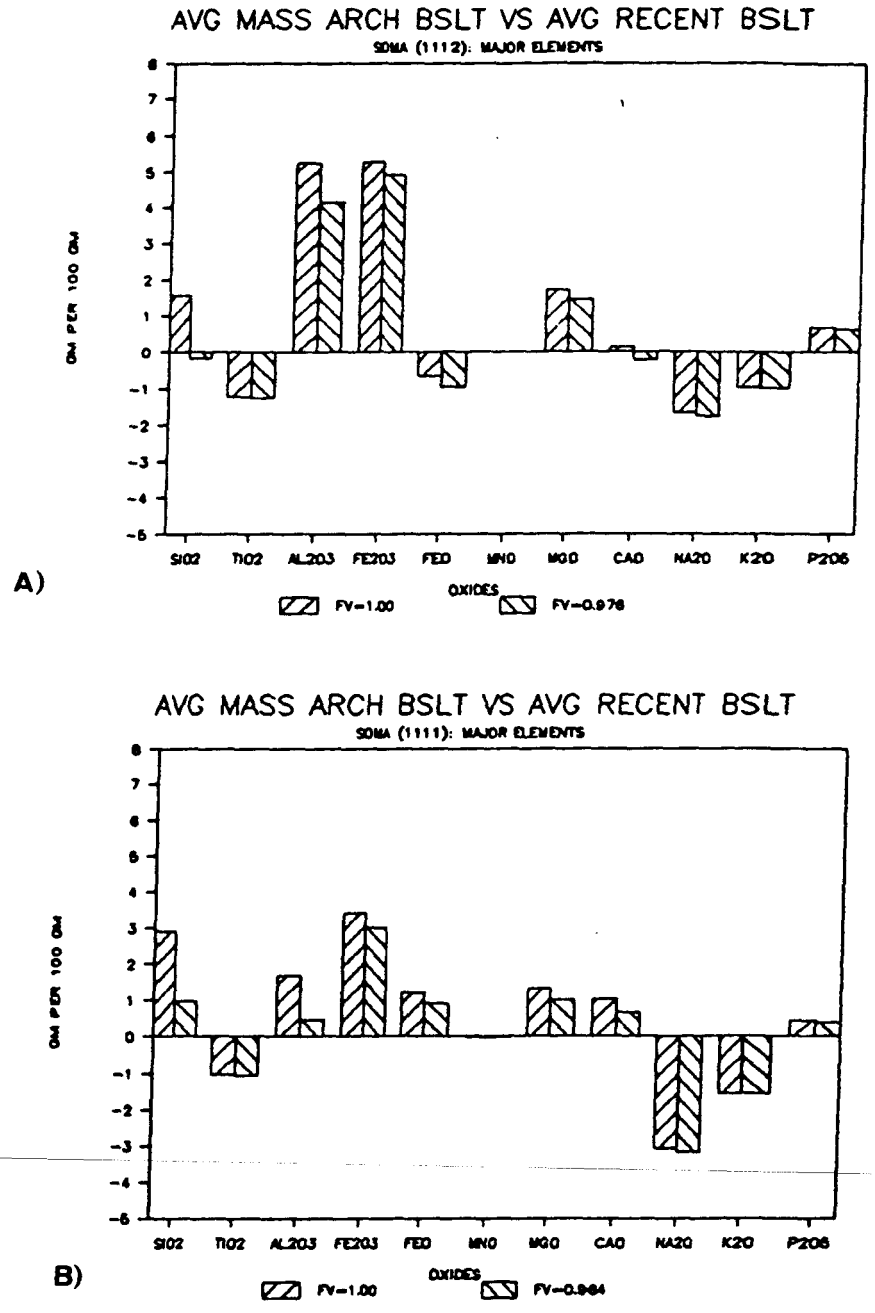

Figure 10: SOMA diagrams exhibiting chemical variations between Kinojevis and Recent basalts.
a) analysis from Nockolds et al. (1979).
b) analysis from Cox et al. (1979).

Diagrammes du logiciel SOMA montrant les variations chimiques entre les basaltes du Kinojévis et les basaltes récents.
a) analyses de Nockolds et al. (1979)
b) analyses de Cox et al. (1979)

defined are entirely due to alteration. The recent basalt was designated as the original rock in both cases, the Archean basalt being the resulting rock. The program was run twice, the first case assumes that there would be no change in volume in producing the Archean basalt from the recent. The second case calculates the change in volume on the basis of the least mobile elements defined by the program. Figure 10 shows that, with the exception of SiO_2 and Al_2O_3, the difference in gains and losses calculated with or without a volume change are very small. The overall difference between the recent basalts and the Archean basalt is, however, large (figure 10 and Table 1). The regional metamorphism of the Archean basalt to prehnite--pumpellyite facies may account for some of the variations, but the fact that Archean tholeiites need not be equivalent to the recent tholeiites, either in that the average analyses taken from the texts do not represent Kinojevis tholeiites or that the chemistry of Archean tholeiites fundamentally differs from the recent, must not be ignored.

Diagrams commonly used to define tectonic affinities of basalts show the problems associated with the assumption that Archean lavas can be successfully compared to Recent lavas. On a Mullen (1983) diagram (figure 11a), the flow falls within the calc-alkaline basalt field; whereas on the Pearce and Cann (1973) diagrams (figure 11b and c), the data falls in the ocean-floor basalt field and along the ocean-floor basalt - island arc tholeiite boundary for Zr - Ti/100 - Sr/2 (figure 11b), and in the ocean-floor - island arc - calc-

alkaline basalt field for Zr - Ti/100 - Yx3 (figure 11c). The ambiguity of the Zr - Ti/100 - Yx3 diagram and the discrepencies between the Mullen (1983) and the Pearce and Cann (1973) diagrams calls into question the validity of using of such diagrams for Archean rocks.

Table 1: Variations in major element chemistry of the average massive Kinojevis basalt compared to average recent tholeiitic basalt analyses.

Variations de la moyenne des éléments majeurs des basaltes massifs du Kinojevis comparée à celle des basaltes récents tholéiitiques.

Average Kinojevis basalt vs. Average Recent basalt

	++	+	=	-	--	+/-
COX ET AL (1980)	Al2O3 Fe2O3	MgO P2O5	MnO	TiO2 FeO Na2O K2O		SiO2 CaO
Nockolds et al (1979)	Fe2O3	SiO2 Al2O3 FeO MgO CaO P2O5	MnO	TiO2 K2O	Na2O	

++ highly enriched + enriched = constant
-- highly depleted - depleted +/- erratic

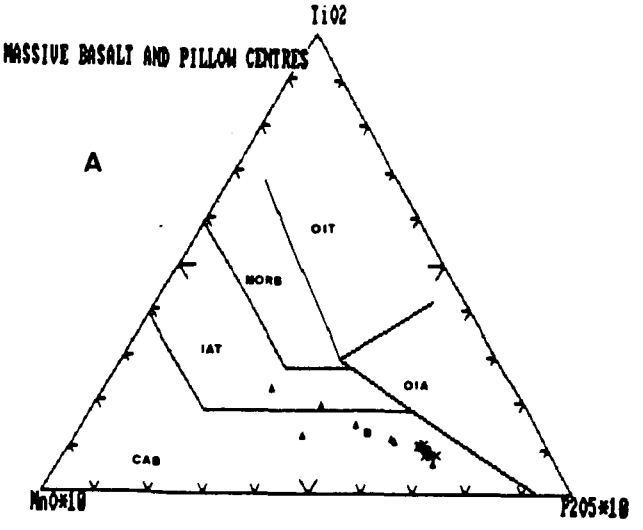

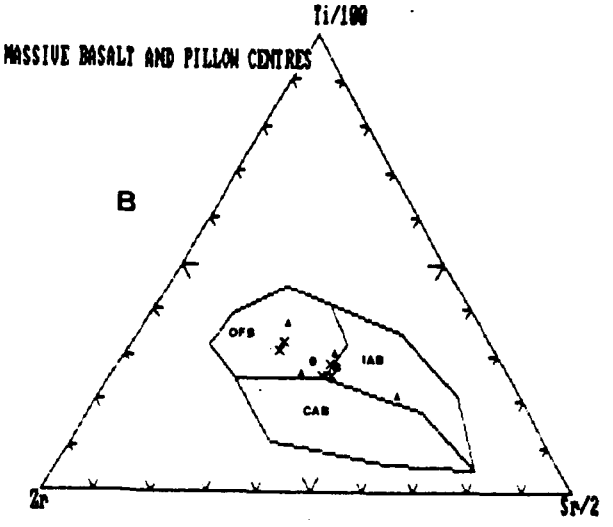

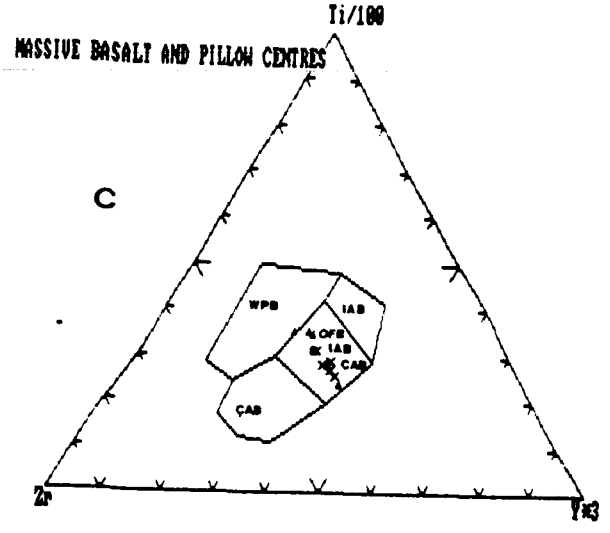

Figure 11: a) Massive basalt and pillow centre analyses, and their averages plotted on a Mullen (1983) MnOx10 - TiO_2 - P_2O_5x10 discrimination diagram.

b) Massive basalt and pillow centre analyses, and their averages plotted on a Pearce and Cann (1973) Zr - Ti/100 - Sr/2 discrimination diagram.

c) Massive basalt and pillow centre analyses, and their averages plotted on a Pearce and Cann (1973) Zr - Ti/100 - Yx3 discrimination diagram.

(symbols are the same as figure 7)

a) Analyses des basaltes massifs et des centres de coussins, et leurs moyennes sur un diagramme MnOx10 - TiO_2 - P_2O_5x10 de Mullen (1983).

b) Analyses des basaltes massifs et des centres de coussins, et leurs moyennes sur un diagramme Zr - Ti/100 - Sr/2 de Pearce and Cann (1973).

c) Analyses des basaltes massifs et des centres de coussins, et leurs moyennes sur un diagramme Zr - Ti/100 - Yx3 de Pearce and Cann (1973).

(Les symboles sont les mêmes qu'à la figure 7)

PILLOW CENTRES VS. MASSIVE BASALT

Seven pillow centre samples were analysed for major elements (Annexe 1: Table III), and four were analysed for trace and REE elements (Annexe 1: Table IV). The average of the analyses was calculated (Annexe 1: Tables III and IV) for use in the comparisons with the average massive basalt analysis.

The Oxide vs SiO_2 diagrams (figure 12 a-k) show that the pillow centre analyses have a much greater scatter than the massive basalt analyses for the major elements. The averages of the two types of analyses, however, exhibit relatively close correspondance. Treatment of the average analyses using the program SOMA (figure 13a), considering the average massive basalt analysis as the parent and the average pillow centre analysis as the daughter, show that the pillow centre is depleted in Al_2O_3, MgO, FeO, K_2O and P_2O_5; and enriched in Fe_2O_3, CaO and Na_2O (Table 2).

The Trace Element vs SiO_2 diagrams (figure 14 a-s) exhibit that the scatter of certain elements (Cu, Ba, Ni, Rb, Cs and Nb) is greater for the massive basalt than for the pillow centre. In fact, the obvious scatter of the pillow centres observed in the diagrams is due to the variation in SiO_2; the scatter of trace element abundances being more restrained than that of the major elements. The average pillow centre and massive basalt analyses exhibit good correspondance. The results of the SOMA analysis of the pillow centre average compared to the average massive basalt

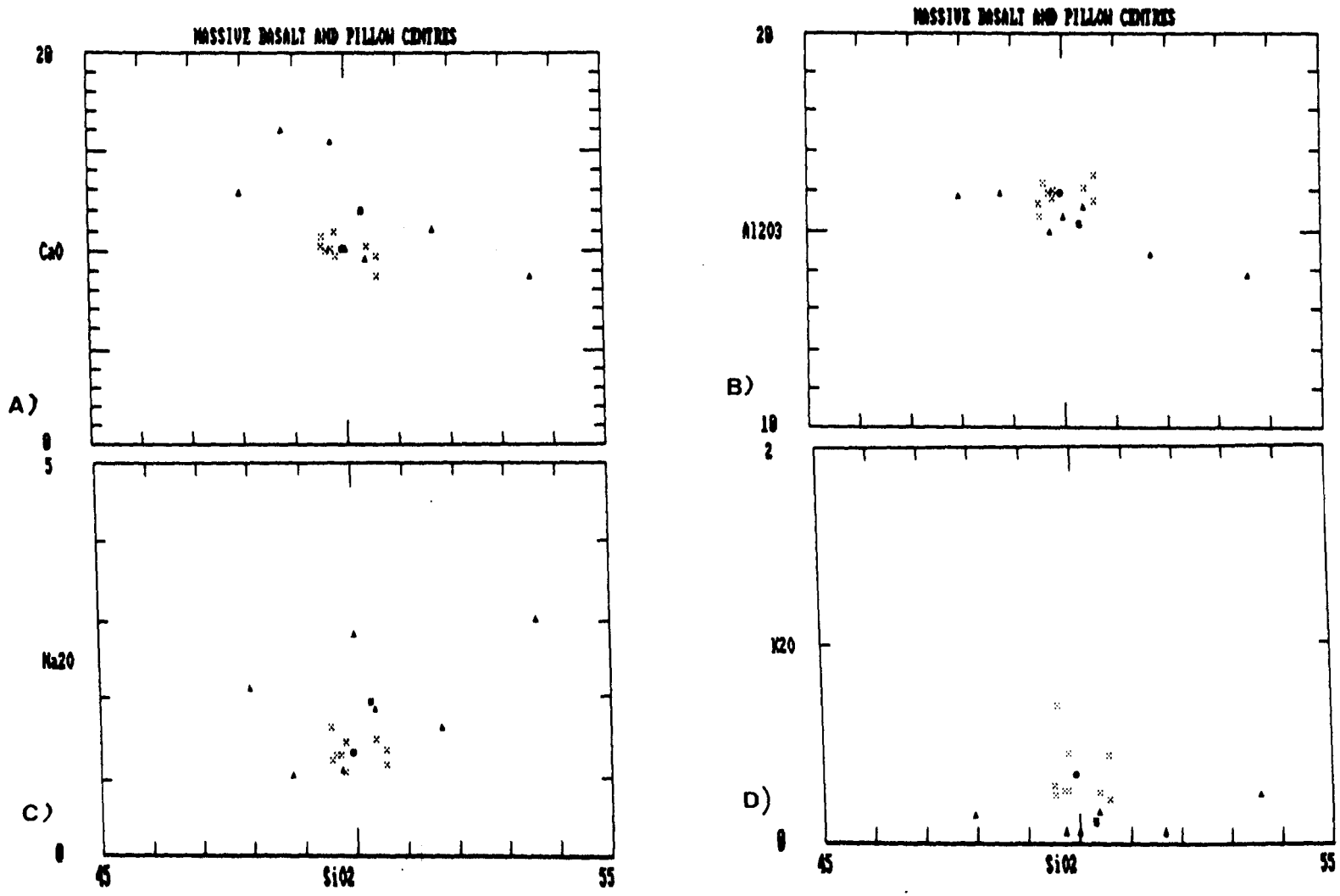

Figure 12: a)-k) Oxide versus SiO_2 diagrams for massive basalt and pillow centre analyses, including averages. (symbols the same as figure 7)

a)-k) Diagrammes des oxydes versus SiO_2 pour les basaltes massifs et les centres de coussins, incluant les moyennes.
(même symboles qu'à la figure 7)

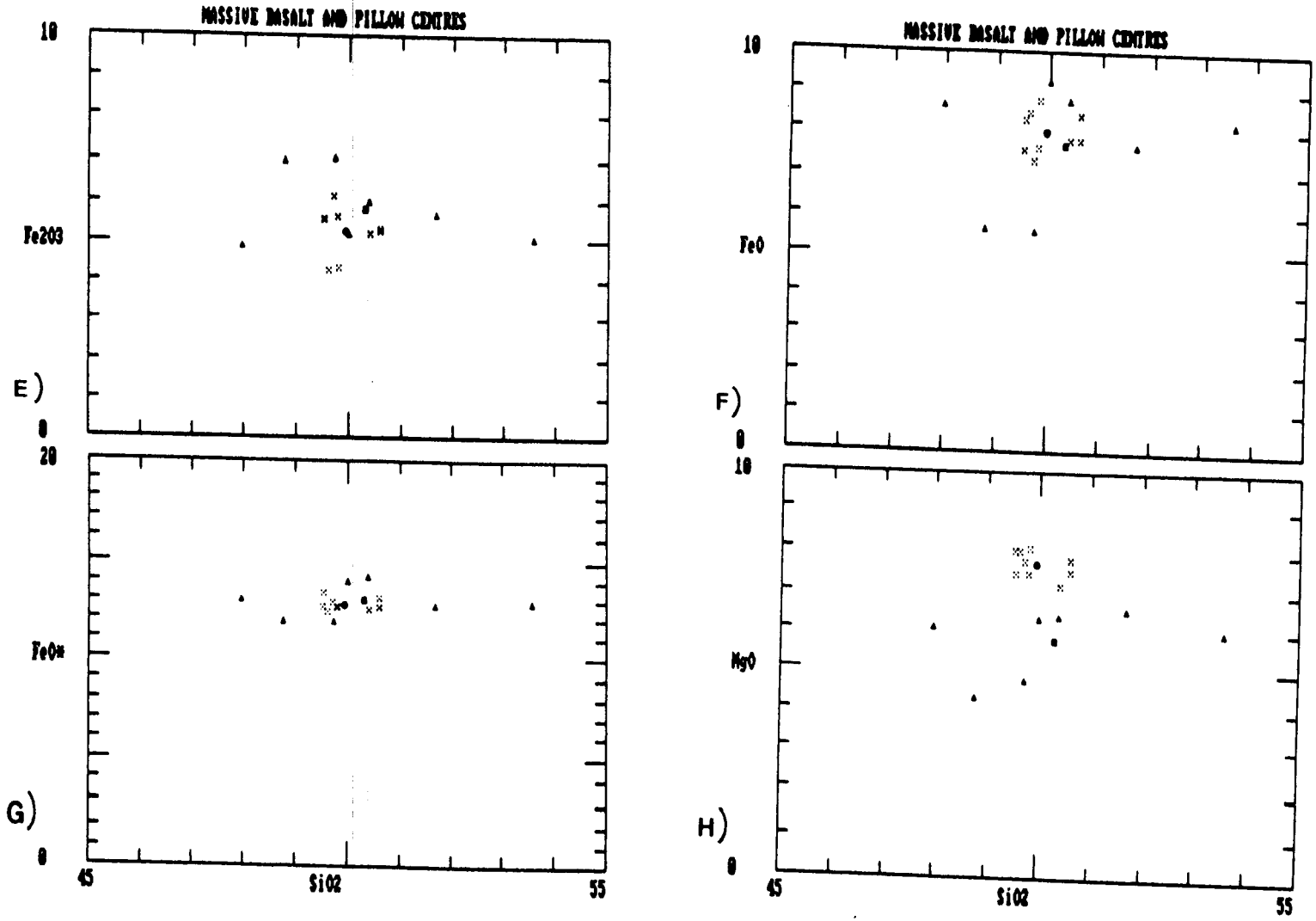

Figure 12 (continued):
(suite):

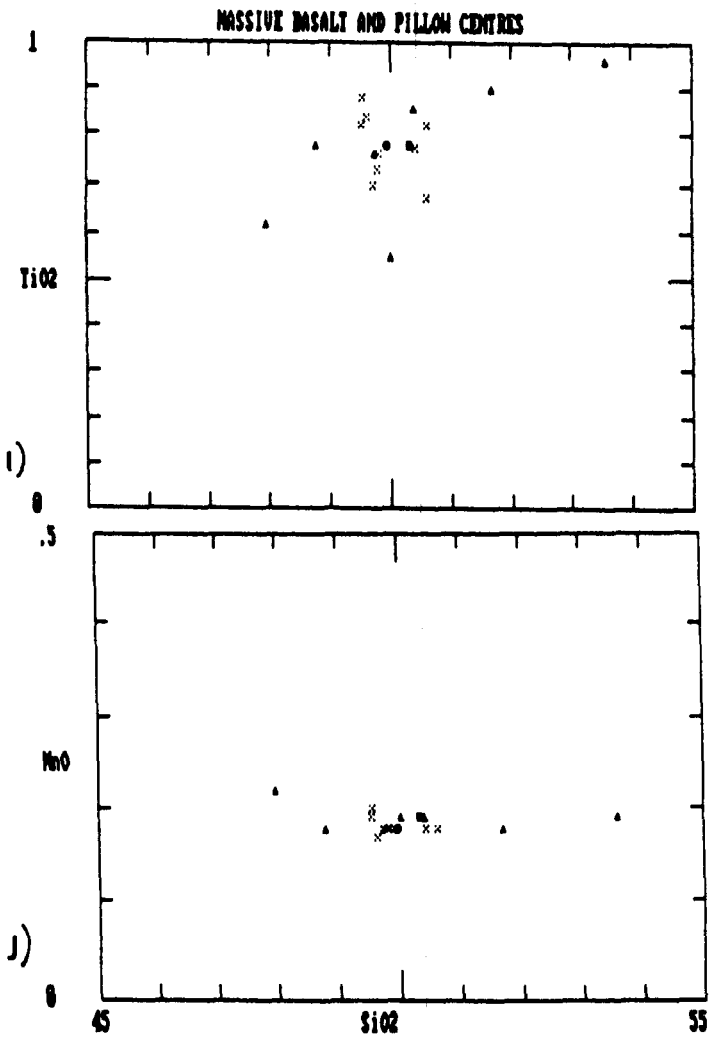

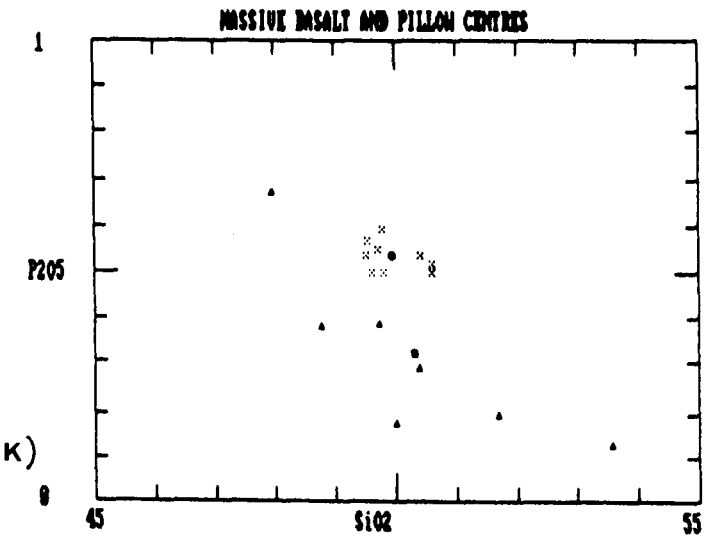

Figure 12 (continued):
(suite):

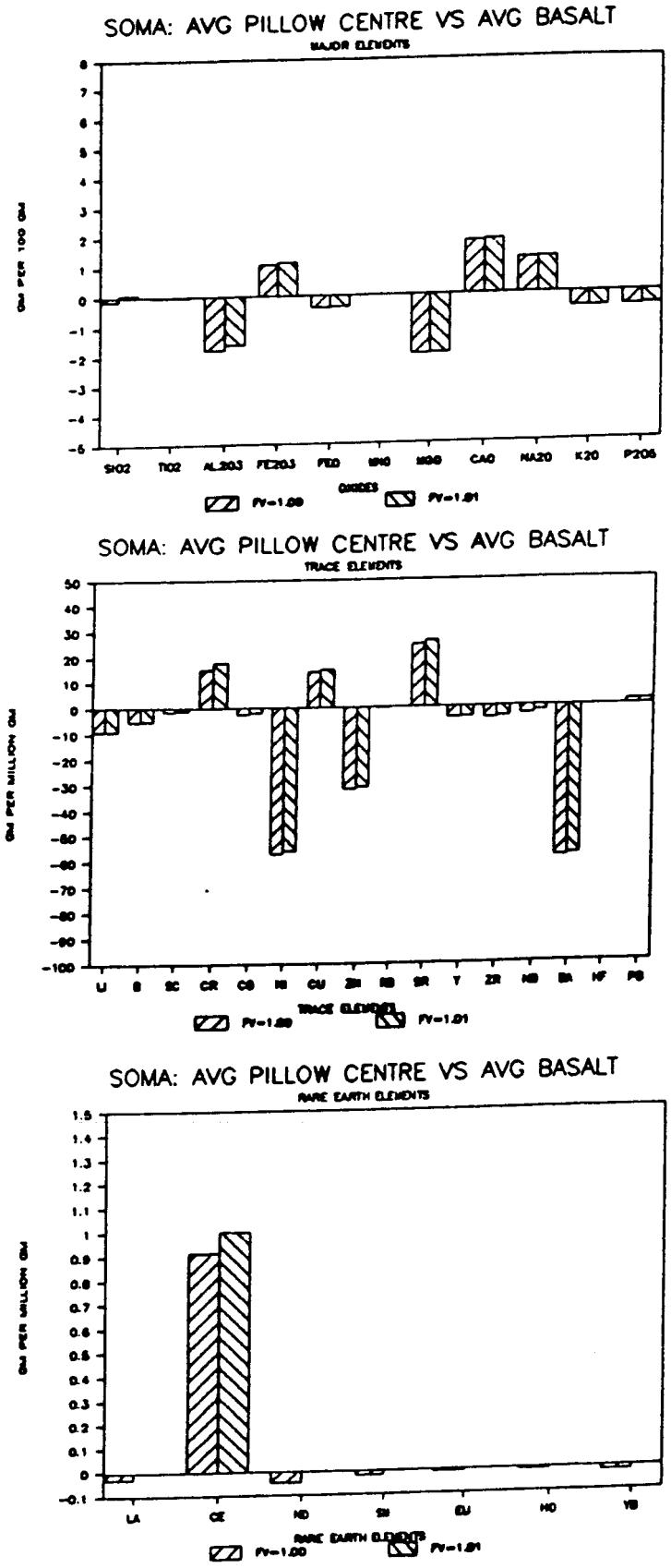

Figure 13: SOMA diagrams exhibiting chemical variations between the average pillow centre and the average massive basalt.

a) major elements
b) trace elements
c) REE

Diagrammes du logiciel SOMA montrant les variations chimiques entre la moyenne des centres de coussins et la moyenne des basaltes massifs.

a) éléments majeurs
b) éléments traces
c) terres rares

Table 2: Variations in the major, trace and REE element chemistry of the pillow centre average compared to the massive basalt average. (symbols the same as in Table 1)

Variations des éléments majeurs, traces et des terres rares de la moyenne des centres de coussins comparée à la moyenne des basaltes massifs. (mêmes symboles qu'au Tableau 1).

Average Pillow Centre vs. Average Massive Basalt

	++	+	=	-	--	+/-
Major Elements		Fe2O3 CaO Na2O	TiO2 MnO	Al2O3 FeO MgO K2O P2O5		SiO2
Trace Elements	Cr Cu Sr	Pb	Rb Hf	Li B Sc Co Y Zr Nb	Ni Zn Ba	
Rare Earth Elements	Ce		Eu Ho	La Nd Sm Yb		

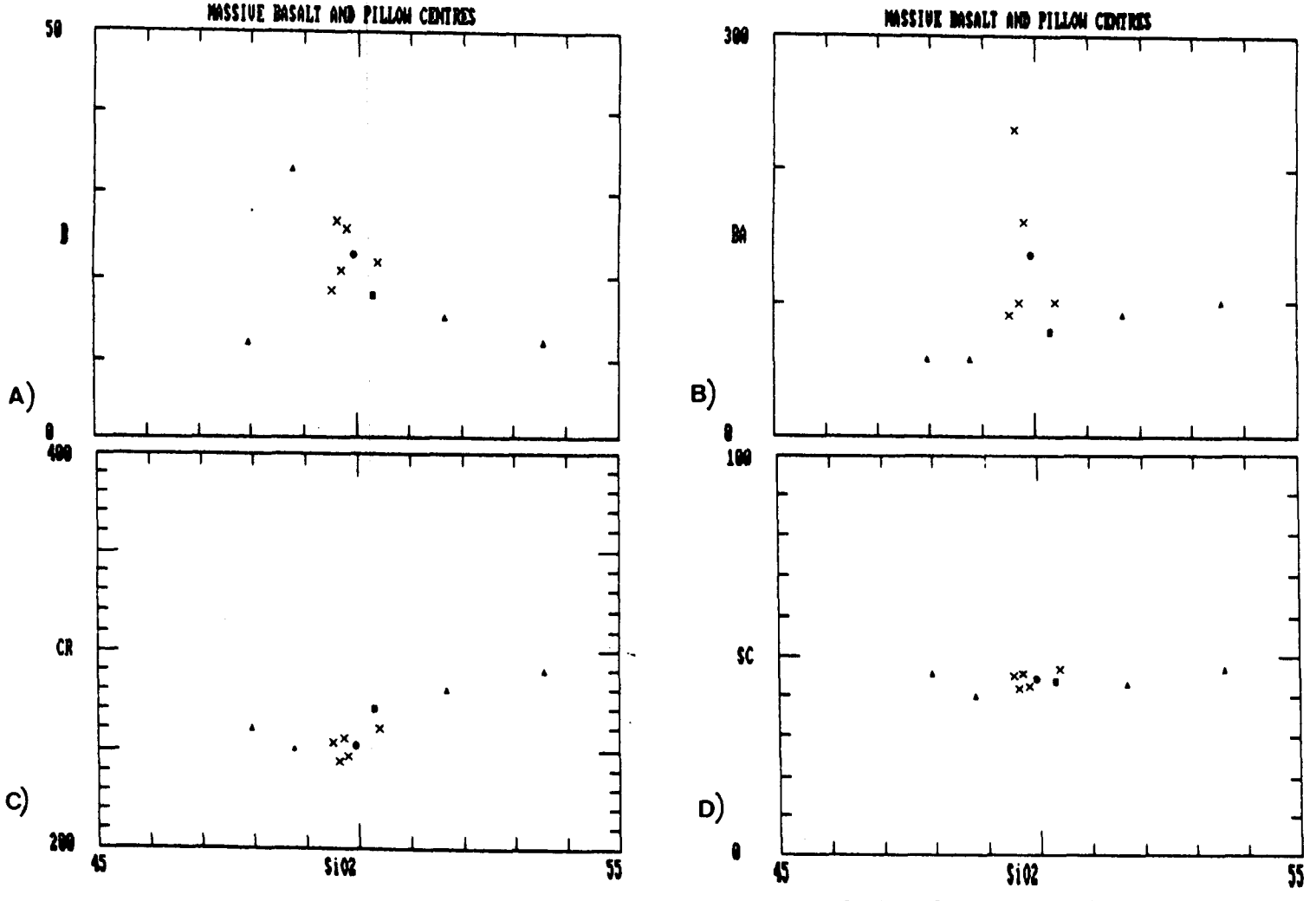

Figure 14: a)-s) Trace element versus SiO_2 diagrams for massive basalt and pillow centre analyses, including averages.
(symbols the same as figure 7)

a)-s) Diagrammes des éléments traces versus SiO_2 pour les basaltes massifs et les centres de coussins, incluant les moyennes.
(mêmes symboles qu'à la figure 7)

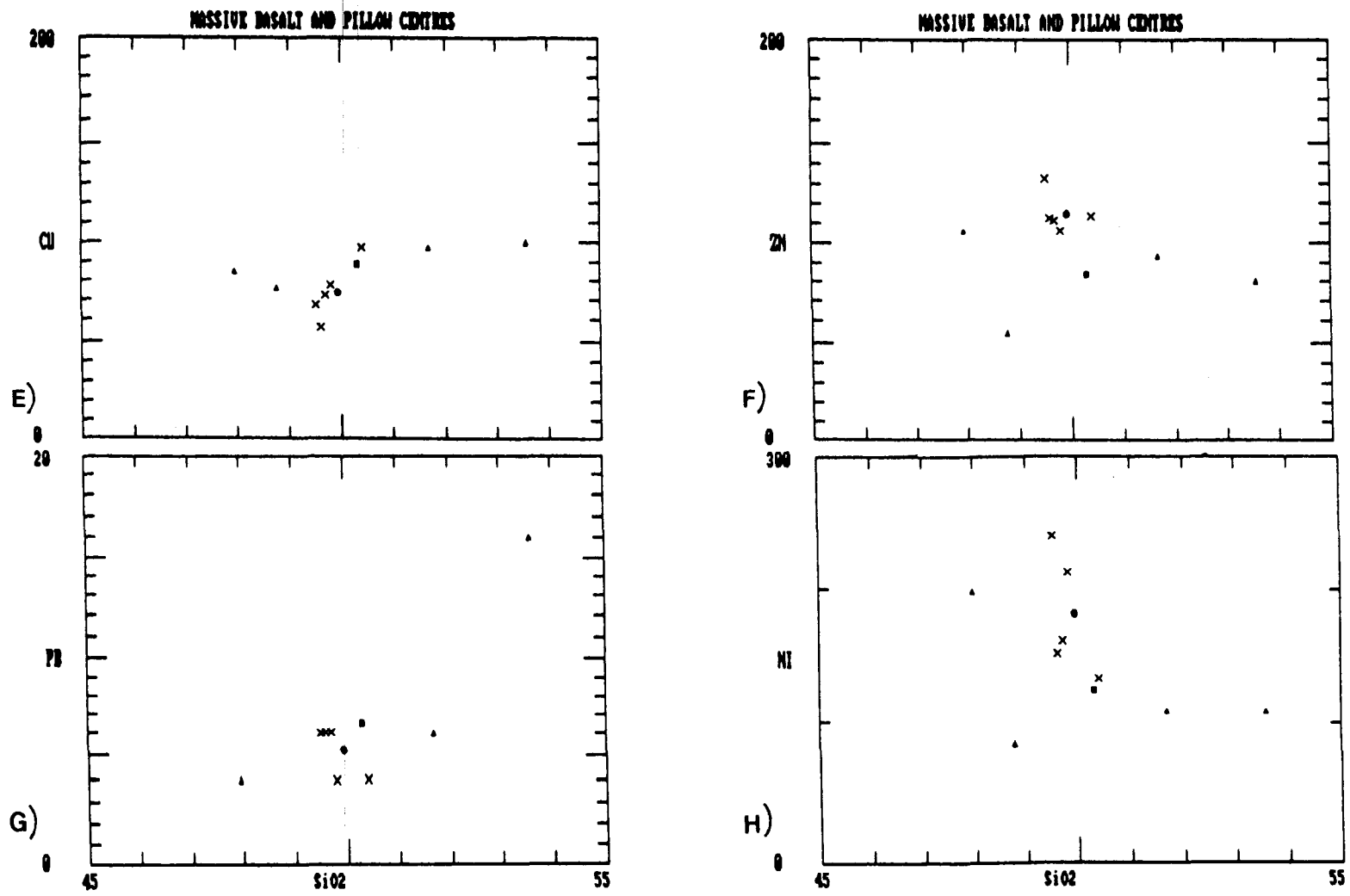

Figure 14 (continued):
(suite):

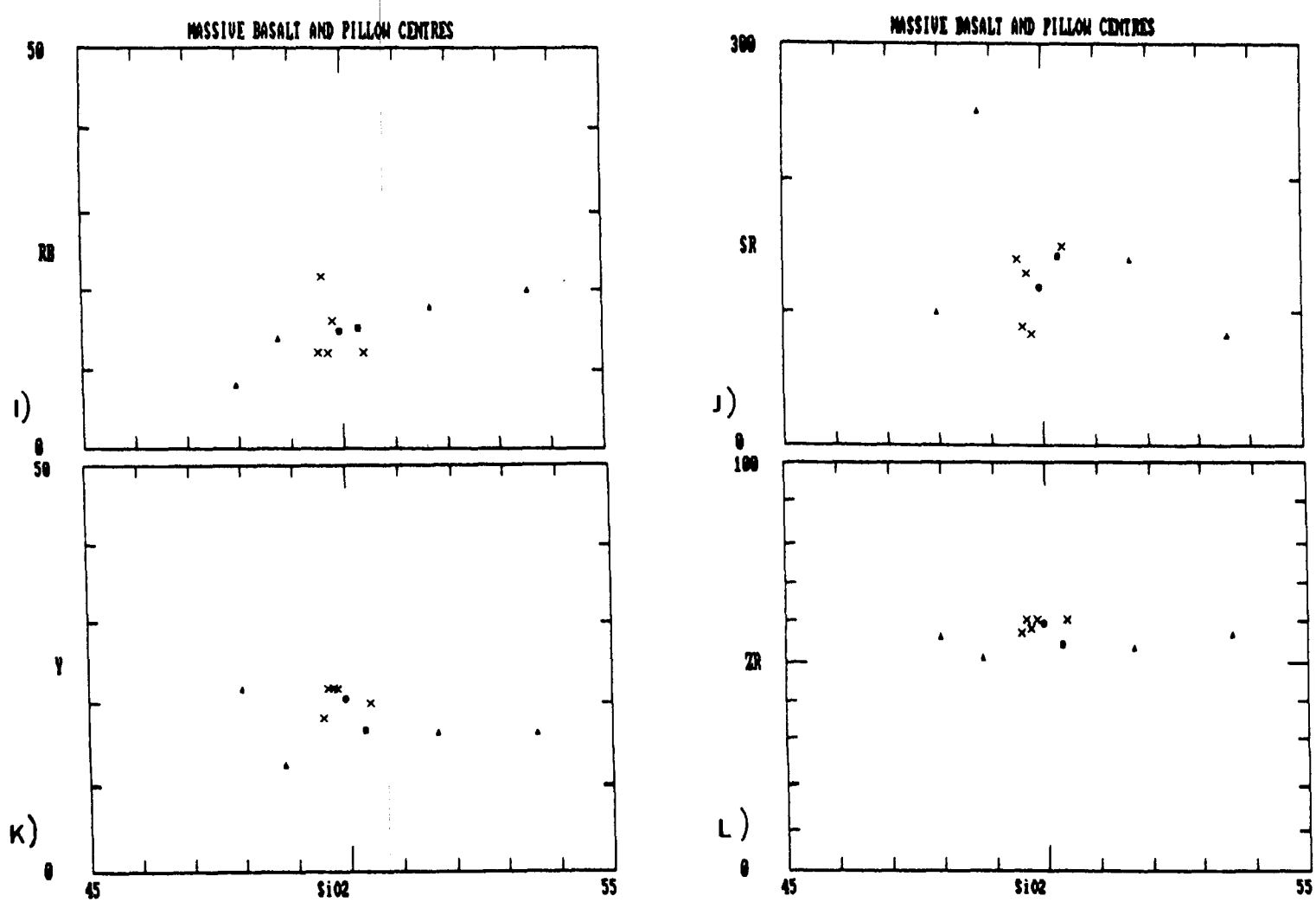

Figure 14 (continued):
(suite):

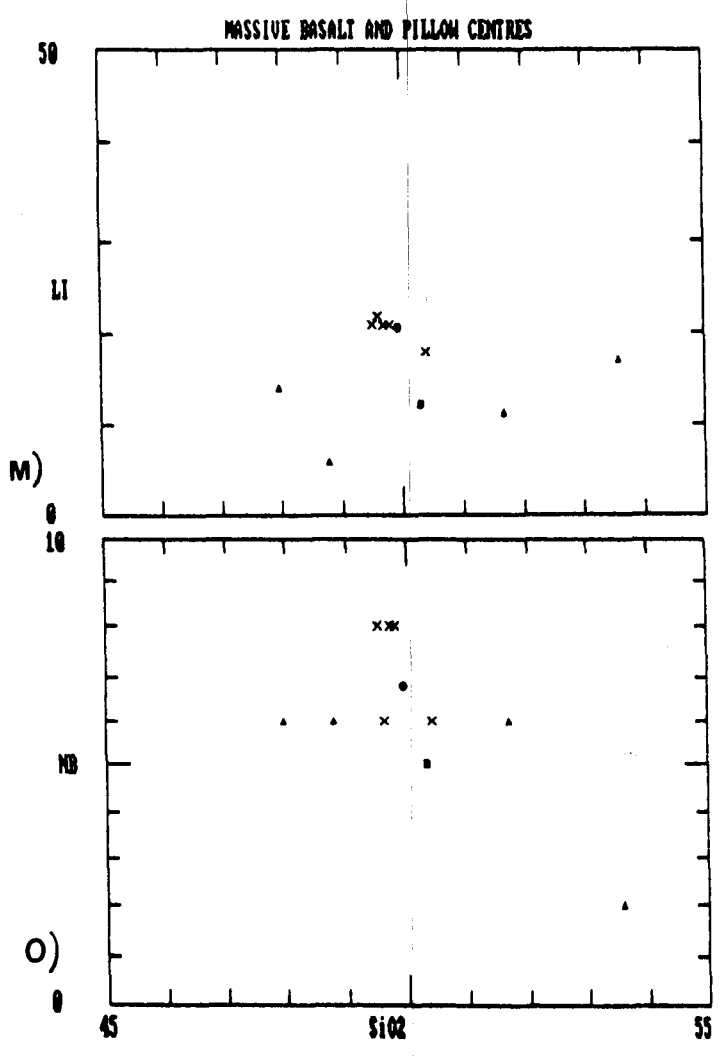

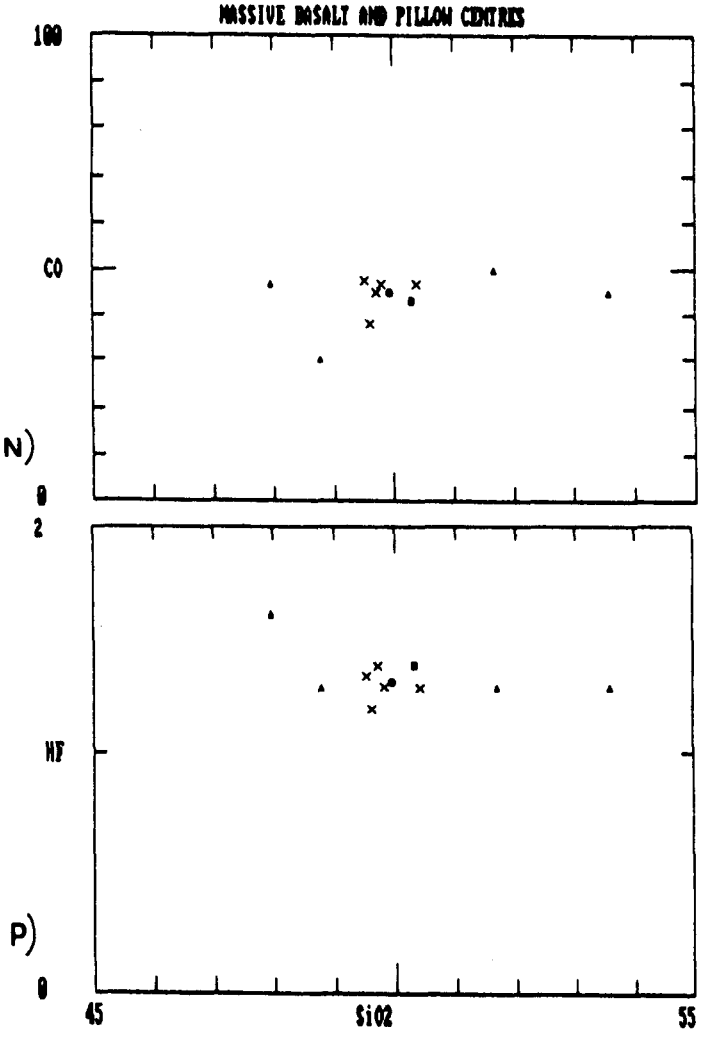

Figure 14 (continued):
(suite):

Figure 14 (continued):
(suite):

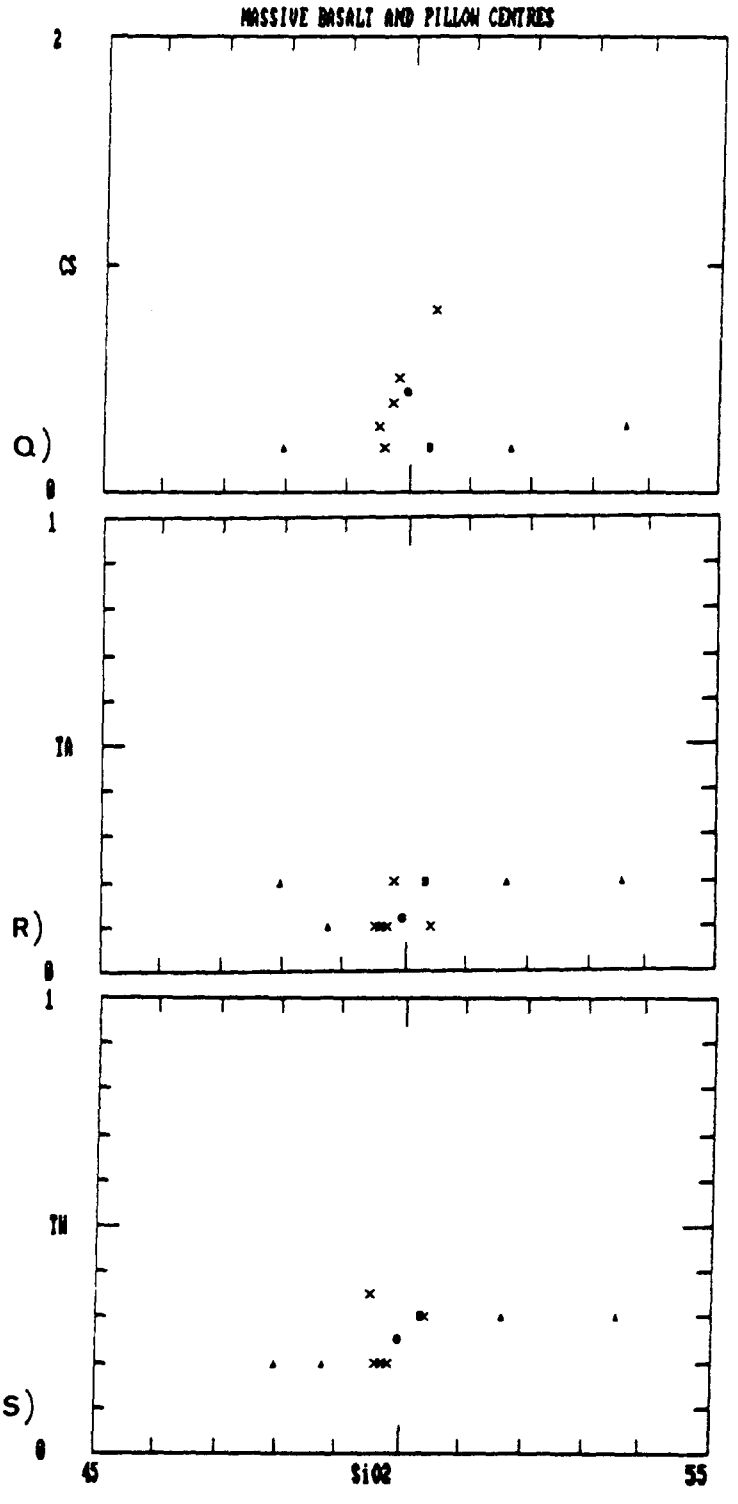

(figure 13b) show major depletion in Ni, Zn and Ba; minor depletion in Li, B, Zr and Nb; and enrichment in Cr, Cu and Sr (Table 2).

On the REE vs SiO_2 diagrams (figures 15 a-i), La, Nd, Ho and Sm show greater scatter for the massive basalts, while Ce and Eu show greater scatter for the pillow centres. The remaining elements are constant for the two sample types (the effect of SiO_2 variation being ignored for the pillow centres); the correspondance between the two average analyses is very close. Treatment of the data using SOMA (figure 13 and Table 2) indicates that only Ce is greatly enriched in the average pillow centre compared to the average massive basalt; the remaining elements being virtually constant. The Spider diagram of the pillow centre REE elements (figure 9) exhibits a flat curve at 10x chondrite similar to that observed for the massive basalt.

The variations in chemistry, major, trace and REE elements, observed between the average pillow centre and the average massive basalt may be explained by a combination of primary chemical variations due to differing crystallization histories between the two facies, and deuteric or high temperature sea-water alteration. Scott and Hajash (1976) explained the variations observed between pristine basalt glass and crystalline pillow cores, where the original chemistry was considered to be that of the glass, using the processes mentionned above. Although the variations described in their study (Table 3) are not reflected in this study (Table 2), the possibility that deuteric alteration

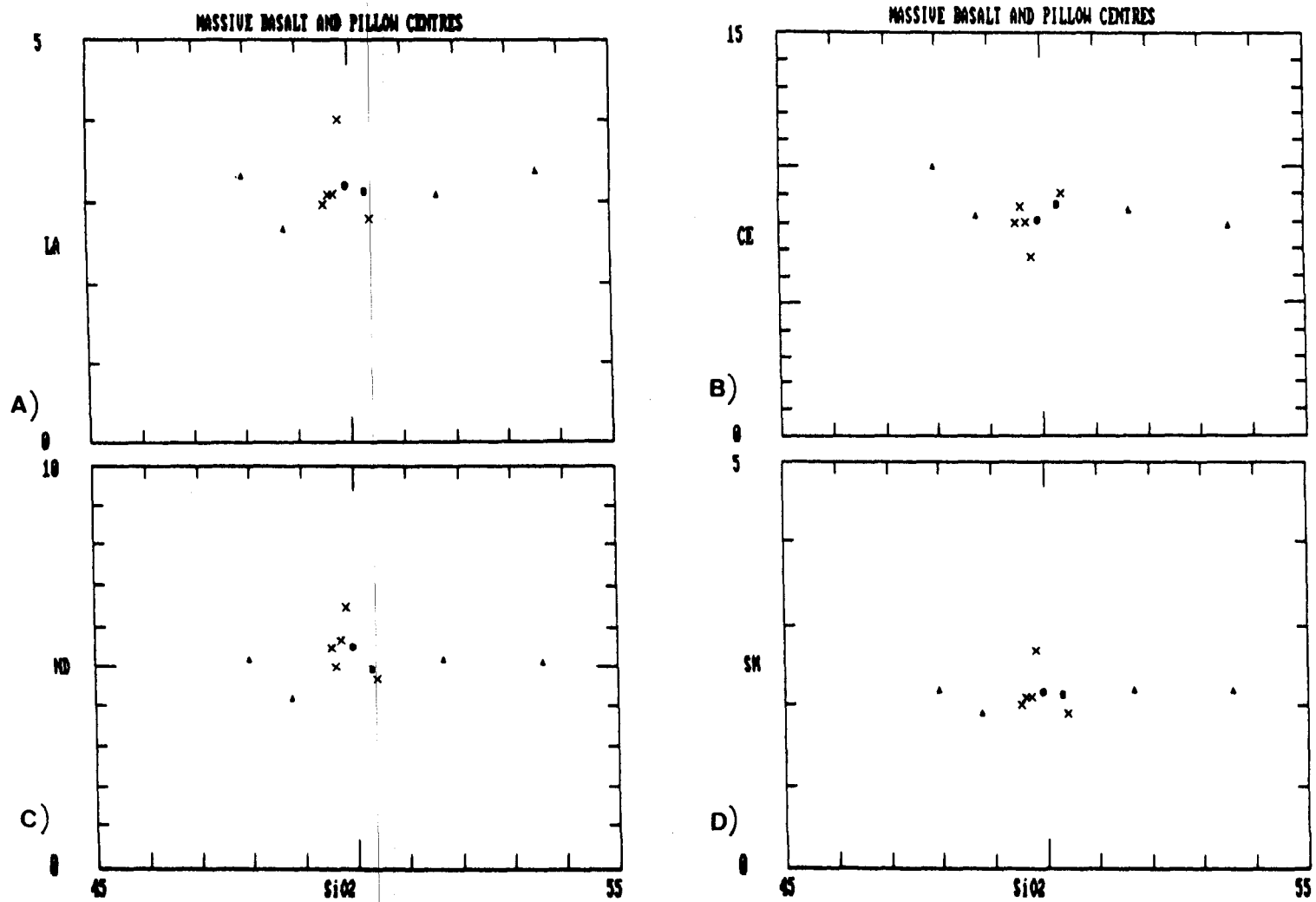

Figure 15: a)-i) REE versus SiO_2 diagrams for massive basalt and pillow centre analyses, including averages.
(symbols the same as figure 7)

a)-i) Diagrammes des éléments des terres rares versus SiO_2 pour les basaltes massifs et les centres de coussins, inclant les moyennes.
(mêmes symboles qu'à la figure 7)

Figure 15 (continued):
(suite):

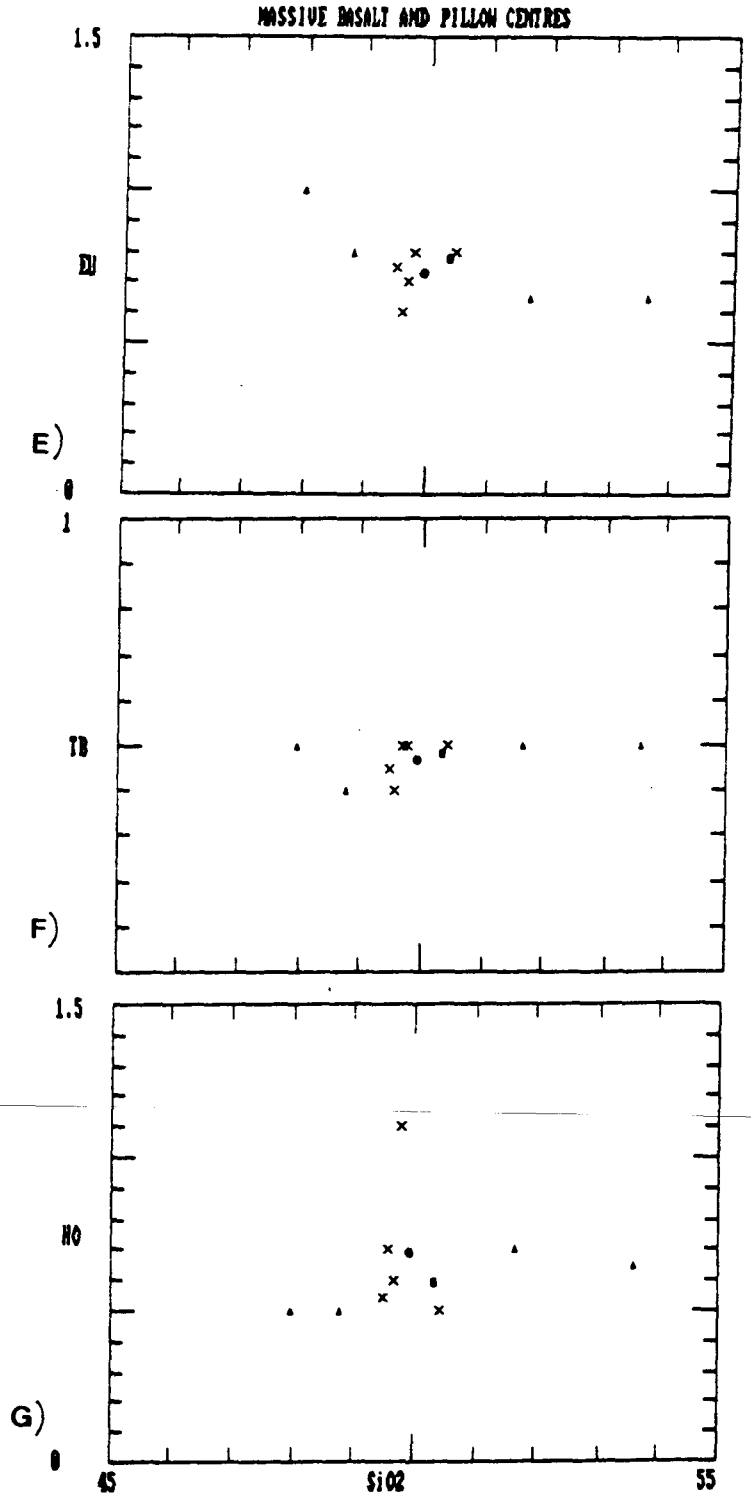

Figure 15 (continued):
(suite):

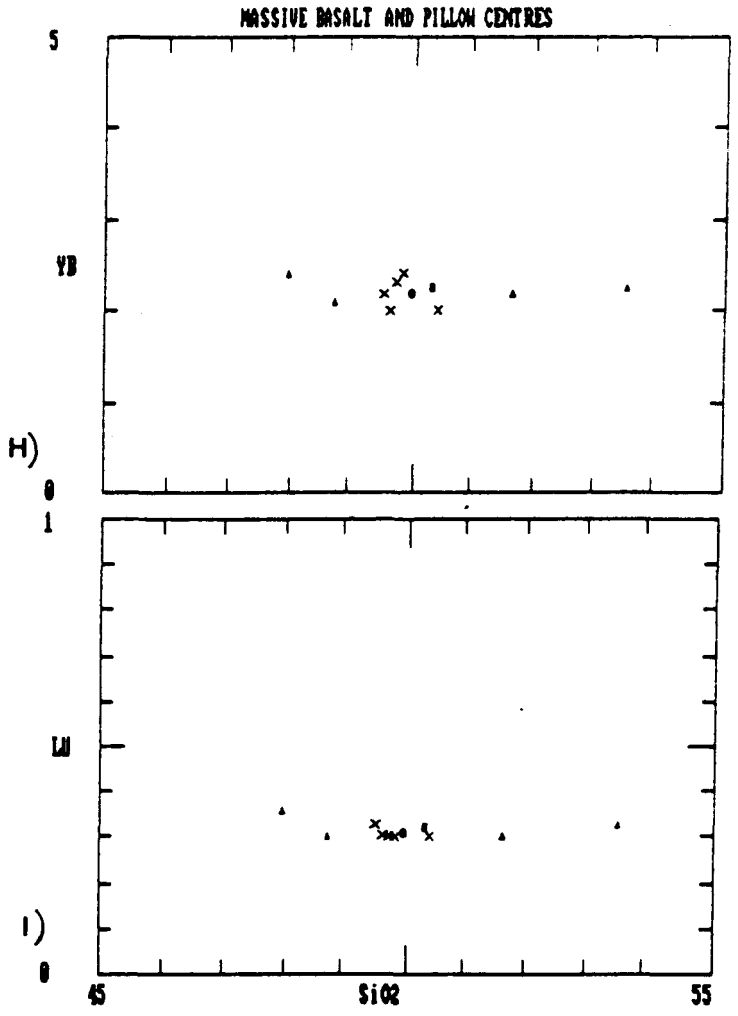

could produce a variety of chemical variations should not be ignored.

The pillow centre data plots in the sub-alkaline field on Alkali vs. Silica, and Nepheline - Olivine - Quartz diagrams (figure 7). The scatter of the data is, however, much greater for the pillow centres than for the massive basalt, and in the Nepheline - Olivine - Quartz plot the average pillow centre analysis does not approach the average massive basalt analysis. On the AFM, FeO/MgO vs. SiO_2, and Al_2O_3 vs. Anorthosite diagrams (figure 8), the pillow centres plot in the tholeiitic field, although their scatter is again greater than the massive basalt analyses. The AFM and FeO/Mgo vs. SiO_2 diagrams show that the pillow centres have higher FeO/MgO ratios than the massive basalt, and the Al_2O_3 vs. Anorthosite diagram shows that the pillow centres, in general, have higher normative Anorthosite values.

On the tectonic setting diagrams, the pillow centre data plots in the Calc-Alkaline Basalt and Island Arc Tholeiite fields on the Mullen (1983) diagram (figure 11a). The average pillow centre analysis falls in the Calc-Alkaline Basalt field, as did the average massive basalt analysis. On the Pearce and Cann (1973) diagrams (figure 11b and c), the pillow centre data plots in the Ocean Floor Tholeiite and Island Arc Basalt fields on the Zr - Ti/100 - Sr/2 diagram. The average pillow centre falls in the Island Arc Tholeiite field, whereas the average massive basalt falls in the Ocean Floor Tholeiite field. On the Zr - Ti/100 - Y*3 diagram, one pillow centre analysis plots in the Within-Plate Basalt

field; the remaining analyses being in the ocean-floor basalt - island-arc tholeiite - calc-alkaline basalt field. The average pillow centre falls in this field, as does the average massive basalt.

Table 3: Initial alteration types affecting pillow basalts and the chemical variations produced.

Types d'altérations initiales des coussins basaltiques et variations chimiques produites.

	Oeuteric Alteration (Pillow centre)	Palagonitization (Hyaloclastite)	Smectitization Interstitial Glass	Smectitization Olivine
SiO2		=	--	-
Al2O3		=	--	+
FeO(T)	-	+	+	-
MgO	-	-	+	--
CaO		-	--	+
Na2O		-	-	+
K2O	+	+	+	+
MnO	-			
TiO2		+	-	=
	Scott & Hajash (1976)	Baragar et al (1979)	Andrews (1980)	Andrews (1980)

PILLOW CROSS-SECTIONS

A single cross-section was analysed in three of the four pillows sampled; in the fourth pillow (SP-S4-P5) two cross-sections were analysed (Annexe 1: Tables V to IX). The graphical representations in this study (figures 18 to 20) compare the pillow cross-sections to the average massive basalt using the SOMA program, and a volume factor (FV) of 0. A comparison of these graphs to those exhibiting elements in weight percent vs. position in centimentres in the pillow (figures 16a and b and 17a and b) show that only minor differences exist between the two representations. This also is true for the SOMA graph of the individual pillow cross-sections compared by the SOMA program to their proper pillow centre (figures 16c and 17c). The only pillow zone exhibiting variation in gain or loss of elements with a calculated FV was the hyaloclastite, and as there exists an inherent error in the SOMA calculation due to the assumption that the density of the original basalt glass was equal to the density of the crystalline basalt, it is here considered that the variations observed did not justify the use of the calculated FV diagrams. The trace elements, Cs, Ta and Th, and the REE elements, Tb and Lu, are present in abundances too small to be treated by the SOMA program (Annexe 1: Tables V to IX), and were, therefore, excluded from the following study.

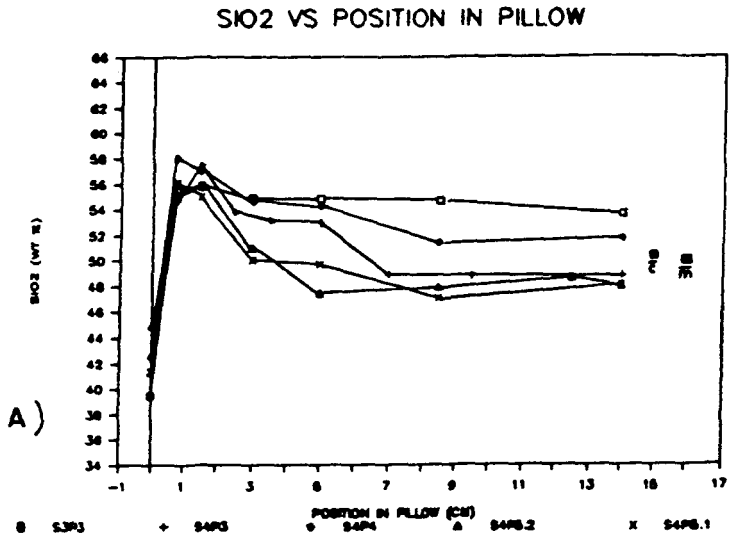

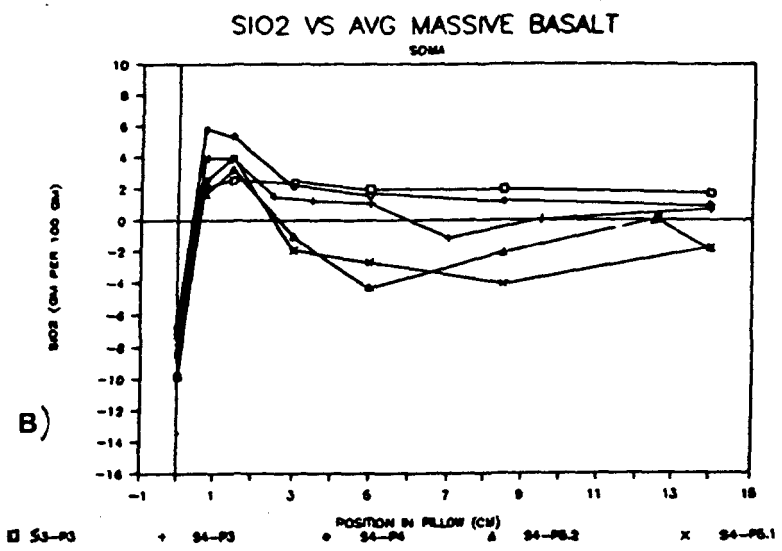

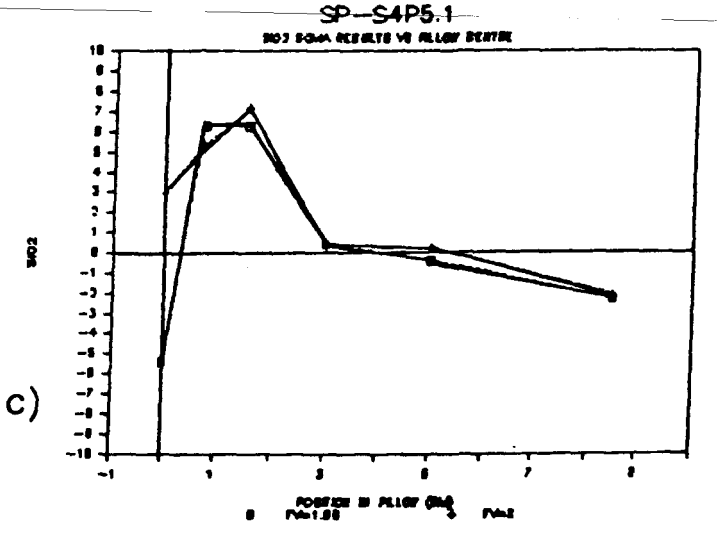

Figure 16: Comparison of various graphic representations of chemical variations in SiO_2 plotted against the samples' position in the pillow:

a) SiO_2 (wt%).

b) Losses and gains of SiO_2 (gm/100gm) calculated by the program SOMA for no volume change (FV = 1.00), and the average massive basalt as parent rock.

c) Losses and gains of SiO_2 (gm/100gm) calculated by the program SOMA with (FV = x) and without (FV = 1.00) a volume change, and the centre of the pillow as parent rock.

Graphiques représentant les variations chimiques du SiO_2 versus la position des échantillons dans les coussins:

a) SiO_2 (%poids).

b) Pertes et gains en SiO_2 (gm/100gm) calculés par le logiciel SOMA, sans changement de volume (FV = 1.00), et avec la moyenne des basaltes massifs comme parent.

c) Pertes et gains en SiO_2 (gm/100gm) calculés par le logiciel SOMA, sans (FV = 1.00) et avec (FV = x) changement de volume, avec le centre du coussin comme parent.

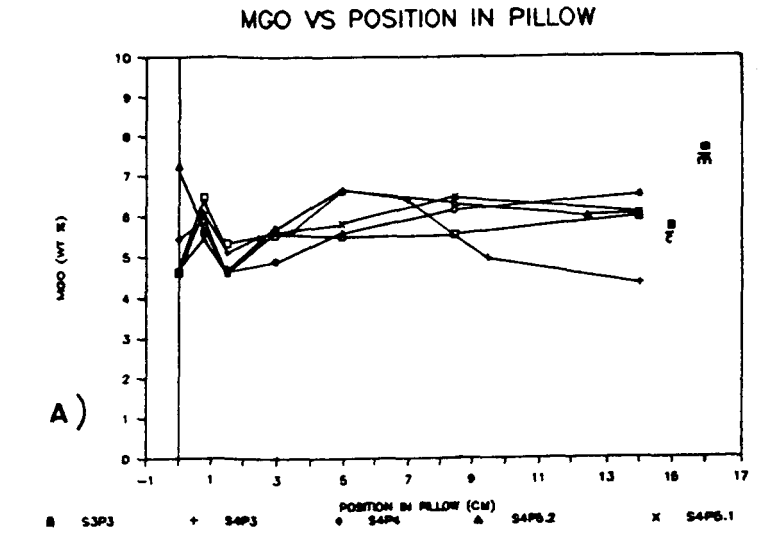

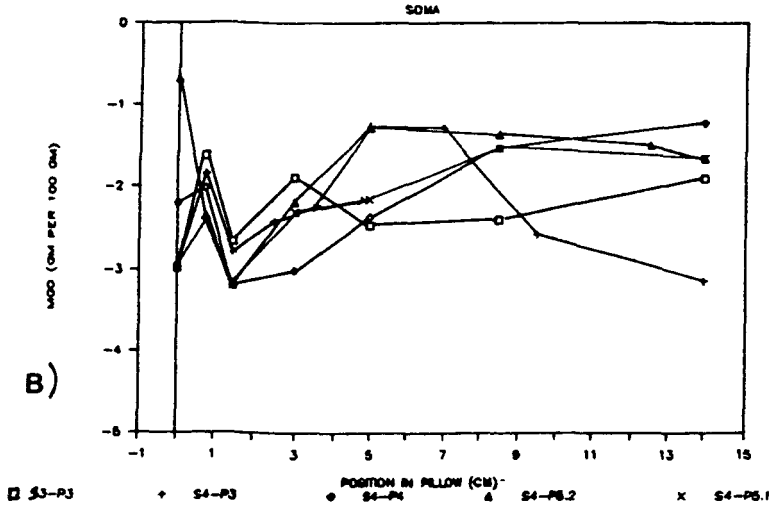

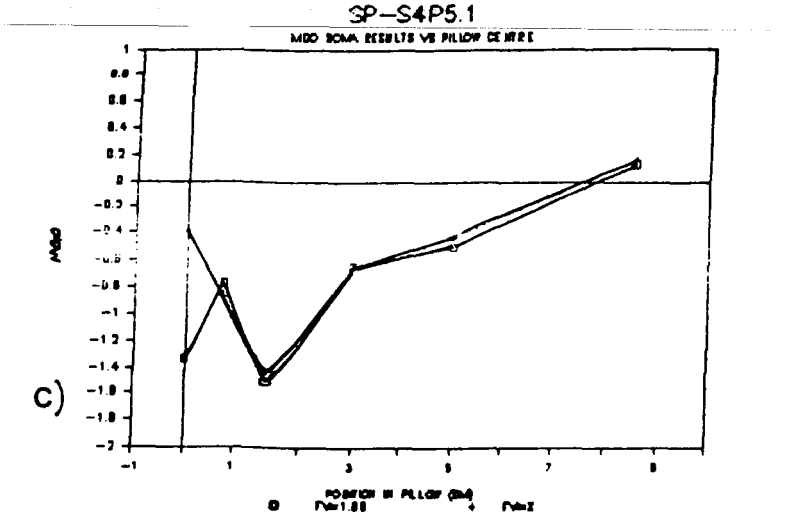

Figure 17: Comparison of various graphic representations of chemical variations in MgO plotted against the samples' position in the pillow:

a) MgO (wt%).

b) Losses and gains of MgO (gm/100gm) calculated by the program SOMA for no volume change (FV = 1.00), and the average massive basalt as parent rock.

c) Losses and gains of MgO (gm/100gm) calculated by the program SOMA with (FV = x) and without (FV = 1.00) a volume change, and the centre of the pillow as parent rock.

Graphiques représentant les variations chimiques du MgO versus la position des échantillons dans les coussins:

a) MgO (%poids).

b) Pertes et gains en MgO (gm/100gm) calculés par le logiciel SOMA, sans changement de volume (FV = 1.00) avec la moyenne des basaltes massifs comme parent.

c) Pertes et gains en MgO (gm/100gm) calculés par le logiciel SOMA, sans (FV = 1.00) et avec (FV = x) changement de volume avec le centre du coussin comme parent.

MAJOR ELEMENTS

The interior zones of the pillow cross-sections exhibit both gains and losses of most elements compared to the average massive basalt (figure 18 and Table 4). The exceptions are MgO and K_2O which are gained only, and Na_2O which is lost. Although gains and losses of the major elements are variable in the Interior zones, trends observed within individual pillows, from the pillow centre to the vesicular zone, are similar (figure 18). SiO_2, K_2O, FeO and TiO_2 have relatively flat curves in the pillow interior. Na_2O exhibits a constant increase from the pillow centre to the vesicular zone, and CaO, Al_2O_3, Fe_2O_3 and P_2O_5 exhibit a constant decrease. FeO is ambiguous, possibly exhibiting an increase from the interior to the exterior; MgO and MnO have no well-defined trend in the interior zones. Pillow S4-P3 (+) exhibits anomalous behavior of CaO, K_2O and Fe_2O_3 (decreases), and FeO, MgO and MnO (increases) in the I2, I3 and I4 (3-7cm) zone. This corresponds with the banded texture observed in this sample.

The major elements in the vesicular zone exhibit greater variation compared to the average massive basalt (Table 4). SiO_2 and NaO_2 are gained, and Al_2O_3, Fe_2O_3, MgO, CaO and K_2O are lost. FeO, MnO, TiO_2 and P_2O_5 exhibit both gains and losses. The trends established in the pillow interior for Na_2O, CaO, K_2O, Al_2O_3, Fe_2O_3, FeO, MgO, TiO_2, and P_2O_3 continue in the vesicular zone. SiO_2 increases here, and no trend can be defined for MnO. (figure 18)

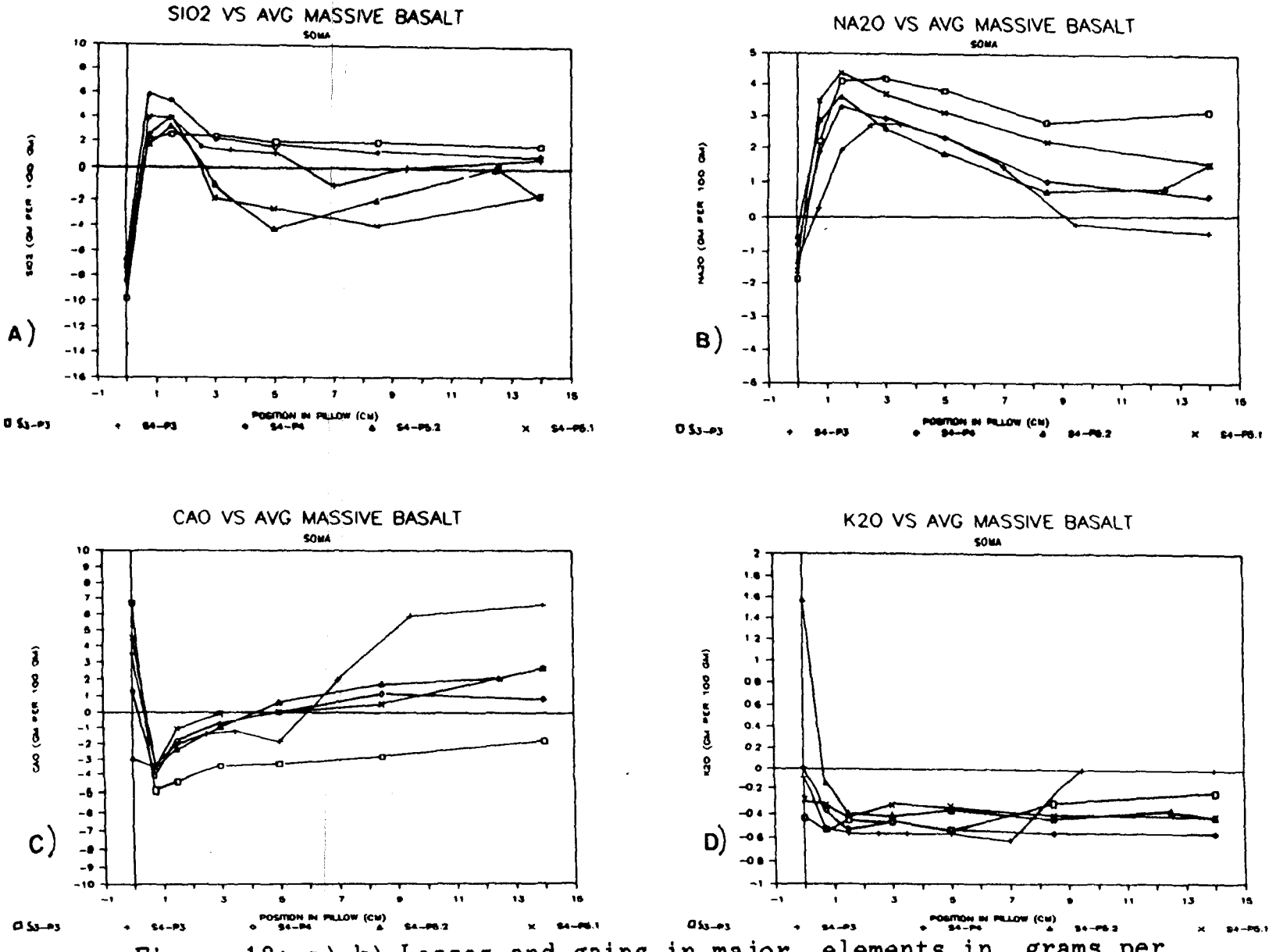

Figure 18: a)-k) Losses and gains in major elements in grams per 100 grams calculated by the program SOMA for no volume change (FV = 1.00), and the average massive basalt as parent rock.

Pertes et gains en éléments majeurs calculés par le logiciel SOMA sans changement de volume (FV =1.00) et avec la moyenne des basaltes massifs comme parent.

Figure 18 (continued):
(suite):

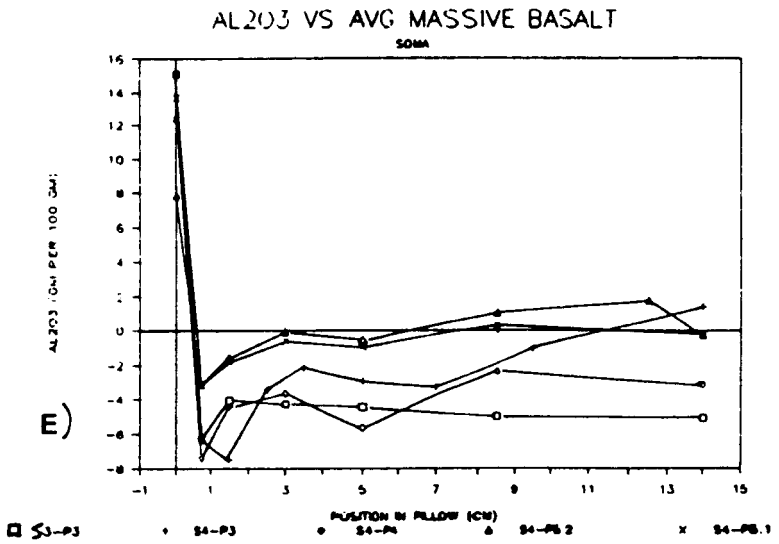

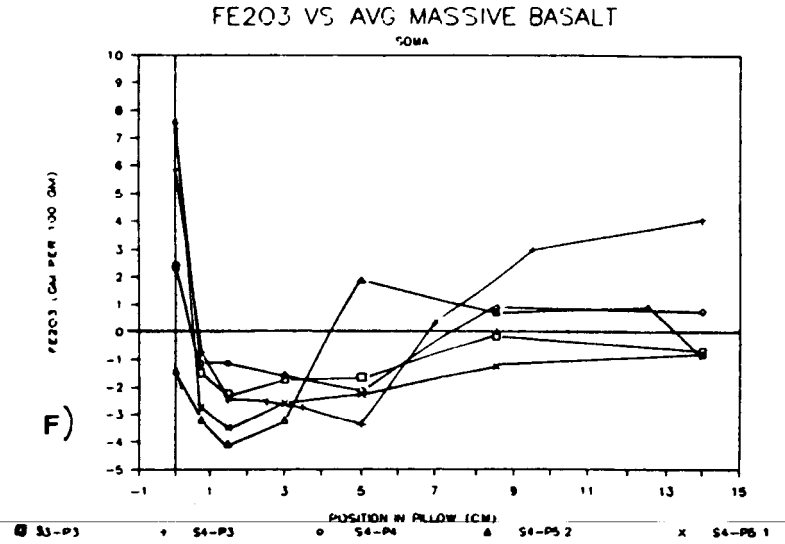

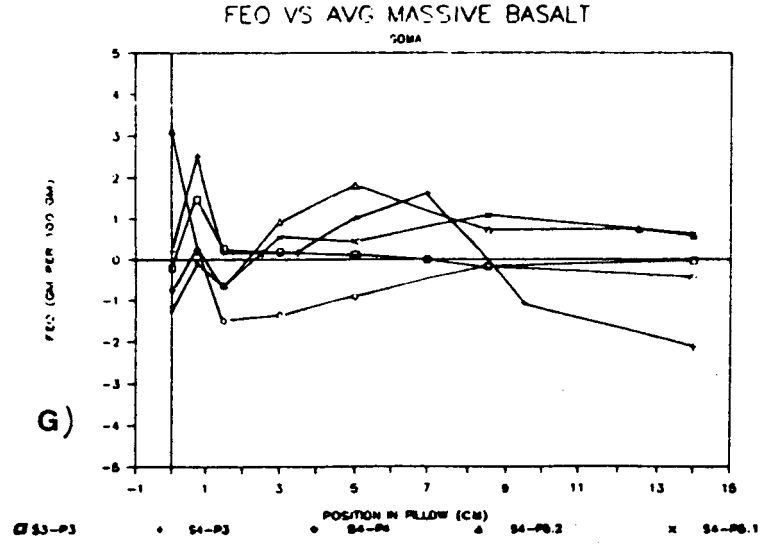

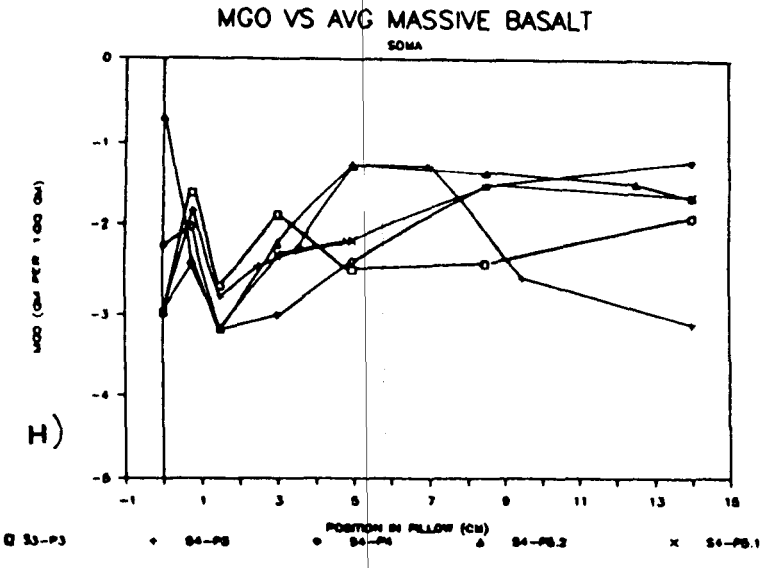

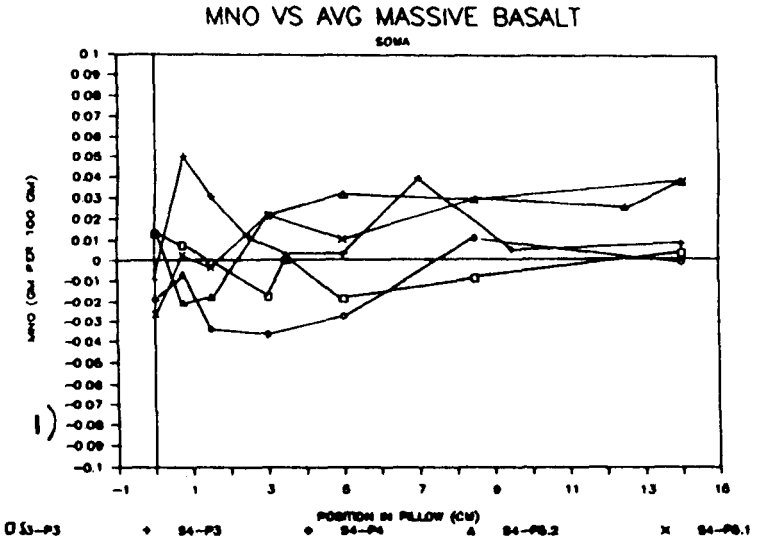

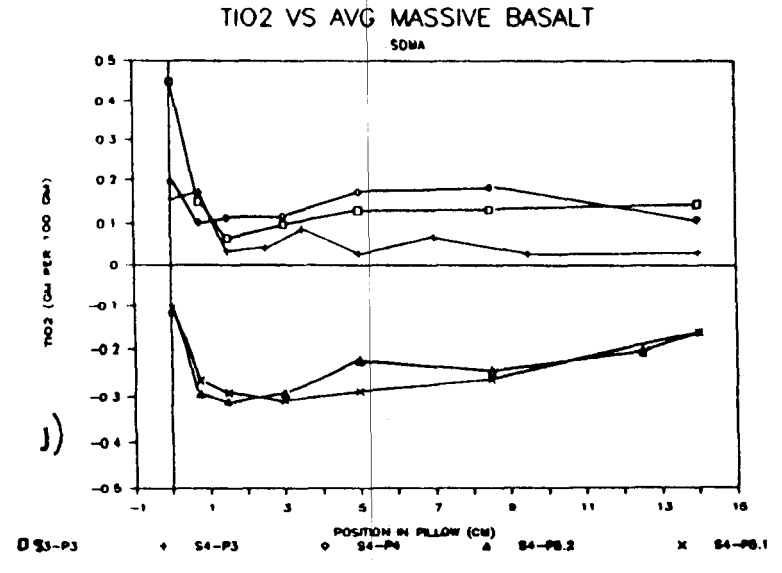

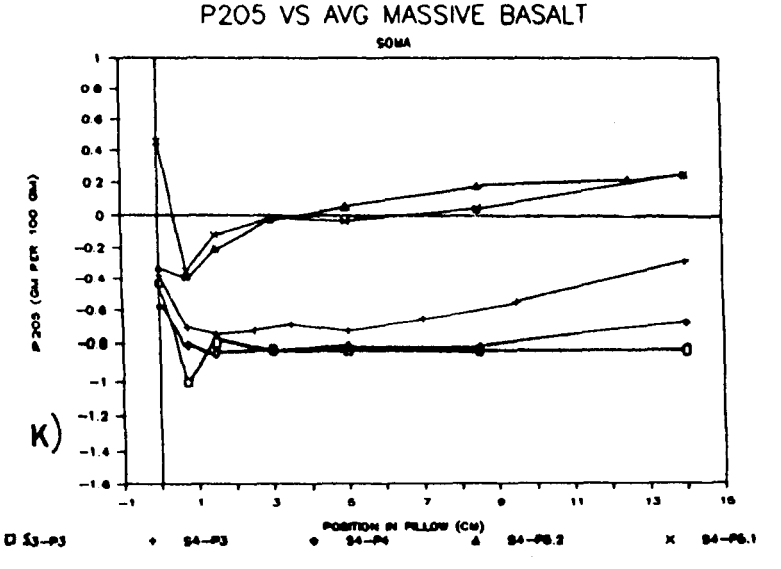

Figure 18 (continued):
(suite):

Table 4: Variations in the major, trace and REE element chemistry of the textural zones of the pillow cross-sections compared to the massive basalt average. (symbols the same as in Table 1)

Variations des éléments majeurs, traces et terres rares dans les zones texturales des coussins comparés à la moyenne des basaltes massifs. (mêmes symboles qu'au Tableau 1).

Pillow Cross-Sections vs. Average Massive Basalt

	Hyaloclastite	Spherulite rim	Vesicular zone	Interior zones	Pillow centre
SiO2	-	+	+	+/-	+/-
Al2O3	+	-	-	+/-	+/-
Fe2O3	+	-	-	+/-	=
FeO	-	+	+/-	+/-	+/-
MgO	-	-	--	-	-
CaO	+	-	-	+/-	+/-
Na2O	-	++	++	+	-
K2O	+/-	-	-	-	-
MnO	+/-	+	+/-	+/-	+/-
TiO2	++	+	+/-	+/-	+/-
P2O5	-	--	-/+	-/+	-/+
Trace Elements	+	-/=	-/=	=	=
Rare Earth Elements	+	-/=	-/=	=	=

In the spherulitic rim SiO_2, FeO, NaO_2, MnO and TiO_2 are gained, while Al_2O_3, Fe_2O_3, MgO, CaO, K_2O and P_2O_5 are lost (Table 4 and figure 18). The trends of the major elements in the spherulite rim commonly resemble those of the vesicular zone (figure 18). Na_2O, CaO, Al_2O_3, and P_2O_5 decrease, while K_2O, Fe_2O_3, FeO, MgO and MnO increase. SiO_2 and TiO_2 are virtually constant.

The hyaloclastite shows the greatest variation in chemistry. SiO_2, Na_2O, FeO, MgO and P_2O_5 are lost; CaO, Al_2O_3, Fe_2O_3 and TiO_2 are gained (Table 4 and figure 18). K_2O and MnO exhibits variable gains and losses (Table 4 and figure 18). On the graphs (figure 18), SiO_2, Na_2O, FeO and MgO decrease from the spherulitic rim to the hyaloclastite, while CaO, K_2O, Al_2O_3, Fe_2O_3, TiO_2 and P_2O_5 increase; MnO is erratic.

A bimodality of analyses is well-defined for TiO_2 and P_2O_5, and less well-defined for Al_2O_3 (figure 18 e, j and k). The two cross-sections of pillow S4-P5 are lower in TiO_2, and higher in P_2O_5 and Al_2O_3 than the other pillows, including those from the same outcrop.

TRACE ELEMENTS

In general, the trace elements exhibit little variation between the pillow interiors and the average massive basalt, slight losses in the vesicular and spherulite rim zones and moderate to large gains in the hyaloclastite (Table 4 and figure 19). Certain elements; Pb, Li, Nb and Hf (figure 19g and m-p); exhibit extremely erratic variations throughout the pillow cross-sections, and have therefore, been left out of the following discussion.

The majority of the trace elements, Ba, Cr, Sc, Cu, Zn, Ni, Rb, Y and Zr (figure 19), remain relatively constant from the pillow centre through the pillow interior, with the exception of pillow SP-S4-P3 which exhibits anomalous increases in Ba, Zn and Ni in the I3 (5cm) banded zone. B and Sr exhibit a general decrease from the pillow centre to the vesicular zone (figure 19a and j); a similar trend for Co is poorly defined (figure 19n). Of these elements, only Co exhibits an anomalous high in the I3-I4 (5-7cm) zone of SP-S4-P3.

Slight decreases in Sc, Cu and Ni occur in the vesicular zone (figure 19d, e and h); all other elements (figure 19) continue along the trends defined for the pillow interiors.

B, Ba, Cr, Sc, Zn, Ni and Zr exhibit slight increases in the spherulitic rim compared to the vesicular zone; while Cu,Rb, Sr and Y exhibit marked decreases (figure 19). Co exhibits no fixed trend in the spherulitic rim.

All elements described for the spherulitic rim exhibit enrichment in the hyaloclastite zone (figure 19) , with the exception of Co which again, exhibits no trend.

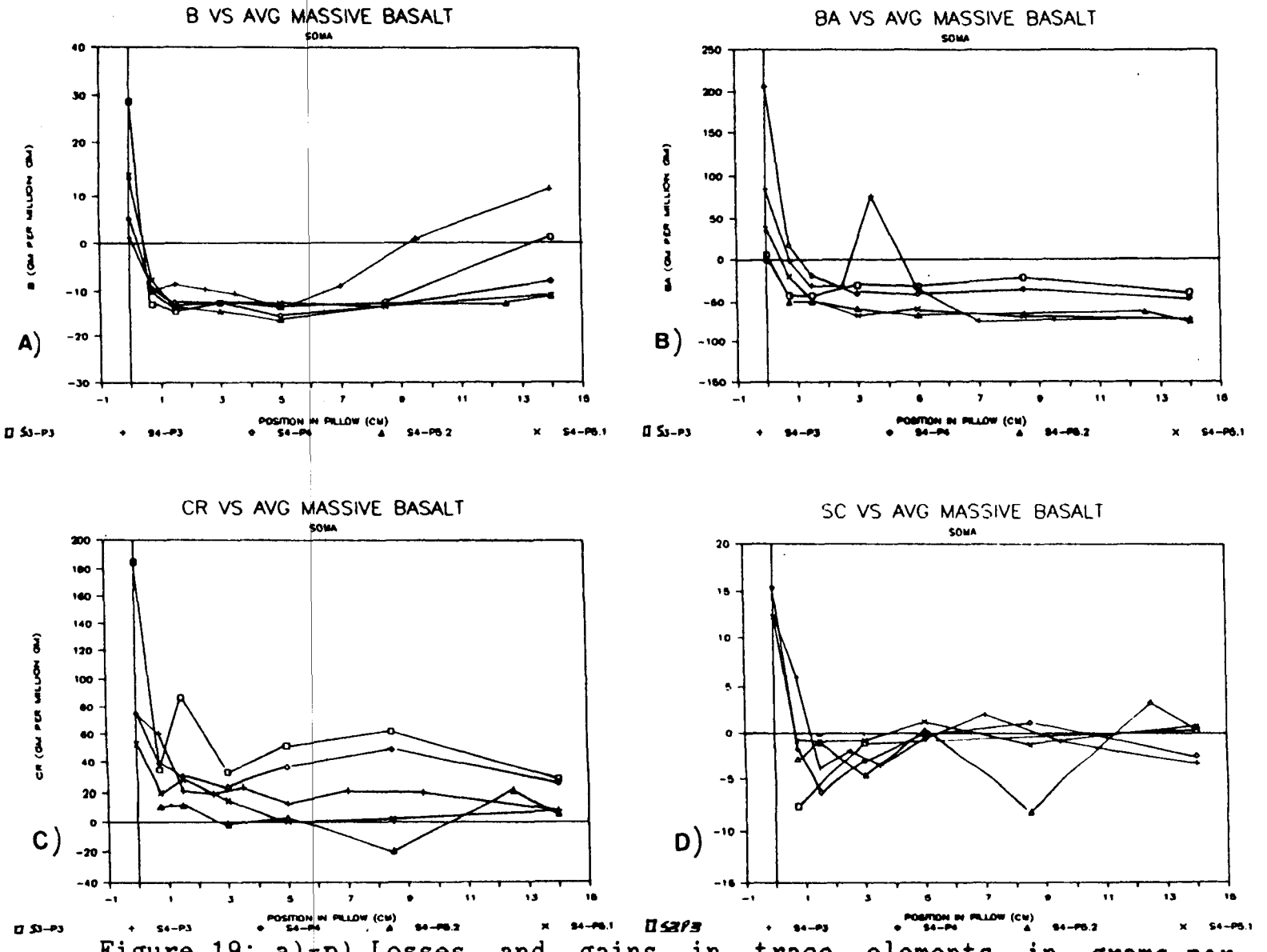

Figure 19: a)-p) Losses and gains in trace elements in grams per million grams calculated by the program SOMA for no volume change (FV = 1.00), and the average massive basalt as parent rock.

Pertes et gains en éléments traces calculés par le logiciel SOMA sans changement de volume (FV =1.00), et avec la moyenne des basaltes massifs comme parent.

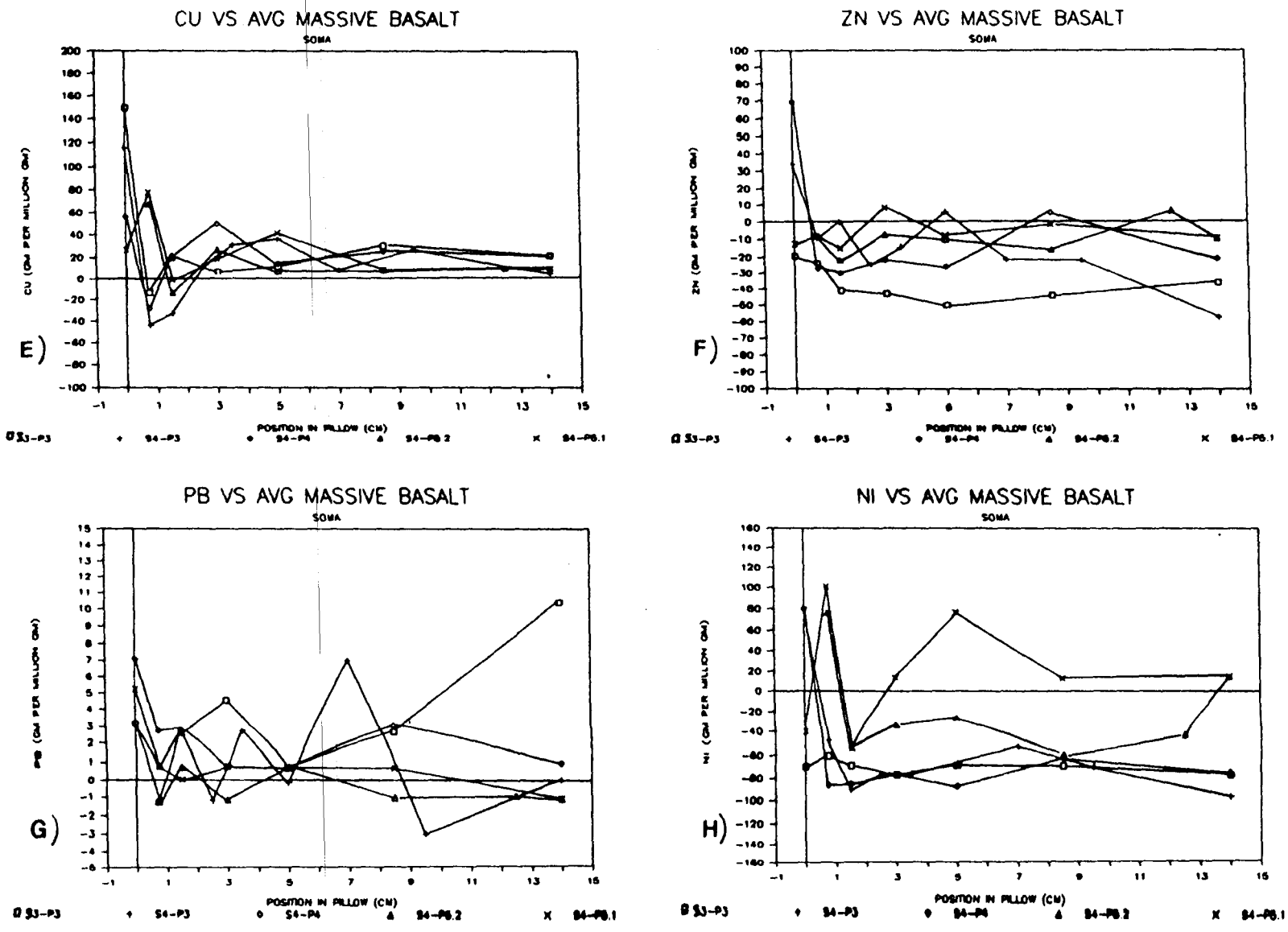

Figure 19 (continued):
(suite):

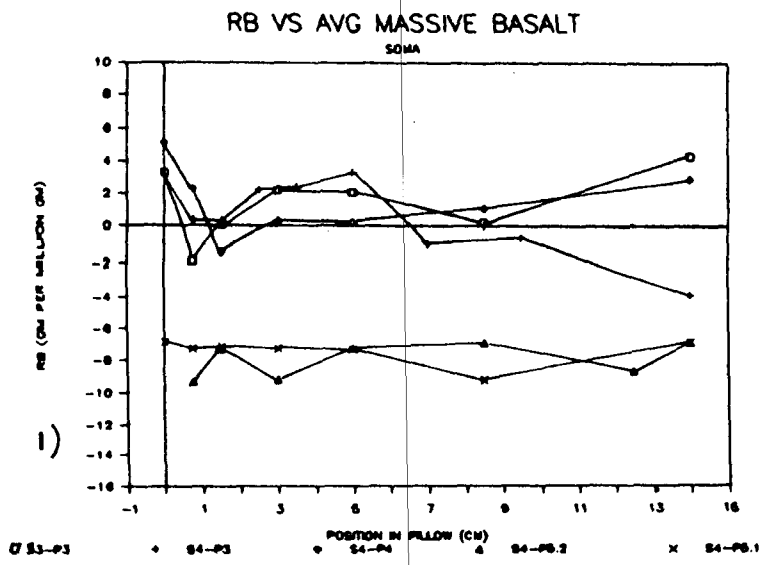

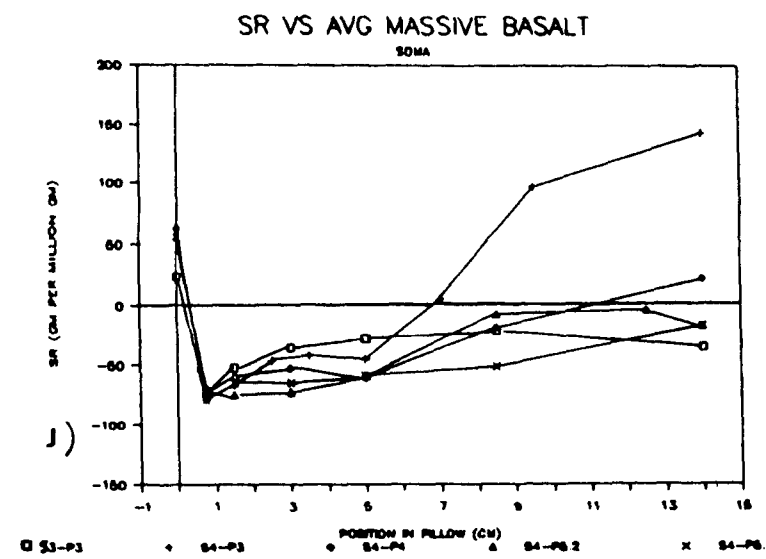

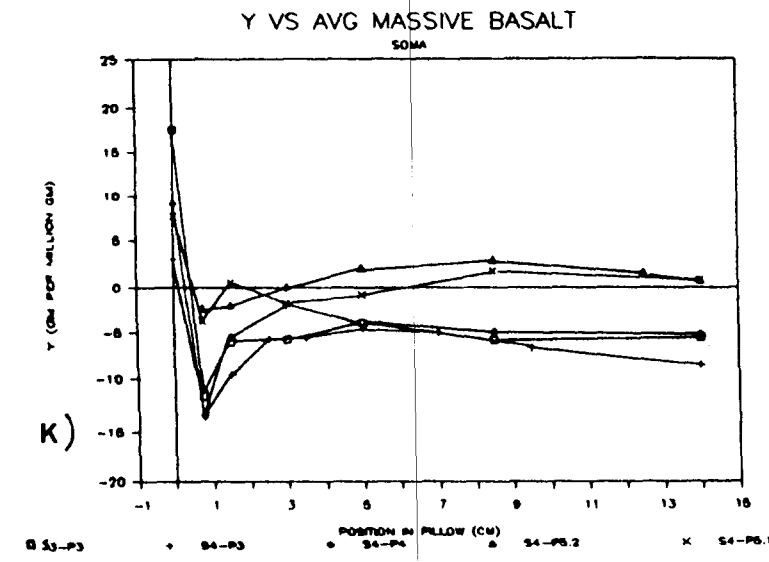

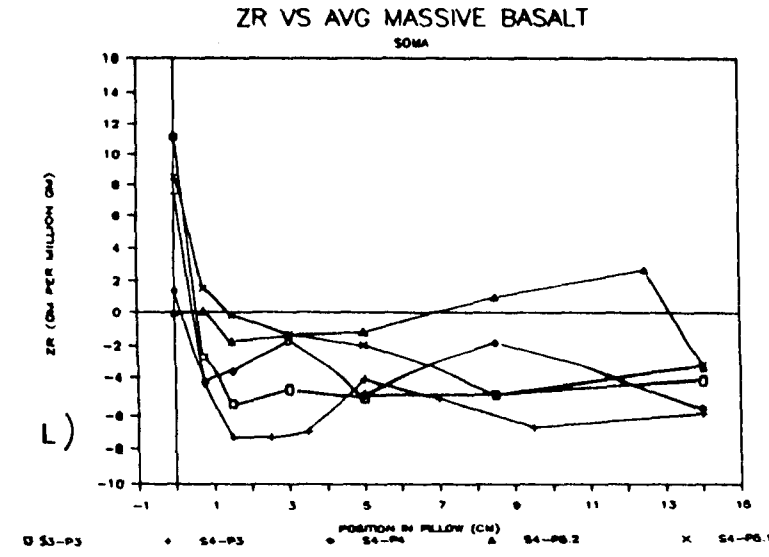

Figure 19 (continued):
(suite):

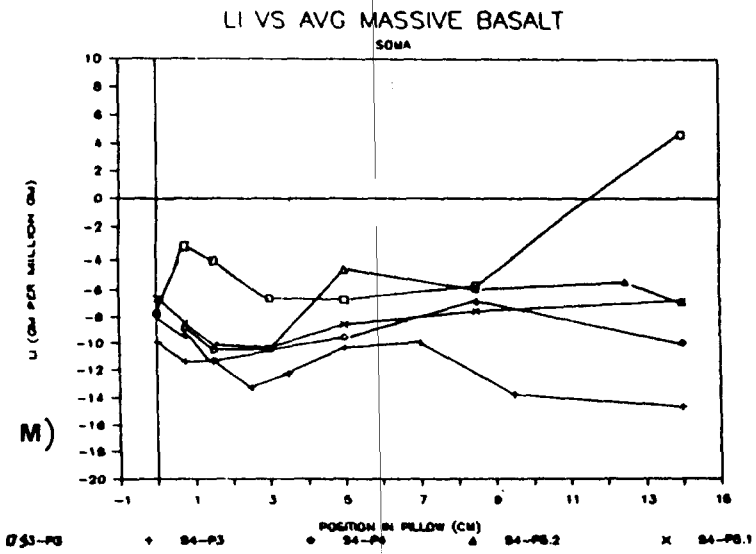

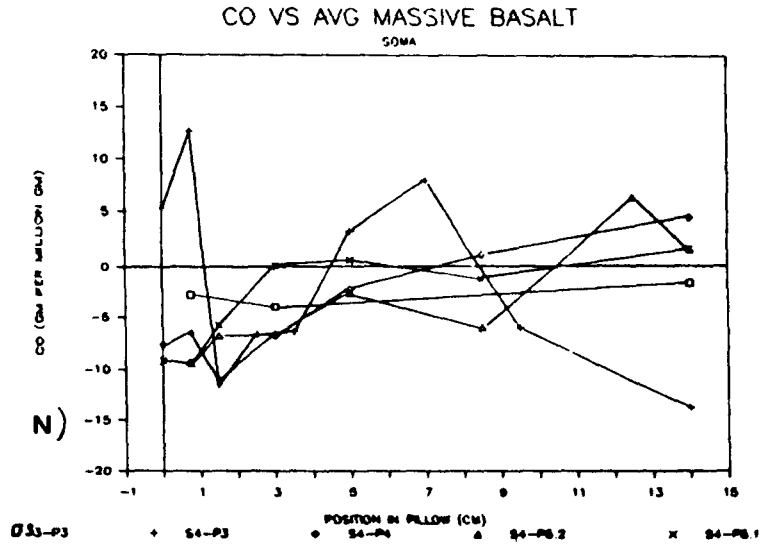

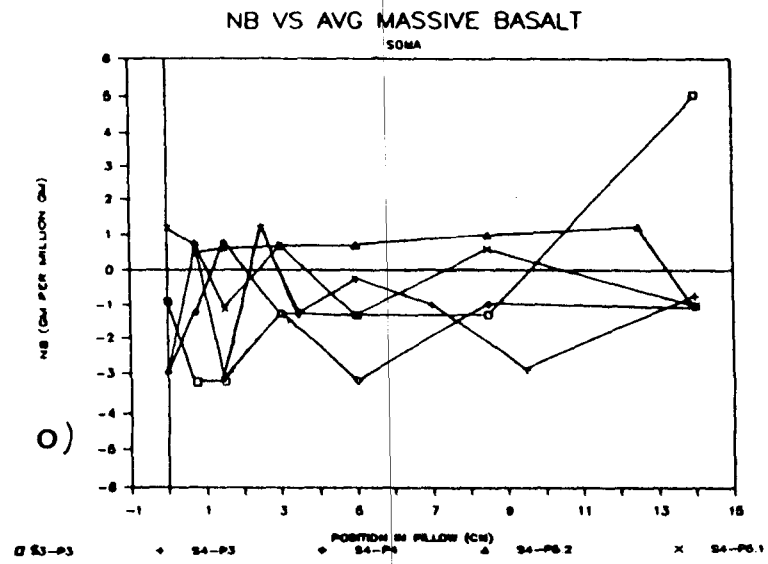

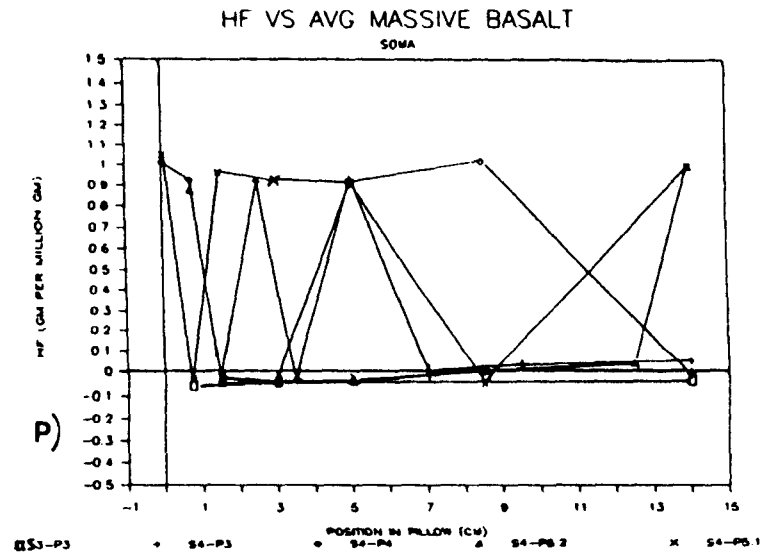

Figure 19 (continued):
(suite):

RARE EARTH ELEMENTS

The gains and losses (Table 4) and trends (figure 20) of the REE elements in the pillow cross-sections greatly resembles those of the trace elements (Table 4 and figure 19). La, Sm, Eu and Ho are constant throughout the pillow interior, while Ce and Yb exhibit positive anomalies in the interior zones of pillows SP-S4-P3 and SP-S4-P5. The anomalies in SP-S4-P3 can be attributed to the banded structure of this pillow, but the anomalies in SP-S4-P5 have no evident explanation. Nd exhibits an overall flat curve, but with a greater scatter between individual pillows than seen for the other REE's.

La, Ce, Nd and Sm exhibit negative anomalies in the vesicular zone and spherulitic rim, while Eu, Ho and Yb remain constant (figures 20). All the REE's are enriched in the hyaloclasitite (figures 20).

The REE curves (figure 9) for the Interior zones ressemble those of the massive basalts and pillow centres; that is, they are flat and 10x chondrite. The Vesicular zone (figure 9) shows no change in abundance for the HREE, but a slight depletion for the LREE. The Spherulitic rim is slightly depleted overall in REE compared to the massive basalt, and more depleted in LREE than in HREE. The Hyaloclastite is enriched in REE, possibly more so in LREE than HREE. Eu exhibits a constant positive anomaly, and Ce, Sm and Ho exhibit erratic distributions.

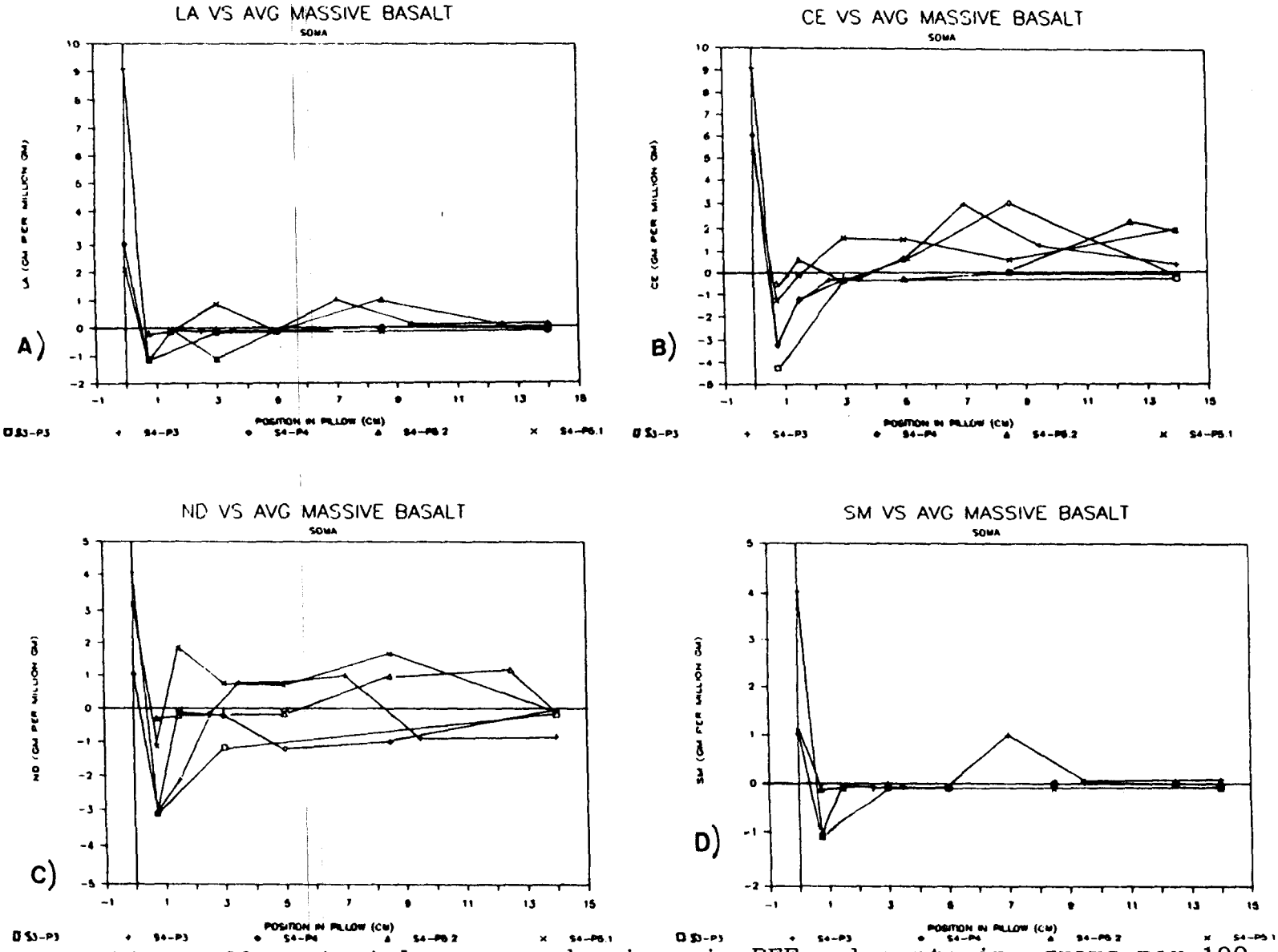

Figure 20: a)-g) Losses and gains in REE elements in grams per 100 grams calculated by the program SOMA for no volume change (FV = 1.00), and the average massive basalt as parent rock.

Pertes et les gains en éléments des terres rares calculés par le logiciel SOMA sans changement de volume (FV =1.00) et avec la moyenne des basaltes massifs comme parent.

Figure 20 (continued):
(suite):

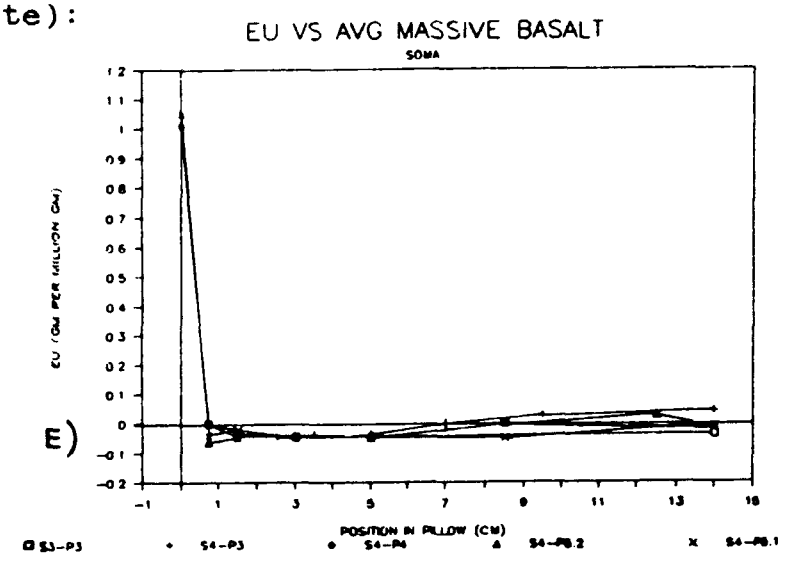

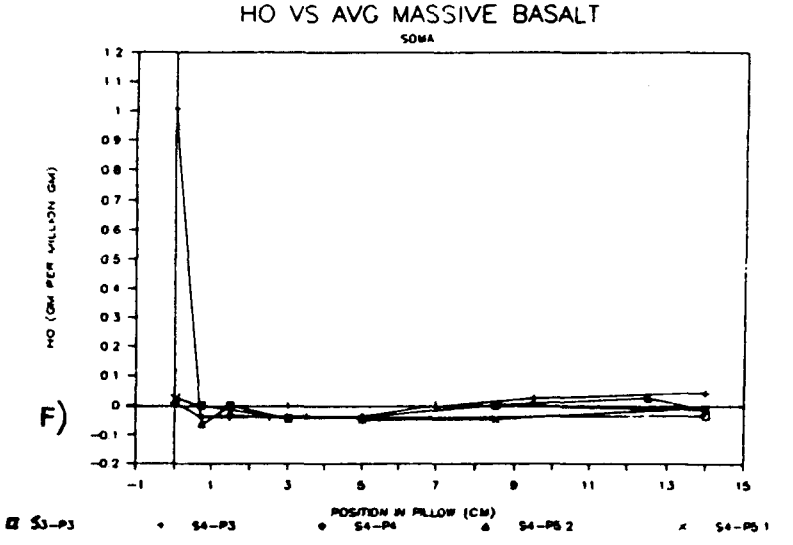

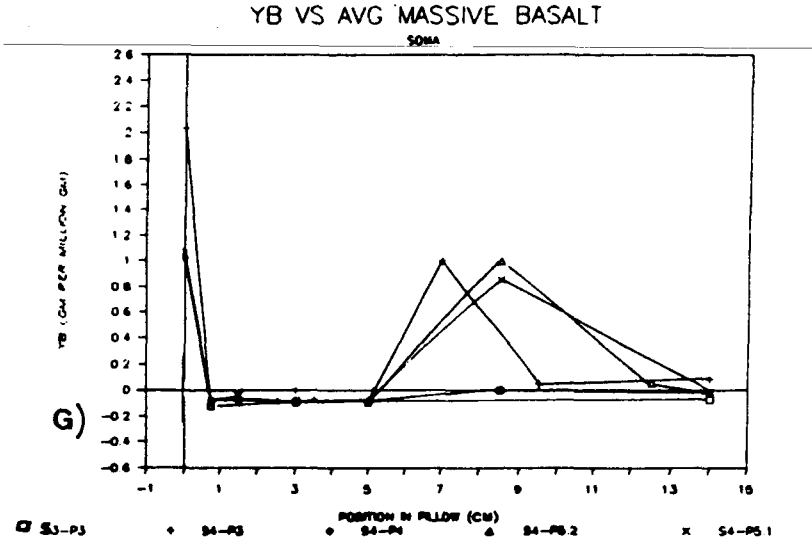

DISCUSSION

The chemical variations observed in the pillow cross-sections of this study resemble those found in other Archean basalt pillows (Baragar et al. 1979, Mellinger 1976). The differences between these variations and those observed in recent pillows (Baragar et al. 1977 and 1979, Dimroth and Lichtblau 1979, Scott and Hajash 1976, Hart 1970, Humphris and Thompson 1978, Humphris et al. 1978, Ludden and Thompson 1979, Mottl 1983) can be explained by the more complexe alteration history expected of Archean basalts.

The alteration of these pillows consists of successive and often overlapping alteration events. Beginning with the primary chemical differences expected in pillow cross-sections (Scott and Hajash 1976, Humphris et al. 1978, Kirkpatrick 1978, Baragar et al. 1977 and 1979), pillows undergo deuteric alteration or autometamorphism (Scott and Hajash 1976, Hart 1970 after Paster (1968)).

This is followed by two stages of basalt - sea water interaction. The first, halmolysis or seafloor weathering, occurs on the seafloor at low temperatures and variable Water/Rock ratios (dependant on the porosity of the rock), and results in palagonitization and smectitization of the glass and smectitization of olivine phenocrysts (Hart 1970 and 1973, Hellman et al. 1979, Ludden and Thompson, 1979, Ludden et al. 1982, Andrews 1977 and 1980, Baragar et al. 1977 and 1979, Edmond et al. 1979, Scott and Hajash 1976, Kinkhammer et al. 1983, Stakes and O'Neil 1982). The second,

sub-seafloor metamorphism, results in zeolite to greenschist facies mineral assemblages, involves increased temperature and pressure due to burial, and in most cases, hydrothermal activity (Hart 1973, Deffeyes 1970 from Hart 1973, Humphris and Thompson 1978, Humphris et al. 1978, Melson and Van Andel 1966, Michard et al. 1983, Mottl 1983, Stakes and O'Neil 1982, Stern et al. 1976, Stern and Elthon 1979). The Water/Rock ratios is again variable depending on the porosity of the rock. The spilitization observed in the submarine environment is commonly attributed to this alteration stage (Cann 1969, Munha and Kerrich 1980, Sivell and Waterhouse 1984, Stern and Elthon 1979, Stern et al. 1976, Vallance 1974, Seyfried et al. 1978).

In this simplified history of the basalt pillows studied, the final alteration event is the burial metamorphism producing prehnite-pumpellyite facies mineral assemblages. Certain authors (Hellman et al. 1979, Smith 1968, Vallance 1965) have suggested that it is at this stage that spilitization occurs.

In addition, numerous experimental studies have been performed to determine the chemical variations produced by basalt - sea water interaction at Water/Rock ratios and temperatures analogous to those expected in the surface and sub-surface oceanic regimes (Bischoff and Dickson 1975, Mottl and Holland 1978, Seyfried and Bischoff 1979 and 1981, Seyfried and Mottl 1982). These studies aid in better defining the conditions under which particular alteration phenomenon, such as spilitization, occur.

The least altered of the pillow cross-section samples are the pillow centres and Interior zones. Some of the chemical variation observed between these samples and the average massive basalt may be primary, due to lateral variations in the flow or differing crystallization histories. Scott and Hajash (1976) found MgO to be more abundant in pillow centres due to crystal fractionation of olivine. Baragar et al. (1977 and 1979) explain the higher abundances of Na_2O and SiO_2 they observed in the pillow centres as due to the fact that the centre is the final zone to crystallize. Gravity settling of the crystals fractionated from the liquid is responsible, according to Baragar et al. (1979), for erratic chemical changes observed in the interior zones of pillows. Humphris et al. (1978) have suggested that the variations in plagioclase crystallization producing spherulitic to microlitic textures may account for some of the primary variations in chemistry observed in the various textural zones. Kirkpatrick (1978), however, rejected this hypothesis in his study of the crystallization textures of basalt pillows.

Upon comparison of the pillow centre average to the massive basalt average (figure 13 and Table 2), the only variation observed, which is described above, is an increase in Na_2O. In Figure 18 (f-i), however, the erratic behavior of FeO, Fe_2O_3, MgO and Mno are evident. These variations may be of primary origin.

The first alteration phase basaltic pillows undergo on the seafloor is deuteric alteration or autometamorphism. Paster (1968 from Hart 1970) and Scott and Hajash (1976) attributed the decrease in MgO and FeO* in pillow centres to deuteric alteration. Comparison of the alteration described by Scott and Hajash (1976) (Table 3) and that seen in the pillow centre average compared to the massive basalt average, indicate only a loss in MgO to occur in the two cases. Thus, to invoke the above processes to explain the chemical variation between the interior zones (including the pillow centres) and the massive basalt average, the deuteric alteration involved would have to be fundamentally different than that observed in recent pillows. This assumption is, however, not without foundation as the chemistry of Archean seawater is unknown.

The second alteration phase is that of seawater - rock interaction at the surface (seafloor weathering or halmolysis). This alteration, consisting of palagonitization of the hyaloclastite and smectitization of the intersitial glass and olivine microphenocrysts in the pillow rim, has been described by numerous authors (Andrews 1977 and 1980, Baragar et al. 1977 and 1979, Hart 1970, Seyfried and Bischoff 1979, Bischoff and Dickson 1975, Stakes and O'Neil 1982). A resume of the chemical variations observed in the recent pillows is given in Table 3. A comparison of these alteration types to the variations in the Hyaloclastite, Spherulitic rim and Vesicular zones of this study (Table 5),shows that with the exception of the MgO loss in the

Table 5: Comparison of gains and losses in major elements due to the palagonitization of basalt glass and the smectitization of pillow rims in recent lavas, to those observed in the Hyaloclastite, the Spherulitic rim and Vesicular zone of the Kinojevis Archean pillows.

Comparaison des gains et des pertes en éléments majeurs dus à la palagonitisation du verre basaltique et la smectitisation des bordures de coussins dans les laves récentes, à ceux observés dans les Hyaloclastites, et les zones de Sphérolites et de Vacuoles des coussins archéens du Kinojévis.

	Palagonitization (Hyaloclastite)	This Study (Hyaloclastite)	Smectitization (Pillow rim)	This Study Spherulitic rim	This Study Vesicular zone
SiO2	=	-	--	+	+
Al2O3	=	+	--	-	-
FeO(T)	+		+		
Fe2O3		+		-	-
FeO		-		+	+/-
MgO	-	-	+	-	--
CaO	-	+	--	-	-
Na2O	-	-	-	++	++
K2O	+	+/-	+	-	-
MnO		+/-		+	+/-
TiO2	+	++	-	+	+/-
	Baragar et al (1979)		Andrews (1980)		

Hyaloclastite and the Al_2O_3 loss in the Spherulitic rim and Vesicular zones, the initial seafloor weathering is no longer evident.

Seafloor weathering generally produces enrichment of trace elements in pillow rims (Hart 1973, Philpotts et al. 1969 and Aumento 1971 in Hart 1973). The data of this study (Table 4) exhibit such an enrichment; the majority of the trace elements are "immobile" in the pillow interior, depleted in the vesicular and spherulitic rim zones, and enriched in the hyaloclastite (figure 19a-1). This may be considered a relict of the seafloor weathering phase of the basalt pillow alteration.

Overall enrichment in the REE elements with a greater LREE enrichement, particularly in the hyaloclastite, occurs during seafloor weathering (Hellman et al. 1979, Ludden and Thompson 1979, Ludden et al. 1982, Menzies et al. 1979, Klinkhammer et al. 1983). The REE patterns of the samples in this study, however, show slight depletion in REE toward the pillow rim with greater depletion in the LREE (figure 9). The Hyaloclastite is the exception to this trend, exhibiting the expected general, albeit erratic, enrichment in REE elements. It may be postulated that the above trend is due to the migration of the REE elements from the Vesicular and Spherulitic Rim zones to the Hyaloclastite, possibly during the seafloor weathering event.

The third alteration stage, involves the sub-surface interaction between sea-water and rock (submarine

metamorphism: diagenesis coupled with hydrothermal activity). This phase produces zeolite to greenschist facies mineral assemblages (Hart 1973, Humphris and Thompson 1978, Humphris et al. 1978, Melson and Van Andel 1966, Munha and Kerrich 1980, Seyfried et al. 1978, Vallance 1974, Baragar et al. 1977 and 1979, Stakes and O'Neil 1982, Stern et al. 1976, Stern and Elthon 1979), and the chemical changes observed are greatly affected by the Water\Rock ratio, or permeability of the rock (Munha and Kerrich 1980, Seyfried and Bischoff 1981, Seyfried and Mottl 1982, Seyfried et al. 1978, Michard et al. 1983, Mottl 1983, Stakes and O'Neil 1982). Albitization of the plagioclase, or spilitization, is commonly attributed to this alteration phase (Munha and Kerrich 1980, Seyfried and Bischoff 1981, Seyfried et al. 1978, Vallance 1974, Stern et al. 1976, Stern and Elthon 1979, Hellman and Henderson 1977). Spilitization is here considered to be a sub-surface phenomenon, as comparisons of experimental results on sea-water - basalt interaction (Table 6) show that the chemical variations due to spilitization at a water/rock ratio of 10 (orthospilitization: spilitization of crystalline basalt; Cann 1969), resemble those of seawater - basalt interaction at 500bars and 200-400°C. The water/rock ratio of 62 in Table 6 represents hyalospilitization, or spilitization of hyaloclastite.

In this study, orthospilitization is observed in the Spherulitic rim and Vesicular zones of the pillows (Table 7). The Pillow Centres and Interior Zones do not, on the other hand, show systematic losses and gains in CaO and Na_2O,

Table 6: Comparison of gains and losses in major elements for seawater - basalt interaction at 500 bars and temperatures of 0-20°C and 200-400°C to experimental albitization (spilitization) at Water/Rock ratios of 10 and 62.

Comparaisons des gains et pertes en éléments majeurs dus à l'interaction eau de mer - basalte à 500 bars pour des températures de 0-20°C et 200-400°C, à ceux dus à l'albitisation (spilitisation) expérimentale pour un rapport eau/roche de 10 et 62.

	Seawater-Basalt Interaction (500 bars)		Spilitization (Albitization)	
	0-20	200-400	W/R=10	W/R=62
SiO2	-	-	-	-
Al2O3				
FeO(T)	-	+/-	-	+
MgO	+/-	+	+	+
CaO	-	-	-	-
Na2O	+/-	+	+	-
K2O	+	-	-	-
MnO	-	-		
TiO2				
	Wolery & Sleep (1976)		Seyfried et al (1978)	

respectively, and cannot, therefore, be considered spilites (Table 4). These oxides do, however, exhibit progressive decreases (CaO) and increases (Na_2O) toward the vesicular zone, indicating a progressive albitization (figure 18b and c). The chemical variations observed in orthospilites and those of the Spherulitic rim and Vesicular zones from this study correspond with the exception of MgO. The Spherulitic rim corresponds better than the Vesicular zone, again indicating that the spilitization progressed from the margin of the pillow toward the centre.

The hyalospilite and hyaloclastite of this study differ in their losses and gains in Al_2O_3, MgO and CaO (Table 7). This can be explained by the epidotization rather than chloritization of the hyaloclastite. Epidotization is generally interpreted as being due to the redistribution of CaO in the rock (Baragar et al. 1977, Humphris and Thompson 1978, Humphris et al. 1978, Melson and Van Andel 1966). Melson and Van Andel (1966), and Seyfried and Bischoff (1981), however, place the appearance of epidote at 300°-500°C and 3-8 kbars; whereas, spilitization occurs at 200°-400°C and 500 bars (Table 6). Thus the epidotization event occurs later than the spilitization at greater depths of burial.

The behavior of REE elements during sub-surface hydrothermal alteration and spilitization is contradictory in the literature. Michard et al. (1983) found that REE elements, and particularly LREE elements were leached from basalt during hydrothermal activity. Hellman and Henderson

(1977) and Hellman et al. (1979) found spilites to be enriched in REE elements, LREE being more enriched than HREE. This behavior is similar to that observed by Ludden and Thompson (1978) for seafloor weathering. Humphris et al. (1978), and Williams and Floyd (1981) suggest that the REE elements are redistributed within the rock during this phase. An increase in mobility with increasing glass abundance, and higher mobility of the LREE elements is used by Humphris et al. (1978) to explain the greater enrichment in REE elements observed in the Hyaloclastite of pillows. Menzies et al. (1979) found the REE elements to be immobile at 150°-350°C and Water\Rock ratios of 10-125 (the temperature and Water\Rock ratio expected during spilitization of both crystalline and vitric basalt; Table 7).

The Spherulitic rim and Vesicular zones of this study (figure 9) exhibit a depletion in REE elements in general and LREE elements in particular, as predicted by Michard et al. (1983). The enrichment of REE elements in the Hyaloclastite may be seen as due to the deposition of the REE leached from the rest of the pillow, with epidote and chlorite accomodating REE elements in their crystal structures (Hellman and Henderson 1977, Humphris et al. 1978).

The final alteration phase of the basalt pillows is the prehnite - pumpellyite facies metamorphism, which may be responsible for the redistribution of some elements (Hellman et al. 1977, Smith 1968, Baragar et al. 1979). For example, the epidotization of the hyaloclastite may be in part metamorphic (Baragar et al. 1979). The overall chemical

variations produced by this phase should, however, be minimal.

Table 7: Comparison of the gains and losses in major elements for ortho- and hyalo-spilites, to those for the Vesicular, Spherulitic rim and Hyaloclastite zones of the pillows in this study.

Comparaison des gains et des pertes en éléments majeurs dans les ortho- et hyalo-spilites, à ceux des zones de Vacuoles, de Sphérolites et d'Hyaloclastites des coussins observés dans cette étude.

	Spilitization (Albitization) Orthospilite	This Study Vesicular zone	This Study Spherulite rim	Spilitization (Albitization) Hyalospilite	This Study Hyaloclastite
SiO2	+	+	+	-	-
Al2O3	-	-	-	-	+
FeO(T)	-			+	
Fe2O3		-	-		+
FeO		+/-	+		-
MgO	+	--	-	+	-
CaO	-	-	-	-	+
Na2O	+	++	++	-	-
K2O	-	-	-	-	+/-
MnO	+	+/-	+	-	+/-
TiO2	+	+/-	+	+	++
	Seyfried et al (1978)			Seyfried et al (1978)	

CONCLUSIONS

The pillows studied in this work are extremely well-preserved prehnite - pumpellyite facies tholeiitic meta-basalts, exhibiting the textural zones observed in recent pillows. These zones are the result of undercooling of the pillow producing skeletal quench crystals and spherulitic overgrowths.

The chemical variations observed between different zones within individual pillows is greater than that seen between specific zones within different pillows. The chemical characteristics of the zones are considered to be a function of their alteration history rather than primary variations.

The successive alteration phases envisioned for Archean basalt pillows are:

1) deuteric alteration of the pillow centre and interior zones: This decreases MgO and FeO* abundances in the pillow interior. Only MgO depletion is observed in the pillow centres of this study, and the possibility that this is a primary variation cannot be ignored.

2) seafloor weathering (water - rock interaction on the seafloor; halmolysis): The chemical effects on major, trace and REE element abundances of this phase are no longer observed in the pillow cross-sections, with the possible exception of the enrichment of trace and REE elements in the hyaloclastite. The mineralogical changes produced at this stage will, however, partially control the succeeding alterations.

3) submarine metamorphism (or sub-seafloor water - rock interaction): This phase produces a progressive albitization (spilitization) from the Spherulitic rim, decreasing toward the Pillow Centre. The albitization is complete in the Vesicular zone and Spherulitic rim, and the REE elements, particularly the LREE's, are depleted. The Hyaloclastite, however, does not exhibit the chloritization and depletion in REE expected of hyalospilites; the enrichment of REE elements in the hyaloclastite may be a relic of the preceding seafloor weathering or may be attributed to the deposition of the REE's leached from the Spherulitic rim and Vesicular zone during spilitization.

4) The final alteration stage is the regional prehnite-pumpellyite facies metamorphism. This stage produces the present mineralogy, but should not produce more than minor chemical changes.

Thus, while it is evident from recent submarine basalt pillow studies that Archean basalt pillows have undergone multiple alteration events, the geochemical variation presently observed in the pillows studied here are, for the most part, the result of a sub-surface hydrothermal event. The primary chemical variations in the basalt pillows, and the results of deuteric alteration and seafloor weathering, cannot be distinguished through the overprint of the submarine metamorphism, and the prehnite-pumpellyite facies regional metamorphism is responsible for only minor redistribution of the elements within the pillow.

ACKNOWLEDGEMENTS

I wish to thank Dr. A.D. Fowler and the late Dr. Erich Dimroth for the conception of this project, and their guidance in the field and during the initial stages of this project. I owe a debt of gratitude to Dr. Gerard Woussen for accepting the direction of this project, and for his assistance and patience in its realisation. I also wish to thank Dr. Jacques Carignan for his assistance throughout the project, and the technicians of the Université du Québec à Chicoutimi for the various preparations involved in this thesis. Sylvain Lacroix, Dr. Gerard Woussen and Dr. Pierre Verpaelst must be given the credit for the readability of the French texts; je les remercie.

Financing of this project was supplied by an E.M.R. grant to Drs. Erich Dimroth and Michel Rocheleau, and funding to the student was provided by an F.C.A.R. Student Scholarship (1984 - 1986) and two U.Q.A.C. Bourses d'Excellence (1985 and 1986).

REFERENCES

ANDREWS, A.J., 1977. Low temperature fluid alteration of oceanic layer 2 basalts, DSDP Leg 37. Canadian Journal of Earth Sciences, v.14, p.911-926.

ANDREWS, A.J., 1980. Saponite and Celadonite in Layer 2 basalts, DSDP Leg 37. Contributions to Mineralogy and Petrology, v.73, p. 323-340.

APPLEYARD, E.C. and de Beer, C.J., 1982. SOMA - A package of fortran IV programs for calculating mass exchange in metasomatic and altered rocks. University of Waterloo, Technical communication 70, pp.75 and CYBER program.

AUMENTO, F., 1971. Uranium content of mid-oceanic basalts. Earth and Planetary Science Letters, v.11, p.1-21.

BARAGAR, W.R.A., Plant, A.G., Pringle, G.J. and Schau, M., 1977. Petrology and alteration of selected units of Mid-Atlantic Ridge basalts sampled from sites 332 and 335, DSDP. Canadian Journal of Earth Sciences, v.14, p.837-874.

BARAGAR, W.R.A., Plant, A.G., Pringle, G.J. and Schau, M., 1979. Diagenetic and postdiagenetic changes in the composition of an Archean pillow. Canadian Journal of Earth Sciences, v.16, p. 2101-2121.

BARTLEY, J.M., 1986. Evaluation of REE mobility in low-grade metabasalts using mass-balance calculations. Norsk Geilogisk Tidsskrift, v.66, p.145-152.

BISCHOFF, J.L. and Dickson, F.W., 1975. Seawater - basalt interaction at 200°C and 500 bars: Implications for origin of sea-floor heavy-metal deposits and regulation of seawater chemistry. Earth and Planetary Science Letters, v.25, p.385-397.

CANN, J.R., 1969. Spilites from the Carlsberg Ridge, Indian Ocean. Journal of Petrology, v.10, p. 1-19.

CARR, M.J., 1987. IGPET-II. pp. 18 and I.B.M.-PC program.

COX, K.G., Bell, J.D. and Pankhurst, R.J., 1979. The interpretation of igneous rocks. Appendix 2. George Allen and Unwin Ltd. pp. 450.

DEFFEYES, K.S., 1970. The acial valley; a steady-state feature of terrain. IN: Johnson, C.H. and Smith, B.C. (eds.),The megatectonics of continenets and oceans. Rutgers University Press, N.J., p.194-222.

DIMROTH, E. and Lichtblau, 1979. Metamorphic evolution of Archean hyaloclastites, Noranda area, Quebec, Part I: Comparison of Archean and Cenozoic sea-floor metamorphism. Canadian Journal of Earth Science. v.16, p. 1315-1340.

DIMROTH, E., Boivin, P., Goulet, N. and Larouche, M., 1973. Tectonic and volcanological studies in the Rouyn-Noranda area. Ministère des Richesse Naturel du Québec, Rapport Finale, GM28491, 59pp.

DIMROTH, E., Imreh, L., Rocheleau, M. and Goulet, N., 1983. Evolution of the south-central segment of the Archean Abitibi Belt, Québec. Part III: Plutonic and metamorphic evolution and geotectonic model. Canadian Journal of Earth Sciences, v.20, p.1374-1388.

EDMONDS, J.M., Measures, C., McDuff, R.E., Chan, L.H., Collier, R., Grant, B., Gordon, L.I. and Corliss, J.B., 1979. Ridge crest hydrothermal activity and the balances of the major and minor elements in the ocean: The Galapagos data. Earth and Planetary Science Letters, v.46, p.1-18.

GELINAS, L., Trudel, P. and Hubert, C., 1984. Chemo-stratigraphic division of the Blake River Group, Rouyn-Noranda area, Abitibi Québec. Canadian Journal of Earth Sciences, v.21, p.220-231.

GRESENS, R.L., 1967. Composition-volume relationships of metasomatism. Chemical Geology. v.2, p. 47-65.

HART, R., 1970. Chemical exchange between sea water and deep ocean basalts. Earth and Planetary Science Letters, v.9, p.269-279.

HART, R.A., 1973. A model for chemical exchange in the basalt - seawater system of oceanic layer II. Canadian Journal of Earth Sciences, v.10, p.799-816.

HELLMAN, P.L. and Henderson, P., 1977. Are rare earth elements mobile during spilitisation? Nature, v.267, p.38-40.

HELLMAN, P.L., Smith, R.E. and Henderson, P., 1979. The mobility of the Rare Earth Elements: Evidence and implications from selected terrains affected by burial metamorphism. Contributions to Mineralogy and Petrology, v.71, p.23-44.

HUMPHRIS, S.E. and Thompson, G., 1978. Hydrothermal alteration of oceanic basalts by seawater. Geochimica et Cosmochimica Acta, v.42, p.107-125.

HUMPHRIS, S.E., Morrison, M.A. and Thompson, R.N., 1978. Influence of rock crystallization history upon subsequent Lanthanide mobility during hydrothermal alteration of basalts. Chemical Geology, v.23, p.125-137.

IRVINE, T.N. and Baragar, W.R.A., 1971. A guide to the chemical classification of the common volcanic rocks. Canadian Journal of Earth Sciences. v.8, p. 523-548.

KIRKPATRICK, R.J., 1978. Processes of crystallization in pillow basalts, Hole 396B, D.S.D.P. Leg 46. IN: Dmitriev, L., Hurtler, J. et al. (eds.), Initial Reports of the D.S.D.P., v.46, p. 271-282.

KLINKHAMMER, G., Elderfield, H. and Hudson, A., 1983. Rare earth elements in seawater near hydrothermal vents. Nature, v.305, p.185-188.

LEDUC, M., 1981. Morphologie des facies volcaniques et structures associees a des coulees basaltiques du Groupe de Kinojevis, canton d'Aiguebelle, Abitibi. Université du Québec à Chicoutimi, Memoire de Maitrise. pp. 169.

LUDDEN, J.N. and Thompson, G., 1979. An evaluation of the behavior of the rare earth elements during the weathering of sea-floor basalt. Earth and Planetary Science Letters, v.43, p.85-92.

LUDDEN, J.N., Gélinas, L. and Trudel, P., 1982. Archean metavolcanics from the Rouyn-Noranda district, Abitibi Greenstone Belt, Quebec. 2. Mobility of trace elements and petrogenetic constraints. Canadian Journal of Earth Sciences, v.19, p.2276-2287.

MELLINGER, M., 1976. Etude de l'altération de laves mafiques archeennes en pillows, dans la region de Rouyn-Noranda (Abitibi, Québec). Memoire de Maîtrise, Université de Montréal, pp. 208.

MELSON, W.G and Van Andel, Tj.-H., 1966. Metamorphism in the Mid-Atlantic Ridge, 22°N latitude. Marine Geology, v.4, p.165-186.

MENZIES, M., Seyfried, W. and Blanchard, D., 1979. Experimental evidence of rare earth element immobility in greenstones. Nature, v.282, p.398-399.

M.E.R.Q. and O.G.S., 1983. Lithostratigraphic map of the Abitibi Sub-Province, 1: 500 000. M.E.R.Q. DV-83-16; O.G.S. Map 2484.

MICHARD, A., Albarede, F., Michard, G., Minster, J.F. and Charlou, J.L., 1983. Rare-earth elements and uranium in high-temperature solutions from East Pacific Rise hydrothermal vent field (13°N). Nature, v.303, p.795-797.

MIYASHIRO, A., 1974. Volcanic rock series in island arcs and active continental margins. American Journal of Science. v.274, p. 321-355.

MOTTL, M.J., 1983. Metabasalts, axial hot springs, and the structure of hydrothermal systems at mid-ocean ridges. Geological Society of America Bulletin, v.94, p.161-180.

MOTTL, M.J. and Holland, H.D., 1978. Chemical exchange during hydrothermal alteration of basalt by seawater - I. Experimental results for major and minor components of seawater. Geochimica et Cosmochimica Acta, v.423, p.1103-1115.

MULLEN, E.D., 1983. $MnO/TiO_2/P_2O_5$: a minor element discriminant for basaltic rocks of oceanic environments and its implications for petrogenesis. Earth and Planetary Science Letters. v.62, p. 53-62.

MUNHA, J. and Kerrich, R., 1980. Sea water basalt interaction in spilites from the Iberian Pyrite Belt. Contributions to Mineralogy and Petrology, v.73, p.191-200.

NATLAND, J.H., 1978. Crystal morphologies in basalts from D.S.D.P. site 395, 23°N, 46°W, Mid-Atlantic Ridge. IN: Melson, W.G., Rabinowitz, P.D. et al. (eds.), Initial Reports of the D.S.D.P., v.45, p. 423-445.

NATLAND, J.H., 1980. Crystal morphologies in basalts dredged and drilled from the East Pacific Rise near 9°N and the Siqueiros fracture zone. IN: Rosendahl, B.R., Hekinian, R. et al. (eds.), Initial Reports of the D.S.D.P., v.54, p. 605-633.

NOCKOLDS, S.R., Knox, R.W.O'B. and Chinner, G.A., 1979. Petrology for students. Table 12.1. Cambridge University Press. pp.435.

PASTER, T.P., 1968. Petrologic variations within submarine basalt pillows of the South Pacific-Antarctic Ocean. Unpublished Ph.D. dissertation, Florida State University, Tallahassee.

PEARCE, J.A, and Cann, J.R., 1973. Tectonic setting of basic volcanic rocks determined using trace element analyses. Earth and Planetary Science Letters. v.19, p. 290-300.

PHILPOTTS, J.A., Schnetzler, C.C. and Hart, S.R., 1969. Submarine basalts: some K, Rb, Sr, Ba, rare earth, H_2O and CO_2 data bearing on their alteration, modification by plagioclase, and possible source materials. Earth and Planetary Science Letters, v.7, p.293-299.

POLDERVAART, A.P., 1953. Petrological calculations in metasomatic processes. American Journal of Science. v.251, p. 481-504.

SANSCHAGRIN, Y., 1981. Etude des variations laterales et verticales de facies dans les coulees de basalte tholeiitiques du Groupe de Kinojevis, canton d'Aiguebelle, Abitibi. Université du Québec à Chicoutimi, Memoire de Maitrise. pp. 114.

SANSCHAGRIN, Y. and Leduc, M., 1979. Quart sud-est du canton d'Aiguebelle. Ministere des Richesse Naturelles du Quebec, Rapport Final, DPV-676. pp.42.

SCHILLING, J.-G. and Winchester, J.W., 1967. Rare-earth fractionation and magmatic processes. IN: Runcorn, S.K. (ed.), Mantles of the Earth and terrestrial planets. John Wiley and Sons, p. 267-283.

SCOTT, R.B. and Hajash, A. Jr., 1976. Initial submarine alteration of basaltic pillow lavas: A microprobe study. American Journal of Science, v.276, p. 480-501.

SEYFRIED, W.E. Jr. and Bischoff, J.L., 1979. Low temperature basalt alteration by seawater: an experimental study at 70°C and 150°C. Geochimica Cosmochimica Acta, v.43, p.1937-1947.

SEYFRIED, W.E. Jr. and Bischoff, J.L., 1981. Experimental seawater - basalt interaction at 300°C, 500 bars, chemical exchange, secondary mineral formation and implications for the transport of heavy metals. Geochimica Cosmochimica Acta, v.45, p.135-147.

SEYFRIED, W.E. Jr. and Mottl, M.J., 1982. Hydrothermal alteration of basalt by seawater under seawater-dominated conditions. Geochimica Cosmochimica Acta, v.46, p.985-1002.

SEYFRIED, W.E. Jr., Mottl, M.J. and Bischoff, J.L., 1978. Seawater/basalt ratio effects of the chemistry and mineralogy of spilites from the ocean floor. Nature. v.275, p. 211-213.

SIVELL, W.J. and Waterhouse, J.B., 1980. Oceanic ridge metamorphism of the Patuki Volcanics, D'Urville Island, New Zealand. Lithos, v.17, p.19-36.

SMITH, R.E., 1968. Redistribution of major elements in the alteration of some basic lavas during burial metamorphism. Journal of Petrology, v.9, p.191-219.

STAKES, D.S. and O'Neil, J.R., 1982. Mineralogy and stable isotope geochemistry of hydrothermally altered oceanic rocks. Earth and Planetary Science Letters, v.57, p.285-304.

STERN, C. and Elthon, D., 1979. Vertical variations in the effects of hydrothermal metamorphism in Chilean ophiolites: Their implications for ocean floor metamorphism. Tectonophysics, v.55, p.179-213.

STERN, C., De Wit, M.J. and Lawrence, J.R., 1976. Igneous and metamorphic processes associated with the formation of Chilean ophiolites and their implication for ocean floor metamorphism, seismic layering, and magnetism. Journal of Geophysical Research, v.81, #23, p.4370-4380.

VALLANCE, T.G., 1965. On the chemistry of pillow lavas and the origin of spilites. Mineralogical Magazine, p.471-481.

VALLANCE, T.G., 1974. Spilitic degradation of a tholeiitic basalt. Journal of Petrology, v.15, p.79-96.

WILLIAMS, C.T. and Floyd, P.A., 1981. The localised distribution of U and other incompatible elements in spilitic pillow lavas. Contributions in Mineralogy and Petrology, v.78, p.111-117.

WOLERY, T.J. and Sleep, N.H., 1976. Hydrothermal circulation and geothermal flux at mid-ocean ridges. Journal of Geology. v.84, p. 249-275.

ANNEXE I

Tables of chemical analyses[1]

Massive basalts
and
Pillow cross-sections

(Tableaux des analyses chimiques
Basaltes massifs
et
Sections des coussins)

[1] All Tables generated by the computer program IGPET II (Carr, 1987).

Table I: Major element analyses and C.I.P.W norms for massive basalt samples, including the average of the analyses.

Analyses des éléments majeurs, et norme C.I.P.W. des échantillons de basaltes massifs, et la moyenne des analyses.

Nom de la filiere C:83-M5.ROC

Echantillon	83-2	83-5	83-6	83-8	83-10	83-11	83-13	83-14	83-15	AVGE
Litho.										
Qualite										
Code	1	1	1	1	1	1	1	1	1	0
Unite										
SiO2	49.52	49.33	49.61	50.59	49.78	50.40	49.80	49.72	50.59	49.95
TiO2	0.82	0.88	0.84	0.82	0.73	0.77	0.76	0.70	0.67	0.78
Al2O3	15.67	15.40	16.16	16.33	15.83	16.07	15.96	15.95	15.73	15.90
Fe2O3	5.54	5.58	4.29	5.24	5.60	5.18	4.30	6.10	5.33	5.24
FeO	7.55	8.25	8.48	8.40	7.57	7.78	8.76	7.30	7.80	7.99
MnO	0.19	0.20	0.17	0.18	0.18	0.18	0.18	0.18	0.18	0.18
MgO	8.03	7.45	8.02	7.50	7.44	7.13	8.06	7.77	7.82	7.69
CaO	10.25	10.69	9.94	8.81	10.96	10.19	9.80	10.18	9.81	10.07
Na2O	1.63	1.24	1.30	1.17	1.08	1.49	1.45	1.31	1.35	1.34
K2O	0.27	0.22	0.68	0.43	0.25	0.24	0.44	0.25	0.20	0.33
P2O5	0.54	0.57	0.50	0.50	0.59	0.54	0.50	0.55	0.52	0.54
Total	100.01	100.01	99.99	99.97	100.01	99.97	100.01	100.01	100.00	100.01
AN	71.52	77.34	76.72	79.35	80.45	74.30	74.44	76.90	76.05	76.25
Q	5.56	7.68	4.73	9.42	8.59	8.03	4.87	8.02	8.54	7.27
or	1.60	1.30	4.02	2.54	1.48	1.42	2.60	1.48	1.18	1.95
ab	13.79	10.49	11.00	9.90	9.14	12.61	12.27	11.08	11.42	11.34
an	34.65	35.81	36.25	38.04	37.61	36.45	35.74	36.90	36.27	36.40
di	10.21	10.94	7.95	1.95	10.43	8.57	7.81	8.05	7.27	8.12
hy	23.36	22.71	27.07	27.81	21.90	22.68	27.88	23.02	25.11	24.61
mt	8.03	8.09	6.22	7.60	8.12	7.51	6.23	8.84	7.73	7.60
il	1.56	1.67	1.60	1.56	1.39	1.46	1.44	1.33	1.27	1.48
ap	1.25	1.32	1.16	1.16	1.37	1.25	1.16	1.27	1.20	1.25
D(M)	3.04	3.11	3.06	3.03	3.10	3.11	3.05	3.07	3.07	3.07
FeO*	12.54	13.27	12.34	13.12	12.61	12.44	12.63	12.79	12.60	12.71
F/F+M	0.613	0.644	0.609	0.639	0.632	0.639	0.614	0.625	0.620	0.626
den	2.67	2.68	2.68	2.66	2.67	2.66	2.68	2.67	2.66	2.67

Nom de la filiere C:\83MJTRE.ROC

Echantillon	83-2	83-6	83-11	83-13	83-14	AVGE
Litho.						
Qualite						
Code	1	1	1	1	1	0
Unite						
SiO2	49.52	49.61	50.40	49.80	49.72	49.95
TiO2	0.82	0.84	0.77	0.76	0.70	0.78
Al2O3	15.67	16.16	16.07	15.96	15.95	15.90
Fe2O3	5.54	4.29	5.18	4.30	6.10	5.24
FeO	7.55	8.48	7.78	8.76	7.30	7.99
MnO	0.19	0.17	0.18	0.18	0.18	0.18
MgO	8.03	8.02	7.13	8.06	7.77	7.69
CaO	10.25	9.94	10.19	9.80	10.18	10.07
Na2O	1.63	1.30	1.49	1.45	1.31	1.34
K2O	0.27	0.68	0.24	0.44	0.25	0.33
P2O5	0.54	0.50	0.54	0.50	0.55	0.54
Total	100.01	99.99	99.97	100.01	100.01	100.01
B	18.5	27.0	22.0	26.0	21.0	22.8
BA	90.0	230.0	100.0	160.0	100.0	136.0
CR	253.3	245.0	260.0	246.5	255.0	252.0
LI	21.0	22.0	18.0	21.0	21.0	20.6
NB	8.0	6.0	6.0	8.0	8.0	6.8
PB	6.0	6.0	4.0	4.0	6.0	5.2
RB	12.0	22.0	12.0	16.0	12.0	14.8
SR	140.0	88.0	150.0	84.0	130.0	118.4
Y	18.0	22.0	20.0	22.0	22.0	20.8
ZR	57.0	60.0	60.0	60.0	58.0	59.0
CS	0.3	0.2	0.8	0.5	0.4	0.4
SC	45.1	42.2	46.7	42.9	45.7	44.5
HF	1.4	1.2	1.3	1.3	1.4	1.3
CO	47.5	38.0	47.0	47.0	45.0	44.9
TH	0.4	0.2	0.3	0.2	0.2	0.3
TA	0.1	0.1	0.1	0.2	0.1	0.1
ZN	132.5	112.0	113.5	106.5	111.0	115.1
CU	68.0	57.0	97.0	78.0	73.0	74.6
NI	243.0	153.0	136.0	213.0	163.0	181.6
LA	3.0	3.1	2.8	4.0	3.1	3.2
CE	8.0	8.5	9.0	6.8	8.0	8.1
ND	5.5	5.0	4.7	6.5	5.7	5.5
SM	2.0	2.1	1.9	2.7	2.1	2.2
EU	0.8	0.6	0.8	0.8	0.7	0.7
TB	0.5	0.4	0.5	0.5	0.5	0.5
HO	0.6	0.7	0.5	1.1	0.6	0.7
YB	2.2	2.0	2.0	2.4	2.3	2.2
LU	0.3	0.3	0.3	0.3	0.3	0.3
D(M)	3.04	3.06	3.11	3.05	3.07	3.07
FeO*	12.54	12.34	12.44	12.63	12.79	12.71
F/F+M	0.613	0.609	0.639	0.614	0.625	0.626
Rb/Sr	0.086	0.250	0.080	0.190	0.092	0.125
K/Rb	187	257	166	228	173	185
K/Ba	24.9	24.5	19.9	22.8	20.8	20.1
den	2.67	2.68	2.66	2.68	2.67	2.67

Table II: Major, trace and REE element analyses for the massive basalt samples, including the average of the analyses.

Analyses des éléments majeurs, traces et des terres rares des échantillons de basaltes massifs, et la moyenne des analyses.

Table III: Major element analyses and C.I.P.W. norms for pillow centre samples, including the average of the analyses.

Analyses des éléments majeurs, et norme C.I.P.W. des échantillons des centres de coussins et la moyenne des analyses.

Nom de la filiere	C:PILCENT.ROC							
Echantillon	83P2C	83P3C	83P4C	84P2C	84P3C	84P4C	84P5C	PCAVG
Litho.								
Qualite								
Code	2	2	2	2	2	2	2	3
Unite					0			
SiO2	50.39	53.57	49.73	50.00	48.76	51.67	47.96	50.30
TiO2	0.86	0.96	0.76	0.55	0.78	0.90	0.62	0.78
Al2O3	15.60	13.87	14.97	15.37	15.93	14.47	15.88	15.16
Fe2O3	5.96	5.08	7.02	5.19	6.98	5.67	4.86	5.83
FeO	8.78	8.24	5.58	9.24	5.60	7.63	8.64	7.67
MnO	0.19	0.19	0.18	0.19	0.18	0.18	0.22	0.19
MgO	6.33	6.00	4.76	6.30	4.35	6.53	6.07	5.76
CaO	9.61	8.72	15.45	10.09	16.00	11.05	12.81	11.96
Na2O	1.86	3.04	1.10	2.83	1.06	1.65	2.14	1.95
K2O	0.13	0.22	0.05	0.05	0.00	0.05	0.12	0.09
P2O5	0.29	0.13	0.39	0.18	0.38	0.20	0.67	0.32
Total	100.00	100.02	99.99	99.99	100.02	100.00	99.99	100.01
AN	68.25	47.80	79.35	54.85	81.19	69.58	64.82	66.22
Q	7.83	7.44	10.71	1.60	9.52	9.97	0.90	6.88
or	0.77	1.30	0.30	0.30	0.00	0.30	0.71	0.53
ab	15.74	25.72	9.31	23.95	8.97	13.96	18.11	16.50
an	33.84	23.55	35.76	29.09	38.71	31.93	33.37	32.35
di	9.74	15.39	30.65	16.24	30.07	17.48	21.14	20.25
hy	21.14	17.13	0.74	19.84	0.00	15.97	15.98	12.83
wo	0.00	0.00	0.00	0.00	0.27	0.00	0.00	0.00
mt	8.64	7.37	10.18	7.53	10.12	8.22	7.05	8.45
il	1.63	1.82	1.44	1.04	1.48	1.71	1.18	1.48
ap	0.67	0.30	0.90	0.42	0.88	0.46	1.55	0.74
D(M)	2.95	2.96	3.12	2.94	3.20	3.04	3.05	3.04
FeO*	14.14	12.81	11.90	13.91	11.88	12.73	13.01	12.92
F/F+M	0.694	0.684	0.717	0.691	0.735	0.664	0.686	0.695
den	2.67	2.63	2.66	2.67	2.67	2.66	2.69	2.66

Table IV: Major, trace and REE element analyses for the pillow centre samples, including the average of the analyses.

Analyses des éléments majeurs, traces et des terres rares des échantillons des centres de coussins et la moyenne des analyses.

Nom de la filiere C:\PCMTREE.ROC

Echantillon	93P3C	84P3C	84P4C	84P5C	PCAVG
Litho.					
Qualite					
Code	2	2	2	2	3
Unite		0			
SiO2	53.57	48.76	51.67	47.96	50.30
TiO2	0.96	0.78	0.90	0.62	0.78
Al2O3	13.87	15.93	14.47	15.88	15.16
Fe2O3	5.08	6.98	5.67	4.86	5.83
FeO	8.24	5.60	7.63	8.64	7.67
MnO	0.19	0.18	0.18	0.22	0.19
MgO	6.00	4.35	6.53	6.07	5.76
CaO	8.72	16.00	11.05	12.81	11.96
Na2O	3.04	1.06	1.65	2.14	1.95
K2O	0.22	0.00	0.05	0.12	0.09
P2O5	0.13	0.38	0.20	0.67	0.32
Total	100.02	100.02	100.00	99.99	100.01
B	12.0	33.0	15.0	12.0	18.0
BA	100.0	60.0	90.0	60.0	77.5
CR	290.0	250.0	280.0	260.0	270.0
LI	17.0	6.0	11.0	14.0	12.0
NB	2.0	6.0	6.0	6.0	5.0
PB	16.0	0.0	6.0	4.0	6.5
RB	20.0	14.0	18.0	8.0	15.0
SR	84.0	250.0	140.0	100.0	143.5
Y	16.0	12.0	16.0	22.0	16.5
ZR	57.0	51.0	54.0	56.0	54.5
CS	0.3	0.0	0.2	0.2	0.2
SC	47.0	40.0	43.0	45.6	43.9
HF	1.3	1.3	1.3	1.6	1.4
CO	45.0	30.0	50.0	47.0	43.0
TH	0.3	0.2	0.3	0.2	0.3
TA	0.2	0.1	0.2	0.2	0.2
ZN	80.5	54.5	94.0	106.0	83.8
CU	100.0	76.0	97.0	85.0	89.5
NI	110.0	84.0	110.0	198.0	125.5
LA	3.4	2.7	3.1	3.3	3.1
CE	7.9	8.2	8.4	10.0	8.6
ND	5.1	4.2	5.2	5.2	4.9
SM	2.2	1.9	2.2	2.2	2.1
EU	0.7	0.7	0.7	1.0	0.8
TB	0.5	0.5	0.5	0.5	0.5
HO	0.7	0.7	0.7	0.5	0.6
YB	2.3	2.2	2.2	2.4	2.2
LU	0.3	0.3	0.3	0.4	0.3
D(M)	2.96	3.20	3.04	3.05	3.04
FeO*	12.81	11.88	12.73	13.01	12.92
F/F+M	0.684	0.735	0.664	0.686	0.693
Rb/Sr	0.238	0.056	0.129	0.080	0.105
K/Rb	91	0	23	125	50
K/Ba	18.3	0.0	4.6	16.6	9.6
den	2.63	2.67	2.66	2.69	2.66

Table Va: Major element analyses and C.I.P.W. norms for pillow cross-section SP-S3-P3.

Analyses des éléments majeurs, et norme C.I.P.W. d'une section du coussin SP-S3-P3.

Nom de la filiere C:\83P3MNO.ROC							
Echantillon	83P3C	83P3I3	83P3I2	83P3I1	83P3V	83P3R	83P3H
Litho.				0			
Qualite							
Code	2	6	7	8	9	10	11
Unite							
SiO2	53.57	54.62	54.77	54.84	55.77	55.53	39.47
TiO2	0.96	0.96	0.96	0.92	0.90	0.99	1.21
Al2O3	13.87	14.09	14.46	14.43	14.74	13.60	23.09
Fe2O3	5.08	5.41	4.66	4.58	4.38	4.80	6.33
FeO	8.24	8.22	8.56	8.58	8.76	10.09	7.65
MnO	0.19	0.18	0.17	0.17	0.19	0.20	0.19
MgO	6.00	5.55	5.51	5.55	5.34	6.47	4.63
CaO	8.72	7.77	7.29	7.09	6.05	5.61	16.61
Na2O	3.04	2.89	3.42	3.60	3.60	2.61	0.39
K2O	0.22	0.18	0.07	0.10	0.11	0.07	0.11
P2O5	0.13	0.13	0.13	0.13	0.15	0.04	0.32
Total	100.02	100.00	99.99	99.99	99.99	100.01	100.00
AN	47.80	50.50	45.22	42.94	43.80	53.28	97.86
Q	7.44	11.05	8.78	7.98	9.89	12.99	0.00
or	1.30	1.06	0.41	0.59	0.65	0.41	0.65
ab	25.72	24.45	28.94	30.46	30.46	22.09	1.33
an	23.55	24.94	23.89	22.92	23.74	25.19	60.93
ne	0.00	0.00	0.00	0.00	0.00	0.00	1.07
di	15.39	10.42	9.38	9.36	4.36	1.96	15.79
hy	17.13	18.10	19.72	19.99	22.48	28.45	0.00
ol	0.00	0.00	0.00	0.00	0.00	0.00	8.01
mt	7.37	7.84	6.76	6.64	6.35	6.96	9.18
il	1.82	1.82	1.82	1.75	1.71	1.88	2.30
ap	0.30	0.30	0.30	0.30	0.35	0.09	0.74
D(M)	2.96	2.92	2.91	2.93	2.89	2.88	3.12
FeO*	12.81	13.09	12.75	12.70	12.70	14.41	13.35
F/F+M	0.684	0.705	0.701	0.699	0.707	0.693	0.745
K/Rb	0	0	0	0	0	0	853
K/Ba	245.4	135.2	66.2	104.0	92.3	44.7	0.0
den	2.63	2.62	2.61	2.61	2.60	2.63	2.76

Table Vb: Major, trace and REE element analyses for pillow cross-section SP-S3-P3.

Analyses des éléments majeurs, traces et des terres rares d'une section du coussin SP-S3-P3.

Nom de la filiere C:S33TRD.ROC

Echantillon	S3P3C	S3P3I3	S3P3I2	S3P3I1	S3P3V	S3P3R	S3P3H
Litho.				o			
Qualite							
Code	2	6	7	8	9	10	11
Unite							
SiO2	53.57	54.62	54.77	54.84	55.77	55.53	39.47
TiO2	0.96	0.96	0.96	0.92	0.90	0.99	1.21
Al2O3	13.87	14.09	14.46	14.43	14.74	13.60	23.09
Fe2O3	5.08	5.41	4.66	4.58	4.38	4.80	6.33
FeO	8.24	8.22	8.56	8.58	8.76	10.09	7.65
MnO	0.19	0.18	0.17	0.17	0.19	0.20	0.19
MgO	6.00	5.55	5.51	5.55	5.34	6.47	4.63
CaO	8.72	7.77	7.29	7.09	6.05	5.61	16.61
Na2O	3.04	2.89	3.42	3.60	3.60	2.61	0.39
K2O	0.22	0.18	0.07	0.10	0.11	0.07	0.11
P2O5	0.13	0.13	0.13	0.13	0.15	0.04	0.32
Total	100.02	100.00	99.99	99.99	99.99	100.01	100.00
B	12.0	11.0	9.9	11.0	9.2	11.0	51.0
BA	100.0	120.0	110.0	110.0	100.0	100.0	140.0
CR	290.0	330.0	320.0	298.0	360.0	305.0	430.0
LI	17.0	16.0	15.0	15.0	18.0	19.0	13.0
NB	2.0	6.0	6.0	6.0	4.0	4.0	6.0
PB	16.0	8.0	6.0	10.0	8.0	4.0	8.0
RB	20.0	16.0	18.0	18.0	16.0	14.0	18.0
SR	84.0	100.0	94.0	86.0	70.0	50.0	140.0
Y	16.0	16.0	18.0	16.0	16.0	10.0	38.0
ZR	57.0	57.0	57.0	57.0	57.0	60.0	69.0
CS	0.3	0.0	0.0	0.3	0.0	0.3	0.0
SC	47.0	0.0	0.0	46.0	0.0	40.0	0.0
HF	1.3	0.0	0.0	1.4	0.0	1.4	0.0
CO	45.0	0.0	0.0	43.0	0.0	45.0	0.0
TH	0.3	0.0	0.0	0.3	0.0	0.3	0.0
TA	0.2	0.0	0.0	0.2	0.0	0.1	0.0
ZN	80.5	74.0	68.0	75.0	78.0	97.0	94.0
CU	100.0	110.0	91.0	90.0	100.0	65.0	220.0
NI	110.0	120.0	120.0	110.0	120.0	130.0	110.0
LA	3.4	0.0	0.0	2.8	0.0	1.5	0.0
CE	7.9	0.0	0.0	7.7	0.0	4.0	0.0
ND	5.1	0.0	0.0	4.4	0.0	1.9	0.0
SM	2.2	0.0	0.0	2.0	0.0	1.2	0.0
EU	0.7	0.0	0.0	0.5	0.0	0.3	0.0
TB	0.5	0.0	0.0	0.5	0.0	0.3	0.0
HO	0.7	0.0	0.0	0.7	0.0	0.4	0.0
YB	2.3	0.0	0.0	2.2	0.0	1.7	0.0
LU	0.3	0.0	0.0	0.3	0.0	0.3	0.0
D(M)	2.96	0.00	2.91	2.93	0.00	2.88	3.12
FeO*	12.81	13.09	12.75	12.70	12.70	14.41	13.35
F/F+M	0.684	0.705	0.701	0.699	0.707	0.693	0.745
Rb/Sr	0.238	0.160	0.191	0.209	0.229	0.280	0.129
K/Rb	91	93	32	46	57	42	31
K/Ba	18.3	12.5	5.3	7.5	9.1	5.8	6.5
den	2.63	2.62	2.61	2.61	2.60	2.63	2.76

Table VIa: Major element analyses and C.I.P.W. norms for pillow cross-section SP-S4-P3.

Analyses des éléments majeurs, et norme C.I.P.W. d'une section du coussin SP-S4-P3.

Nom de la filiere C:\S4P3M.ROC									
Echantillon	S4P3C	S4P3I5	S4P3I4	S4P3I3	S4P3I2	S4P3I1	S4P3V	S4P3R	S4P3H
Litho.									
Qualite									
Code	2	4	5	6	7	8	9	10	11
Unite	0								
SiO2	48.76	48.73	48.85	52.94	53.12	53.76	57.44	54.62	41.15
TiO2	0.78	0.79	0.85	0.84	0.90	0.86	0.85	0.99	0.93
Al2O3	15.93	14.99	14.28	14.98	15.37	14.82	12.70	13.23	22.05
Fe2O3	6.98	6.55	5.39	3.68	4.01	4.15	4.17	5.07	8.13
FeO	5.60	6.73	9.61	9.33	8.47	8.53	8.52	10.94	8.14
MnO	0.18	0.18	0.22	0.19	0.19	0.20	0.22	0.24	0.17
MgO	4.35	4.98	6.41	6.67	5.64	5.50	5.10	6.09	4.63
CaO	16.00	15.59	12.07	8.55	9.22	9.12	8.37	7.01	13.53
Na2O	1.06	1.20	2.07	2.60	2.82	2.82	2.41	1.54	0.64
K2O	0.00	0.00	0.02	0.05	0.05	0.05	0.05	0.07	0.28
P2O5	0.38	0.26	0.21	0.18	0.20	0.18	0.17	0.19	0.35
Total	100.02	100.00	99.98	100.01	99.99	99.99	100.00	99.99	100.00
AN	81.19	77.77	62.84	56.91	54.97	53.66	53.74	68.98	91.25
Q	9.52	7.60	2.59	6.55	7.17	8.39	16.68	16.11	0.06
or	0.00	0.00	0.12	0.30	0.30	0.30	0.30	0.41	1.65
ab	8.97	10.15	17.52	22.00	23.86	23.86	20.39	13.03	5.42
an	38.71	35.52	29.62	29.06	29.13	27.63	23.69	28.98	56.47
di	30.07	32.46	23.70	10.00	12.56	13.51	13.78	3.76	6.81
hy	0.00	2.68	16.53	24.76	18.98	18.24	17.11	28.02	15.22
wo	0.27	0.00	0.00	0.00	0.00	0.00	0.00	0.00	0.00
mt	10.12	9.50	7.81	5.34	5.81	6.02	6.05	7.35	11.79
il	1.48	1.50	1.61	1.60	1.71	1.63	1.61	1.88	1.77
ap	0.88	0.60	0.49	0.42	0.46	0.42	0.39	0.44	0.81
D(M)	3.20	3.15	3.07	2.96	2.96	2.94	2.94	2.95	3.09
FeO*	11.88	12.63	14.46	12.64	12.08	12.27	12.27	15.50	15.46
F/F+M	0.735	0.720	0.696	0.658	0.685	0.694	0.710	0.721	0.771
K/Ba	0.0	0.0	64.1	63.4	57.9	49.5	24.9	36.1	138733.3
den	2.67	2.68	2.70	2.65	2.63	2.63	2.61	2.66	2.74

Table VIb: Major, trace and REE element analyses for pillow cross-section SP-S4-P3.

Analyses des éléments majeurs, traces et des terres rares d'une section du coussin SP-S4-P3.

Nom de la filiere C:S4P3MTR.ROC

Echantillon	S4P3C	S4P3I5	S4P3I4	S4P3I3	S4P3I2	S4P3I1	S4P3V	S4P3R	S4P3H
Litho.									
Qualite									
Code	2	4	5	6	7	8	9	10	11
Unite	0								
SiO2	48.76	48.73	48.85	52.94	53.12	53.76	57.44	54.62	41.15
TiO2	0.78	0.79	0.85	0.84	0.90	0.86	0.85	0.99	0.93
Al2O3	15.93	14.99	14.28	14.98	15.37	14.82	12.70	13.23	22.05
Fe2O3	6.98	6.55	5.39	3.68	4.01	4.15	4.17	5.07	8.13
FeO	5.60	6.73	9.61	9.33	8.47	8.53	8.52	10.94	8.14
MnO	0.18	0.18	0.22	0.19	0.19	0.20	0.22	0.24	0.17
MgO	4.35	4.98	6.41	6.67	5.64	5.50	5.10	6.09	4.63
CaO	16.00	15.59	12.07	8.55	9.22	9.12	8.37	7.01	13.53
Na2O	1.06	1.20	2.07	2.60	2.82	2.82	2.41	1.54	0.64
K2O	0.00	0.00	0.02	0.05	0.05	0.05	0.05	0.07	0.28
P2O5	0.38	0.26	0.21	0.18	0.20	0.18	0.17	0.19	0.35
Total	100.02	100.00	99.98	100.01	99.99	99.99	100.00	99.99	100.00
B	33.0	23.0	14.0	9.9	13.0	14.0	15.0	14.0	24.0
BA	60.0	60.0	60.0	105.0	220.0	110.0	110.0	140.0	220.0
CR	250.0	265.0	272.5	275.0	285.0	282.5	285.0	325.0	325.0
LI	6.0	7.0	11.0	10.5	9.0	8.0	10.0	10.0	11.0
NB	6.0	4.0	6.0	7.0	6.0	6.0	4.0	8.0	4.0
PB	0.0	2.0	12.0	5.0	8.0	4.0	8.0	6.0	8.0
RB	14.0	14.0	14.0	19.0	18.0	18.0	16.0	16.0	18.0
SR	250.0	210.0	120.0	75.0	78.0	74.0	54.0	42.0	170.0
Y	12.0	14.0	16.0	17.0	16.0	16.0	12.0	8.0	24.0
ZR	51.0	51.0	54.0	57.0	54.0	54.0	54.0	57.0	66.0
CS	0.0	0.0	0.2	0.2	0.3	0.2	0.2	0.3	0.4
SC	40.0	43.0	47.0	46.0	43.0	45.0	43.0	53.0	57.0
HF	1.3	1.1	104.0	1.6	1.4	1.5	1.4	1.7	1.9
CO	30.0	38.0	53.0	50.0	40.0	40.0	35.0	60.0	50.0
TH	0.2	0.2	0.2	0.2	0.3	0.2	0.3	0.3	0.4
TA	0.1	0.1	0.1	0.1	0.2	0.2	0.2	0.1	0.1
ZN	54.5	90.0	92.5	125.0	104.0	93.5	120.0	110.0	147.5
CU	76.0	99.0	83.0	115.0	110.0	90.0	43.0	32.0	190.0
NI	84.0	110.0	130.0	120.0	110.0	110.0	96.0	140.0	100.0
LA	2.7	3.1	3.7	3.0	3.2	3.3	2.6	1.6	12.2
CE	8.2	9.0	10.6	8.8	8.2	8.0	6.5	5.0	17.0
ND	4.2	4.4	5.6	5.7	6.4	4.8	3.0	2.3	8.9
SM	1.9	2.0	2.5	2.1	2.2	2.2	1.8	1.2	6.3
EU	0.7	1.2	0.9	0.6	0.6	0.6	0.5	0.3	2.4
TB	0.5	0.5	0.5	0.5	0.5	0.5	0.4	0.3	0.8
HO	0.7	0.6	0.7	0.6	0.6	0.6	0.6	0.5	2.3
YB	2.2	2.1	2.5	2.2	2.3	2.3	2.0	1.8	4.3
LU	0.3	0.3	0.4	0.3	0.3	0.3	0.3	0.3	0.6
D(M)	3.20	3.15	3.07	2.94	2.96	2.94	2.94	2.95	3.09
FeO*	11.88	12.63	14.46	12.64	12.08	12.27	12.27	15.50	15.46
F/F+M	0.735	0.720	0.696	0.658	0.685	0.694	0.710	0.721	0.771
Rb/Sr	0.056	0.067	0.117	0.253	0.231	0.243	0.296	0.381	0.106
K/Rb	0	0	12	22	23	23	26	36	129
K/Ba	0.0	0.0	2.8	4.0	1.9	3.8	3.8	4.2	10.6
den	2.67	2.68	2.70	2.65	2.63	2.63	2.61	2.66	2.74

Table VIIa: Major element analyses and C.I.P.W. norms for pillow cross-section SP-S4-P4.

Analyses des éléments majeurs et norme C.I.P.W. d'une section du coussin SP-S4-P4.

Nom de la filiere C:S4P4NOD.ROC							
Echantillon	S4P4C	S4P4I3	S4P4I2	S4P4I1	S4P4V	S4P4R	S4P4M
Litho.							
Qualite							
Code	2	6	7	8	9	10	11
Unite							
SiO2	51.67	51.33	54.18	54.61	56.96	58.02	42.51
TiO2	0.90	0.96	1.00	0.94	0.92	0.92	0.97
Al2O3	14.47	14.66	13.75	14.75	14.11	12.72	21.91
Fe2O3	5.67	5.65	4.39	4.67	4.81	4.86	8.97
FeO	7.63	7.81	7.44	6.94	6.67	8.57	7.19
MnO	0.18	0.19	0.16	0.15	0.15	0.18	0.16
MgO	6.53	6.15	5.59	4.90	4.62	5.89	5.45
CaO	11.05	11.21	10.64	9.84	8.49	6.17	11.33
Na2O	1.65	1.85	2.64	2.95	3.08	2.38	0.93
K2O	0.05	0.05	0.07	0.10	0.07	0.15	0.33
P2O5	0.20	0.13	0.14	0.13	0.12	0.14	0.25
Total	100.00	99.99	100.00	99.98	100.00	100.00	100.00
AN	69.38	66.84	53.27	51.69	48.42	53.94	0.00
Q	9.97	8.72	9.57	10.17	14.47	18.52	0.00
or	0.30	0.30	0.41	0.59	0.41	0.89	0.00
ab	13.96	15.65	22.34	24.96	26.06	20.14	0.00
an	31.93	31.55	25.46	26.71	24.47	23.58	0.00
di	17.48	18.85	21.52	17.32	13.74	5.00	0.00
hy	15.97	14.60	12.11	11.37	11.85	22.75	0.00
mt	8.22	8.19	6.37	6.77	6.97	7.05	0.00
il	1.71	1.82	1.90	1.79	1.75	1.75	0.00
ap	0.46	0.30	0.32	0.30	0.28	0.32	0.00
D(M)	3.04	3.08	2.92	2.93	2.98	2.95	3.09
FeO*	12.73	12.90	11.39	11.14	11.00	12.94	15.26
F/F+M	0.664	0.680	0.674	0.697	0.707	0.690	0.739
den	2.66	2.66	2.62	2.60	2.58	2.60	2.71

Nom de la filiere C:S4P4MTR.ROC

Echantillon	S4P4C	S4P4I3	S4P4I2	S4P4I1	S4P4V	S4P4R	S4P4H
Litho.							
Qualite							
Code	2	6	7	8	9	10	11
Unite							
SiO2	51.67	51.33	54.18	54.61	56.96	58.02	42.51
TiO2	0.90	0.96	1.00	0.94	0.92	0.92	0.97
Al2O3	14.47	14.66	13.75	14.75	14.11	12.72	21.91
Fe2O3	5.67	5.65	4.39	4.67	4.81	4.86	8.97
FeO	7.63	7.81	7.44	6.94	6.67	8.57	7.19
MnO	0.18	0.19	0.16	0.15	0.15	0.18	0.16
MgO	6.53	6.15	5.59	4.90	4.62	5.89	5.45
CaO	11.05	11.21	10.64	9.84	8.49	6.17	11.33
Na2O	1.65	1.85	2.64	2.95	3.08	2.38	0.93
K2O	0.05	0.05	0.07	0.10	0.07	0.15	0.33
P2O5	0.20	0.13	0.14	0.13	0.12	0.14	0.25
Total	100.00	99.99	100.00	99.98	100.00	100.00	100.00
B	15.0	9.8	8.1	11.0	11.0	14.0	28.0
BA	90.0	100.0	100.0	100.0	120.0	160.0	340.0
CR	280.0	300.0	302.5	287.5	290.0	302.5	325.0
LI	11.0	14.0	12.0	11.0	10.0	12.0	13.0
NB	6.0	6.0	4.0	6.0	8.0	6.0	4.0
PB	6.0	8.0	6.0	6.0	8.0	8.0	12.0
RB	18.0	16.0	16.0	16.0	14.0	18.0	20.0
SR	140.0	98.0	60.0	68.0	60.0	44.0	180.0
Y	16.0	16.0	18.0	20.0	16.0	8.0	30.0
ZR	54.0	57.0	57.0	60.0	57.0	57.0	60.0
CS	0.2	0.4	0.0	0.4	0.0	0.4	0.5
SC	43.0	46.0	47.0	44.0	40.0	45.0	60.0
HF	1.3	1.7	1.6	1.4	1.2	1.6	1.7
CO	30.0	46.0	45.0	40.0	35.0	40.0	37.0
TH	0.3	0.3	0.2	0.3	0.2	0.2	0.3
TA	0.2	0.2	0.1	0.2	0.2	0.2	0.2
ZN	94.0	119.5	93.0	97.0	87.0	90.5	183.0
CU	97.0	100.0	94.0	130.0	99.0	48.0	130.0
NI	110.0	120.0	100.0	110.0	100.0	100.0	260.0
LA	3.1	3.2	2.9	3.0	2.6	1.7	5.5
CE	8.4	10.8	9.0	8.0	7.1	5.0	1.4
ND	5.2	4.2	4.4	4.8	4.5	2.2	6.4
SM	2.2	2.0	2.1	2.1	2.0	1.3	3.3
EU	0.7	1.0	0.6	0.5	0.5	0.4	2.0
TB	0.5	0.6	0.5	0.4	0.4	0.3	0.8
HO	0.7	1.5	0.6	0.7	0.6	0.5	0.9
YB	2.2	2.2	2.0	2.4	2.0	1.7	3.3
LU	0.3	0.3	0.3	0.3	0.3	0.3	0.5
D(M)	3.04	3.08	2.92	2.93	2.98	2.95	3.09
FeO*	12.73	12.90	11.39	11.14	11.00	12.94	15.26
F/F+M	0.664	0.680	0.674	0.697	0.707	0.690	0.739
Rb/Sr	0.129	0.163	0.267	0.235	0.233	0.409	0.111
K/Rb	23	26	36	52	42	69	137
K/Ba	4.6	4.2	5.8	8.3	4.8	7.8	8.1
den	2.66	2.66	2.62	2.60	2.58	2.60	2.71

Table VIIb: Major, trace and REE element analyses for pillow cross-section SP-S4-P4.

Analyses des éléments majeurs, traces et des terres rares d'une section du coussin SP-S4-P4.

Table VIIIa: Major element analyses and C.I.P.W. norms for pillow cross-section SP-S4-P5.1.

Analyses des éléments majeurs et norme C.I.P.W. d'une section du coussin SP-S4-P5.1.

Nom de la filiere C:S4P51MND.ROC

Echantillon	S4P5C	S4P51I	S4P51I	S4P51I	S4P51V	S4P51R	S4P51H
Litho.							
Qualite							
Code	2	6	7	8	9	10	11
Unite							
SiO2	47.96	47.01	49.66	50.00	54.95	56.06	41.35
TiO2	0.62	0.55	0.52	0.49	0.50	0.54	0.66
Al2O3	15.88	16.89	16.21	16.22	15.29	14.91	22.25
Fe2O3	4.86	4.85	4.31	4.10	3.56	4.02	8.66
FeO	8.64	9.52	8.87	8.88	7.49	8.20	6.60
MnO	0.22	0.22	0.20	0.21	0.18	0.19	0.15
MgO	6.07	6.48	5.82	5.61	4.62	5.48	4.61
CaO	12.81	11.18	10.66	10.46	9.21	6.84	14.27
Na2O	2.14	2.58	3.05	3.31	3.59	3.21	0.52
K2O	0.12	0.13	0.17	0.17	0.12	0.17	0.18
P2O5	0.67	0.59	0.55	0.55	0.49	0.38	0.75
Total	99.99	100.00	100.02	100.00	100.00	100.00	100.00
AN	64.82	60.98	53.79	50.78	45.39	48.69	92.93
Q	0.90	0.00	0.00	0.00	7.39	11.11	2.15
or	0.71	0.77	1.00	1.00	0.71	1.00	1.06
ab	18.11	21.83	25.81	28.01	30.38	27.16	4.40
an	33.37	34.12	30.04	28.90	25.25	25.77	57.85
di	21.14	14.37	15.84	15.99	14.21	4.67	6.46
hy	15.98	12.40	18.50	16.20	14.81	22.55	12.53
ol	0.00	7.07	0.32	1.75	0.00	0.00	0.00
mt	7.05	7.03	6.25	5.94	5.16	5.83	12.56
il	1.18	1.04	0.99	0.93	0.95	1.03	1.25
ap	1.55	1.37	1.27	1.27	1.14	0.88	1.74
D(M)	3.05	2.92	2.92	2.95	3.01	2.95	3.14
FeO*	13.01	13.89	12.75	12.57	10.69	11.82	14.39
F/F+M	0.686	0.685	0.690	0.695	0.702	0.687	0.759
K/Ba	1106.7	0.0	0.0	0.0	134.8	127.0	694.9
den	2.69	2.70	2.66	2.66	2.59	2.59	2.72

Table VIIIb: Major, trace and REE element analyses for pillow cross-section SP-S4-P5.1.

Analyses des éléments majeurs, traces et des terres rares d'une section du coussin SP-S4-P5.1.

Nom de la filiere C:\S4BZTRE.ROC

Echantillon	S4P5C	S4P5II	S4P5II	S4P5II	S4P5IV	S4P5IR	S4P5IM
Litho.							
Qualite							
Code	2	6	7	8	9	10	11
Unite							
SiO2	47.96	47.01	49.66	50.00	54.95	56.06	41.35
TiO2	0.62	0.55	0.52	0.49	0.50	0.54	0.66
Al2O3	15.88	16.89	16.21	16.22	15.29	14.91	22.25
Fe2O3	4.86	4.85	4.31	4.10	3.56	4.02	8.66
FeO	8.64	9.52	8.87	8.88	7.49	8.20	6.60
MnO	0.22	0.22	0.20	0.21	0.18	0.19	0.15
MgO	6.07	6.48	5.82	5.61	4.62	5.48	4.61
CaO	12.81	11.18	10.66	10.46	9.21	6.84	14.27
Na2O	2.14	2.58	3.05	3.31	3.59	3.21	0.52
K2O	0.12	0.13	0.17	0.17	0.12	0.17	0.18
P2O5	0.67	0.59	0.55	0.55	0.49	0.38	0.75
Total	99.99	100.00	100.02	100.00	100.00	100.00	100.00
B	12.0	9.9	11.0	11.0	10.0	16.0	36.0
BA	60.0	70.0	80.0	70.0	90.0	120.0	170.0
CR	260.0	267.5	265.0	277.5	285.0	282.5	298.0
LI	14.0	14.0	13.0	11.0	11.0	13.0	14.0
NB	6.0	8.0	6.0	8.0	6.0	8.0	8.0
PB	4.0	6.0	6.0	6.0	0.0	6.0	10.0
RB	8.0	6.0	8.0	8.0	8.0	8.0	8.0
SR	100.0	70.0	62.0	56.0	54.0	42.0	170.0
Y	22.0	24.0	22.0	20.0	22.0	18.0	28.0
ZR	56.0	57.0	60.0	60.0	60.0	63.0	66.0
CS	0.2	0.2	0.3	0.5	0.2	0.3	0.4
SC	45.6	46.4	46.2	46.0	45.0	46.0	56.2
HF	1.6	1.4	1.5	1.6	1.5	1.3	1.6
CO	47.0	46.0	48.0	47.0	40.0	37.0	35.0
TH	0.2	0.2	0.2	0.3	0.2	0.4	0.4
TA	0.2	0.1	0.1	0.1	0.2	0.2	0.1
ZN	106.0	118.5	112.5	128.0	101.5	110.5	99.5
CU	85.0	88.0	122.0	97.0	75.0	139.0	99.0
NI	198.0	205.0	272.0	203.0	132.0	294.0	139.0
LA	3.3	2.9	3.4	3.6	2.6	2.4	5.2
CE	10.0	8.5	9.5	10.0	8.0	7.0	13.0
ND	5.2	7.0	6.4	5.6	7.3	3.9	7.5
SM	2.2	2.2	2.3	2.4	2.0	1.8	3.1
EU	1.0	0.7	0.9	0.7	0.5	0.5	2.3
TB	0.5	0.5	0.6	0.6	0.5	0.4	0.7
HO	0.5	0.5	0.7	0.5	0.6	0.4	0.9
YB	2.4	2.5	2.4	2.4	2.2	1.9	3.2
LU	0.4	0.4	0.4	0.4	0.4	0.3	0.4
D(M)	3.05	2.92	2.92	2.95	3.01	2.95	3.14
FeO*	13.01	13.89	12.75	12.57	10.69	11.82	14.39
F/F+M	0.686	0.685	0.690	0.695	0.702	0.687	0.759
Rb/Sr	0.080	0.086	0.129	0.143	0.148	0.190	0.047
K/Rb	125	180	176	176	125	176	187
K/Ba	16.6	15.4	17.6	20.2	11.1	11.8	8.8
den	2.69	2.70	2.66	2.66	2.59	2.59	2.72

Table IXa: Major element analyses and C.I.P.W. norms for pillow cross-section SP-S4-P5.2.

Analyses des éléments majeurs et norme C.I.P.W. d'une section du coussin SP-S4-P5.2.

Nom de la filiere C:84P5MND.ROC

Echantillon	84P5C	84P521	84P521	84P521	84P521	84P52V	84P52R	84P52H
Litho.								
Qualite								
Code	2	5	6	7	8	9	10	11
Unite								
SiO2	47.96	48.56	47.87	47.42	50.98	55.75	55.06	44.95
TiO2	0.62	0.56	0.54	0.58	0.51	0.49	0.52	0.69
Al2O3	15.88	16.31	16.43	16.23	16.49	15.83	15.27	20.56
Fe2O3	4.86	5.52	5.60	4.46	3.79	3.37	3.90	4.72
FeO	8.64	8.49	8.72	10.18	9.29	7.71	8.76	11.53
MnO	0.22	0.20	0.21	0.22	0.21	0.17	0.17	0.20
MgO	6.07	6.02	6.33	6.65	5.72	4.70	5.68	7.26
CaO	12.81	11.85	11.86	11.17	9.57	8.11	7.02	7.44
Na2O	2.14	1.72	1.71	2.35	2.76	3.29	2.97	1.10
K2O	0.12	0.14	0.11	0.15	0.13	0.14	0.27	1.16
P2O5	0.67	0.63	0.63	0.59	0.55	0.46	0.37	0.39
Total	99.99	100.00	100.01	100.00	100.00	100.02	99.99	100.00
AN	64.82	71.42	71.80	62.61	57.98	50.16	52.29	78.69
Q	0.90	4.61	3.34	0.00	3.33	10.03	9.73	0.93
or	0.71	0.83	0.65	0.89	0.77	0.83	1.60	6.86
ab	18.11	14.55	14.47	19.89	23.35	27.84	25.13	9.31
an	33.37	36.37	36.83	33.30	32.22	28.01	27.54	34.36
C	0.00	0.00	0.00	0.00	0.00	0.00	0.00	4.90
di	21.14	14.97	14.63	15.05	9.63	7.61	4.01	0.00
hy	15.98	18.14	19.49	17.41	22.96	18.83	24.49	34.59
ol	0.00	0.00	0.00	4.55	0.00	0.00	0.00	0.00
mt	7.05	8.00	8.12	6.47	5.50	4.89	5.65	6.84
il	1.18	1.06	1.03	1.10	0.97	0.93	0.99	1.31
ap	1.55	1.46	1.46	1.37	1.27	1.07	0.86	0.90
D(M)	3.05	3.16	3.07	2.96	2.95	2.93	2.88	2.96
FeO*	13.01	13.46	13.76	14.19	12.70	10.74	12.27	15.78
F/F+M	0.686	0.694	0.688	0.684	0.693	0.699	0.687	0.688
K/Ba	1106.7	252.1	273.4	0.0	324.0	115.9	230.3	X10352.7
den	2.69	2.68	2.69	2.71	2.65	2.59	2.61	2.72

Table IXb: Major, trace and REE element analyses for pillow cross-section SP-S4-P5.2.

Analyses des éléments majeurs, traces et des terres rares d'une section du coussin SP-S4-P5.2.

Nom de la filiere C:\S4S2MTR.ROC								
Echantillon	S4P5C	S4P521	S4P521	S4P521	S4P521	S4P52V	S4P52R	S4P52H
Litho.								
Qualite								
Code	2	5	6	7	8	9	10	11
Unite								
SiO2	47.96	48.56	47.87	47.42	50.98	55.75	55.06	44.95
TiO2	0.62	0.56	0.54	0.58	0.51	0.49	0.52	0.69
Al2O3	15.88	16.31	16.43	16.23	16.49	15.83	15.27	20.56
Fe2O3	4.86	5.52	5.60	4.46	3.79	3.37	3.90	4.72
FeO	8.64	8.49	8.72	10.18	9.29	7.71	8.76	11.53
MnO	0.22	0.20	0.21	0.22	0.21	0.17	0.17	0.20
MgO	6.07	6.02	6.33	6.65	5.72	4.70	5.68	7.26
CaO	12.81	11.85	11.86	11.17	9.57	8.11	7.02	7.44
Na2O	2.14	1.72	1.71	2.35	2.76	3.29	2.97	1.10
K2O	0.12	0.14	0.11	0.15	0.13	0.14	0.27	1.16
P2O5	0.67	0.63	0.63	0.59	0.55	0.46	0.37	0.39
Total	99.99	100.00	100.01	100.00	100.00	100.02	99.99	100.00
B	12.0	10.0	10.0	7.4	9.4	10.0	14.0	0.0
BA	60.0	70.0	70.0	70.0	80.0	90.0	90.0	0.0
CR	260.0	265.0	232.5	265.0	260.0	276.5	281.0	0.0
LI	14.0	15.0	15.0	17.0	11.0	11.0	13.0	0.0
NB	6.0	8.0	8.0	8.0	8.0	8.0	8.0	0.0
PB	4.0	4.0	4.0	6.0	4.0	6.0	4.0	0.0
RB	8.0	6.0	8.0	8.0	6.0	8.0	6.0	0.0
SR	100.0	110.0	110.0	62.0	48.0	46.0	52.0	0.0
Y	22.0	22.0	24.0	24.0	22.0	20.0	20.0	0.0
ZR	56.0	60.0	60.0	60.0	60.0	60.0	63.0	0.0
CS	0.2	0.2	0.2	0.3	0.2	0.3	0.2	0.0
SC	45.6	47.0	37.0	47.0	41.8	46.0	45.0	0.0
HF	1.6	1.3	1.1	1.3	1.3	1.3	1.6	0.0
CO	47.0	50.0	39.0	44.0	40.0	40.0	38.0	0.0
TH	0.2	0.3	0.2	0.3	0.2	0.3	0.2	0.0
TA	0.2	0.1	0.1	0.2	0.2	0.1	0.1	0.0
ZN	106.0	118.0	98.5	109.0	112.0	97.0	113.5	0.0
CU	85.0	82.0	83.0	85.0	106.0	64.0	152.0	0.0
NI	198.0	136.0	124.0	161.0	154.0	136.0	275.0	0.0
LA	3.3	3.2	3.6	2.7	2.4	2.6	2.7	0.0
CE	10.0	9.6	8.2	7.8	8.0	8.6	8.0	0.0
ND	5.2	6.0	6.4	5.0	4.3	5.3	4.7	0.0
SM	2.2	2.2	2.4	2.0	1.6	1.9	2.0	0.0
EU	1.0	0.9	0.7	0.5	0.5	0.6	0.6	0.0
TB	0.5	0.6	0.4	0.5	0.5	0.5	0.5	0.0
HO	0.5	0.6	0.7	0.5	0.5	0.4	0.5	0.0
YB	2.4	2.4	2.6	2.2	1.8	2.0	2.0	0.0
LU	0.4	0.4	0.4	0.3	0.3	0.4	0.3	0.0
D(M)	3.05	3.16	3.07	2.96	2.95	2.93	2.88	2.96
FeO*	13.01	13.46	13.76	14.19	12.70	10.74	12.27	15.78
F/F+M	0.686	0.694	0.688	0.684	0.693	0.699	0.687	0.688
Rb/Sr	0.080	0.055	0.073	0.129	0.125	0.174	0.115	0.000
K/Rb	125	194	114	156	180	145	374	0
K/Ba	16.6	16.6	13.0	17.8	13.5	12.9	24.9	0.0
dsn	2.69	2.68	2.69	2.71	2.65	2.59	2.61	2.72